

# POLITECNICO DI TORINO

**Corso di Laurea Magistrale  
in Ingegneria Civile**



Tesi di Laurea Magistrale

## **Structural Health Monitoring of the Forth Road Bridge**

**Relatore**

Prof. Rosario Ceravolo

**Candidato**

Greta Lentini

**Corelatore**

Prof. Daniele Zonta

A.A.2018/2019



## Abstract

Structural Health Monitoring (SHM) is a helpful tool for engineers in order to control and verify the structural behaviour. SHM also guides the engineers in decision making concerning the maintenance, economy and safety of structures.

Bridges play a fundamental role in infrastructure assets of a country, stimulating regional cooperation and economic development. However, the inevitable aging process and the accumulation of damage resulting from traffic and weather effects can adversely affect their performance. For these and more reasons long-span bridges, in particular, need care and attention and constant controls to be sure they are behaving as designed. Ordinary maintenance with visual inspection alone, is not sufficient to prevent the risk of failure.

An installation of Structural Health Monitoring system on long-span bridges is strongly recommended to ensure their safety and serviceability. However, the diagnosis of the reliability and damage detection of bridges are challenged by the sensitivity of structural performances and monitoring parameters to environmental conditions. The aim of the project is therefore to present a SHM data strategy to separate the effects induced by temperature and evaluate the structural health status of a long-span bridge.

In this thesis is presented the case study of the Forth Road Bridge (FRB), a long span suspended bridge opened in 1964. The monitoring system was developed on the FRB after the discovery of a fractured steel member, known as the truss end link, in December 2015. After about one year, the truss end links were replaced with new sliding bearings and brackets details to support the bottom corner of a new truss-end post.

The deployment of the FRB SHM system and sensors technology are described in order to give the reader a good understanding of the subsequent data analysis and condition assessment.

The data analysed, regarding strain, temperature and displacement measurements, were gathered from January 2016 until November 2018. Results indicating the change

in the structural elements strain are presented, in particular changes of strain associated with changes in temperature are observed.

The results allow to control the maximal strain and displacement, to detect the structural behaviour of the elements analysed to report strain trend compared with the temperature trend over the time and to compare the two different structural schemes.

The evidence to support the conclusion of the analysis is provided by both qualitative and quantitative methods.

# Contents

1.	Introduction.....	1
1.1	Aims .....	2
1.2	Structural Health Monitoring.....	2
1.3	SHM on long-span bridges.....	5
1.4	Motivation for implementation of SHM systems.....	6
1.5	Case study on SHM: Forth Road Bridge.....	7
2.0	History of the Forth Road Bridge.....	8
2.1	Site Location.....	8
2.2	Bridge Design .....	10
2.2.1	Structural scheme.....	10
2.2.2	Foundations.....	13
2.2.3	Main towers.....	15
2.2.4	Side towers .....	17
2.2.5	Main cables.....	18
2.2.6	Anchorage.....	22
2.2.7	Suspended structure .....	24
3.0	Case study maintenance and repair work.....	29
3.1	Truss end links repair.....	30
3.1.1	First phase.....	32
3.1.2	Second phase.....	33
3.1.3	Third phase .....	34
4.0	Structural Health Monitoring system.....	35
4.1	Integrated systems on FRB .....	36
4.2	Sensors arrangement.....	37

4.3	Sensor technology.....	40
4.3.1	Strain gauges .....	41
4.3.2	Displacement transducers .....	42
4.3.3	Tiltmeter .....	43
4.3.4	GPS.....	44
4.3.5	Temperature sensors.....	45
4.3.6	Anemometers .....	46
5.0	Methodology .....	48
5.1	Data acquisition .....	49
5.2	Data analysis .....	51
5.2.1	Sensor specifications .....	51
5.3	Data processing.....	53
5.3.1	Linear parametric model .....	55
5.3.2	Parameter estimation using least squares analysis .....	56
6.0	Results and Discussion.....	59
6.1	Full time history of strain and temperature .....	59
6.2	Strain data shifted.....	63
6.3	Different period within the year.....	64
6.3.1	Summer solstice .....	64
6.3.2	Winter solstice.....	67
6.4	Daily temperature effect .....	68
6.5	Strain and temperature trend with reduced data set .....	69
6.6	Strain-temperature correlation .....	73
6.6.1	Other studies supporting the monitoring .....	76
6.7	Full time history of displacement and temperature.....	78
6.8	Displacement trend with reduced data set .....	80

6.9	Displacement-temperature correlation.....	81
6.10	Least square analysis.....	82
7.0	New bearing results and discussion .....	87
7.1	Full time history of strain and temperature .....	87
7.2	Different periods within the year .....	89
7.2.1	Summer solstice .....	90
7.2.2	Winter solstice.....	91
7.3	Strain and temperature trend with reduced data set .....	92
7.4	Strain-temperature correlation .....	94
7.5	Displacement and temperature trend.....	95
7.6	Displacement and temperature trend with reduced data set .....	96
7.7	Displacement-temperature correlation.....	97
7.8	Least square analysis .....	98
8.0	Conclusion and recommendations.....	103
	References.....	104



# 1. Introduction

Long-span bridges are often among the key transportation infrastructure assets of a country, stimulating regional cooperation and economic and social development. The inevitable aging process and the accumulation of damage resulting from wind, traffic and the surrounding environment can adversely affect their performance. For these and more reasons long span bridges need care and attention and constant controls to be sure they are behaving as designed. Suspension bridges in particular, as their parts move, are at risk of unforeseen element failures, and visual inspection alone is not sufficient to evaluate the risk of such failures.

Without proper monitoring, maintenance and warning, the closure or collapse of these bridges is possible. This can lead to significant economic and societal impacts and, in some cases, heavy casualties as seen with the incident of the Seongsu Bridge (Seoul, 1998), the I-35W highway bridge (Minnesota, 2007) and, more recently, the newly installed pedestrian bridge at Florida International University (Miami, 2018). Therefore, civil structures in general should be monitored both during the construction process and during the service life. Data collected from real time monitoring can then be used for damage assessment and health evaluation of the civil engineering structures in service. The continuously measured data from the monitoring system can provide the basis for predicting future performance and determining optimum maintenance strategy for the existing structures.

Structural Health Monitoring (SHM) has been developed significantly thanks to the evolution of sensing and communication technologies as well as data processing methodologies, including the application of machine learning and pattern recognition.

SHM allows keeping track of every structural element of a civil engineering infrastructure, analysing big amount of data and correlating different data types. In addition, this monitoring system enables setting automatic alerts and predicting future trends.

Structural Health Monitoring is vital to ensure the safety and serviceability of these structures, reducing the risk of malfunction due to extreme loading and long-term degradation.

## 1.1 Aims

The general aims of this thesis are to:

- Explain the principles of Structural Health monitoring
- Present the advantages of SHM providing as a case study the Forth Road Bridge
- Present a state-of-the-art rapport over monitoring and sensory technologies
- Increase the understanding for the behaviour of the structure after a fracture was found
- Increase the understanding for the behaviour of the Forth Road Bridge by reporting strain changes in the structure
- Analyse structural monitoring data
- Evaluate trends and historic events
- Investigate correlations between different types of data
- Understand relationships and behaviour of key elements of the bridge

## 1.2 Structural Health Monitoring

The aim of this section of the thesis is to provide the reader with a basic knowledge on monitoring, as an introduction to the topic before the Forth Road Bridge and its Structural Health Monitoring (SHM) deployment are discussed. In addition, the advantages of using this system will be provided.

Structural health monitoring is a process of characterization of existing works with which we propose to identify and analyse some properties of the structure in order to obtain information. This information enables to develop analytical models for the evaluation of the construction status and they play an important role in the operations of maintenance of structures. Moreover, SHM allows evaluating real time changes in the structural behaviour such as damage to the material or structural elements, changes in the behaviour of constraints and connection systems or other changes that may affect the performance of the structure.

Damage is defined as changes to the material and/or geometric properties of the infrastructure, including changes to the boundary conditions and system connectivity (*Health Monitoring of Bridges, Helmut Wenzel*). Damage is responsible of the present

and future performance of these systems. The damage identification process is generally structured into the following levels:

- Damage detection, where the presence of damage is identified.
- Damage location, where the location of damage is determined.
- Damage typification, where the type of damage is determined.
- Damage extent, where the severity of damage is assessed.

SHM systems generally fall into two categories, global and local. A global SHM system will provide information about the behaviour of the structure as a whole. Whereas local SHM will provide information on local behaviour of critical points of the structure.

Damage detection is not the only purpose of SHM systems. Other goals of an SHM deployment can be:

1. Estimate remaining service life of a structure
2. Optimise the decision-making process for maintenance efforts to avoid costly replacements
3. Verify design models of a structure

Though the deployment of a SHM system can vary significantly due to its components which are application-dependent, the general aspect of most of the SHM system have the same fundamental elements: measurements by sensors and instrumentation, structural assessment and condition assessment to support maintenance and rehabilitation related decision-making (Duzgun Agdas et al., 2015)

The functionality of an SHM system depends heavily on the types and number of sensors used. Sensors can capture a variety of physical measurements associated with load, environmental conditions or bridge responses. There are countless sensing technologies, either emerging or established that can be considered for the monitoring. Standard strain gages and accelerometers have been in wide use for decades to measure structural responses. More recently, optical fibre sensors have been applied for strain, temperature and vibration measurement and GPS sensors to measure bridge deflection that can be problematic due to the need for a fixed reference point (Duzgun Agdas et al., 2015).

The amount of data gathered from these sensors will be massive and will require condensation. This will make data processing more efficient. This process can be achieved through feature selection, which is used to identify data features that can be used to determine if a system is damaged or undamaged. Following this the structural health can be determined.

Taking all this into account the field of application of SHM results wide and it goes from mechanical engineering to aerospace and civil engineering.

While in mechanical and aerospace engineering most of the monitoring systems are designed to work permanently over the lifetime of a structure or a component, in civil engineering often we have to deal with structures that already exist with a widely unknown history. Sometimes like in the Forth Road Bridge the monitoring system is implemented only after damage is detected. This certainly leads to a lot more time to collect data, then analyse them and after all a permanent system can be designed.

During years long-span bridges, which are the focus of this work, attracted attention because a considerable number of bridges that should meet the requirement of the serviceability, safety and sustainability during their lifecycle, were destroyed due to natural and artificial hazards. Others have been damaged by the deterioration of structural components, exceptional vehicle load and faster material deterioration (Zengshun Chen et al., 2017).

Since bridges play an important role in the infrastructure system, it was immediately looked for a solution to keep them under control. For this reason, structural health monitoring systems that are used for surveillance, evaluation and assessment of the condition of existing long-span bridges have been widely developed, and the recently-developed long-term SHM system is one of cutting-edge systems for monitoring the serviceability, safety, and sustainability of long-span bridges (Zengshun Chen et al., 2017).

However, every bridge's monitoring system differs from the others and has to be studied and designed for that specific case because bridges are individual structures that have very little in common with each other. The combination of structural scheme, boundary conditions, materials and properties create a huge number of

unknown. In general past and current bridge monitoring applications can be subdivided into two categories: monitoring systems deployed to track a previously identified concern and monitoring system that are deployed pre-emptively during original construction to track general structural health. The Forth Road Bridge falls into the first category and its SHM system will be later analysed in detail.

### 1.3 SHM on long-span bridges

Long-span bridges are known in the world for their attractive appearance, due to their tall towers and large slender spans; they are undoubtedly a marvel of civil engineering. Moreover, they are key assets of infrastructure and transportation facilities, which provide connections between regions and facilitate regional cooperation as well as economic and social development of countries. A collapse or closure of bridges can lead to traffic chaos in regions, significant financial losses, and, in some cases, heavy casualties. For example, before the open of the Queensferry Crossing, the Forth Road Bridge was the major road link across the Fifth of Forth, Scotland; a single-lane closure of the FRB was estimated to cause a £650,000 loss daily (Meng et al., 2018).

Learning also from the collapse of the Tacoma Narrows Bridge, long-span bridges have been designed with efficient aerodynamic characteristics to limit wind-induced effects. However, extreme events, such as large temperature variation, hurricanes, storms or devastating earthquakes are now stronger and occur more frequently, continuously challenging long-span bridges resistance. Adverse weather conditions coupled with an increase in usage, these inevitably accelerate the aging process and deterioration of structural elements, particularly for some bridges located in harsh environments (X. Meng, 2018).

It is therefore important put the attention in the safety, serviceability and sustainability of these structures during their construction and especially after. Hence SHM systems are being actively developed to fulfil this role (X. Meng, 2018).

In many countries, such as China and Japan, it is now mandatory to implement Structural Health Monitoring systems on long-span bridges for monitoring and evaluating their current health status. The Tsing Ma Bridge, which is a 1337 m long suspension bridge in Hong Kong, has been equipped with probably the most complete

and sophisticated SHM system. This so-called Wind and Structural Health Monitoring System (WASHMS) consists of more than 800 sensors of different types permanently installed on the bridge, including Global Position System (GPS) sensors, accelerometers, and strain gauges (X. Meng, 2018).

SHM systems on long-span bridges have taken greatly advantage from new sensor technologies such as wireless sensors, fibre optic sensors (FOSs) and microelectromechanical sensors.

Wireless sensor networks (WSNs) have attracted a lot of attention recently due to their low cost, high flexibility, and high efficiency. Many SHM systems on bridges have been equipped with FOS sensors, providing reliable measurements of strain and temperature from multiple locations, including the Tsing Ma Bridge, the Yonghe Bridge, the Ebian Bridge and the Siggenthal Bridge (X. Meng, 2018).

#### 1.4 Motivation for implementation of SHM systems

The monitoring of infrastructure such as bridges is very important for several reasons. First of all, it allows detecting and localizing damage, then to validate the structural designs and characterize performance, to assist with infrastructure maintenance, to improve seismic risk assessment, to monitor and control the construction process, to characterize loads in situ, and last but not least reduce inspection cost, while providing increased public safety.

Nowadays, the use of monitoring in the study of civil structures is increasing and it involves both existing and new construction structures and infrastructures on which it is possible to assess the structural reliability allowing a more prolonged use and in total safety. Unnecessary periodical inspections can be avoided leading to a reduction of maintenance costs by using permanent monitoring systems. More and more large-scale monitoring systems have been designed and implemented in existing structures and during the construction stages. However, the application of monitoring systems on existing structures requires a careful strategy to allow the structure to be maintained efficiently with a high level of safety and, at the same time, it limits its maintenance costs. The problem becomes even more relevant when it is necessary to assess the

performance level of structures potentially damaged by traumatic events such as seismic events.

Before the SHM was introduced the only way to detect damage was the visual inspection. This methodology has some limitations that affect the efficiency of decision-making and resource utilization. The visual inspections need lot of time and are not continuous. Moreover, visual inspections depend on inspector's subjective assessment. (Duzgun Agdas et al., 2015).

On the contrary SHM system continuously records data. It can monitor the whole bridge at the same time and it doesn't have problems of accessibility for example to detect an internal structural problem.

## 1.5 Case study on SHM: Forth Road Bridge

Once the topic of the thesis has been selected the second passage was to choose a relevant infrastructure with a structural health monitoring system and with at least a year of data acquisition that could be utilised for the thesis purpose.

It was decided the Forth Road Bridge was an ideal case study because a Structural Health Monitoring system was developed since December 2015 after a fracture was discovered at the north east main span during a routine inspection, it has a significant role in the Scottish highway network and there is a lot of literature available about this bridge.

In order to let the reader understand the event that consequently brought to the installation of the SHM system, it is important to know how a suspended bridge works. For this reason, the second part of the thesis is focused on the structural scheme and on the history of the bridge. The textbooks mainly utilised to undertake this task are titled "Forth Road Bridge" published by the Institute of Civil Engineers (ICE, 1967) and "Forth Road Bridge" by Joint Board that contains information about the history of the bridge.

## 2.0 History of the Forth Road Bridge

The Forth Road Bridge on the Firth of Forth links Fife and the North with Edinburgh and the South; carrying modern traffic over a waterway where for more than eight hundred years the only way to get to the other side was the ferryboat. The Forth Road Bridge was designed, and the construction supervised, by two firms of Consulting Engineers, Messrs. Mott Hay and Anderson and Sir Freeman Fox and Partners. The bridge was built by a consortium, known as the ACD group, which involved Sir William Arrol & Company, The Cleveland Bridge & Engineering Company and Dorman Long. The bridge's construction started in 1958 and it ended in 1964.

The decision to build a new infrastructure came up by 1920's when road traffic was increasing and a new link to the north was necessary. In the following years lots of surveys were conducted to find the perfect site to build the bridge. Then, because of the national economic crisis, bridge building was temporarily halted. After the 1939/45 War the Local Authorities signed an agreement with the Government both to the erection of a new road bridge on the Mackintosh Rock site and to the arrangements for meeting the cost. In 1947 the Forth Road Bridge Order approved the construction of the bridge. On February 10, 1958, the Government gave approval for work to begin. Thus, began the construction of the largest suspension bridge in Europe, fourth largest in the world (*FRB Joint Board, 1964*).

### 2.1 Site Location

Three initial sites were proposed for the FRB in 1929 based on the work carried out by Messrs John Cochrane and Sons Limited (ICE, 1967). The sites planned to span the Firth of Forth and connect the North Queensferry with the South. With reference to Figure 2.1, the first proposal was located approximately one kilometre and a half above of the existing Forth Railway Bridge, the second proposal was located downstream but adjacent to the railway bridge and the third was located one kilometre and a half downstream of the Forth Railway Bridge (ICE, 1967).

The initial site location seemed reasonable for the presence of the beamer rock as a foundation for the large pier of the north tower. However, it was noted from the bore

logs conducted by Messrs John Cochrane and Sons Limited that the south foundation would have to be dug at a great depth (ICE, 1967).

The second proposed location posed two problems, the first of which being that the railway company would rejected the proposed location, due to the close proximity to the Forth Railway Bridge (ICE, 1967). The second issue arose from the suspension bridge design, in that it would experience aerodynamic buffeting effects, which are undesirable for long span suspension bridges (ICE, 1967).

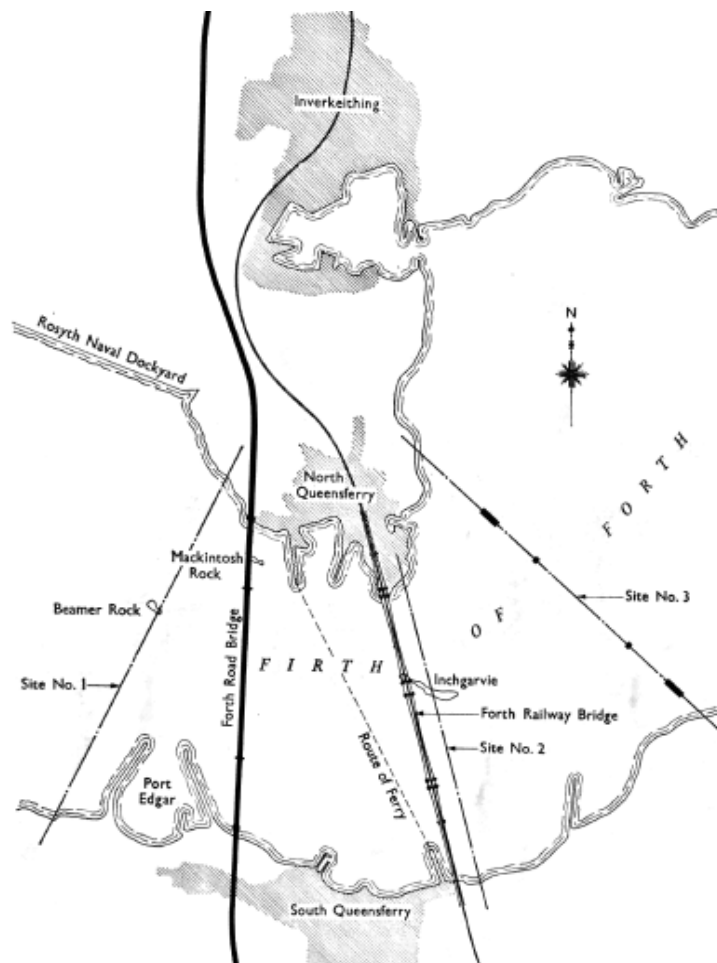


**Figure 2.1:** FRB proposed site locations (ICE, 1967)

The final site proposal was similar to the initial, engineers found an appropriate bedrock on which the piers could be built but at rather great depths (ICE, 1967). It should be noted that this location was the one in which engineers gave their backing to which they established a proposed design (ICE, 1967).

Following the preliminary investigations in 1929, the engineers continued to propose other possible location and in 1931 the survey led to the discovery of another site. This

one was located approximately half way between the existing Forth Railway Bridge and beamer rock site. This location was found to contain suitable bedrock at shallower depths on both sides of the estuary (ICE, 1967). In the North, a submerged rock the Mackintosh Rock was more than capable of withstanding a bridge pier and in the South, the bedrock was found to be no more than 34 metres below the highest water level (ICE, 1967). By 1939 the Ministry of Transport deemed this site proposal acceptable based on the cost and traffic possibilities (ICE, 1967).

## 2.2 Bridge Design

The structural form of the bridge follows the American style of suspension bridge construction, prevalent when the bridge was constructed, and it was designed following the British Standard BS 153 (Penistone, 2009).

### 2.2.1 Structural scheme

The Forth Road Bridge is a long span suspension bridge which when opened in 1964 was the largest in the world outside the United States and, together with the approach viaducts is a little over 2.5 km in length. The bridge has a main span of 1006 metres between the two main towers. The side spans which carry the deck to the side towers are each 408 metres long. The approach viaducts are 252 metres and 438 metres long on the north and south sides respectively. Figure 2.1 shows the general elevation of bridge and viaducts.

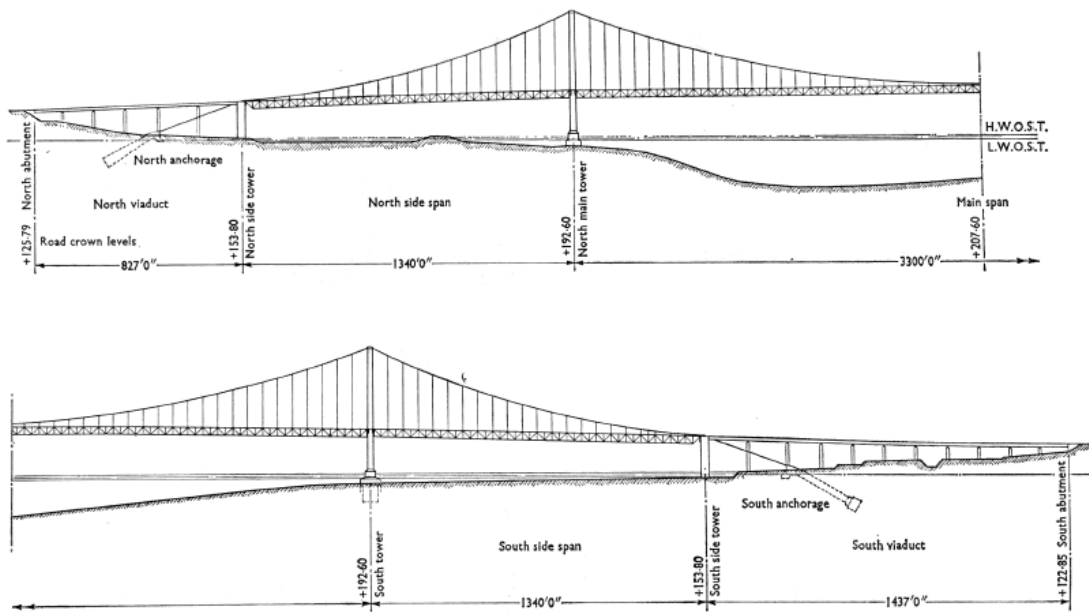


Figure 2.2: FRB detailed design (ICE, 1967)

Dead, traffic and wind load from the deck are taken as tension within the suspender cables, which load the main cables uniformly in tension along the bridge deck's length. Accordingly, the main cables deflect into a parabolic shape. The cables rest on the towers with saddles, which transfer compression vertically to the towers. Differences in load between the spans are accommodated by sliding of the cable over the saddle (Penistone, 2009).

The side towers support the main cables, at the end of each side span as they are deflected down towards the anchorages, and the carriageways, cycle tracks, and footpaths between the side spans and the viaducts.

The north and the south viaducts support the carriageways, footpaths, and cycle tracks between the ends of the approach road embankments and the side towers. The south viaduct is longer and has eleven spans, while the north one has six spans. Figure 2.3 shows a detail of the viaducts. On both sides reinforced concrete piers support the deck structure in spans varying from 34 metres to 50 metres.

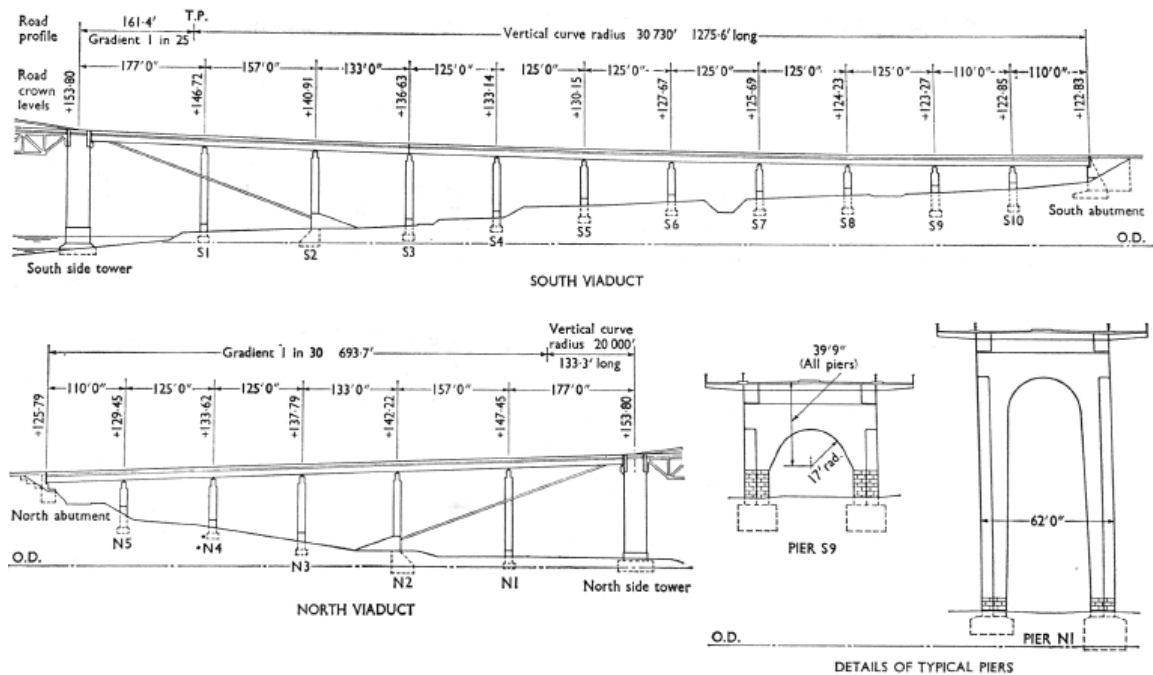


Figure 2.3: General elevation of viaducts and piers (ICE, 1967)

The main suspended structure is made up of a steel stiffening truss, with three longitudinal air gaps at roadway level to improve aerodynamic stability. The deck, simply supported by the stiffening truss, is made of panels with an expansion joint, offset from the cross girders to obtain the advantage in panel design of continuity over the supports. All the material in the deck panel is mild steel. On the side spans for a cheaper solution a composite concrete slab and steel stringer design was adopted.

The suspended structure on the viaducts is a prefabricated box girder made of welded high tensile steel. The cross girders, which occur at 3 metres centres, are made continuous trough the box beams to the outriggers where an edge beam provide end restraint.



*Figure 2.4: Construction of the deck on the south viaduct (Transport of Scotland, 1964)*

### 2.2.2 Foundations

The geological conditions varied greatly across the river and required quite different construction methods to be used for each pier. The realization of the south pier proved much more difficult as the bedrock was much deeper on this side. The construction started with the building of a large figure of eight frames at the suitable side on the north shore, which consisted of twin circular welded steel box members. Then it was floated across the river to the position of the south pier. Sheet piles were driven around the frame to form a cofferdam. Inside these two 18 metres diameter caissons were built, which were sunk through gravel and boulder clay until they reached rock about 30 metres below the surface. The caissons were then filled with concrete to form the foundation for the tower.

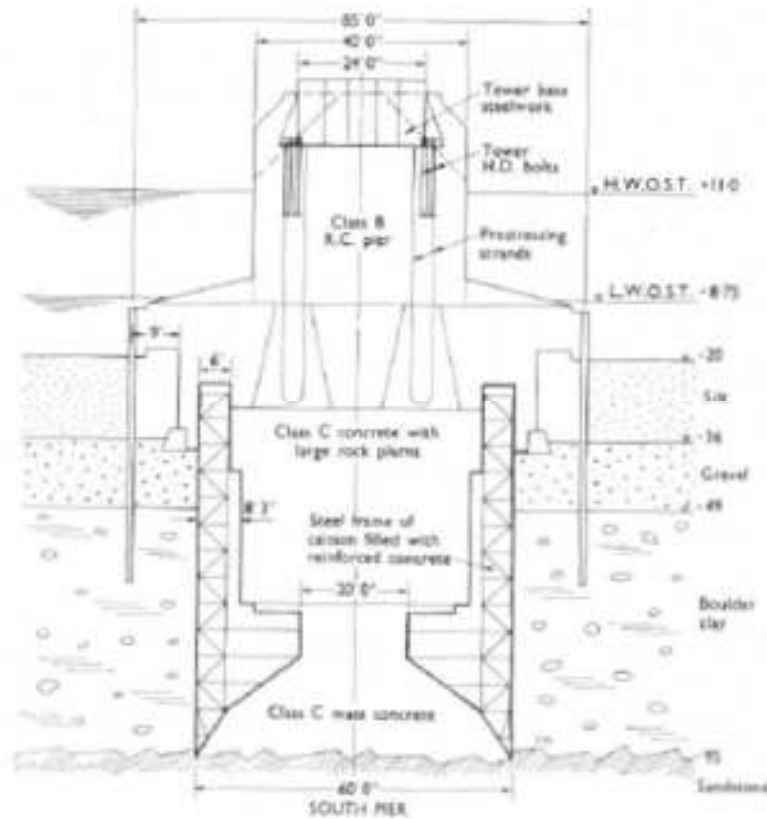


Figure 2.5: Cross section of south pier (ICE, 1967)

The north main pier is found on the mackintosh rock. First level was took off by underwater blasting, then the broken rock was grab out and piles forming the base of the pier were driven straight into the bedrock. Prefabricated waling unit was built, floated out to the site and landed on the small piers where it was secured. Side walls shutters were erected and the struts positioned, then erected stressing columns and concreted sidewalls. Then strands were inserted and stressed, and at the end dewatered cofferdam to enable the pier to be completed in the dry.

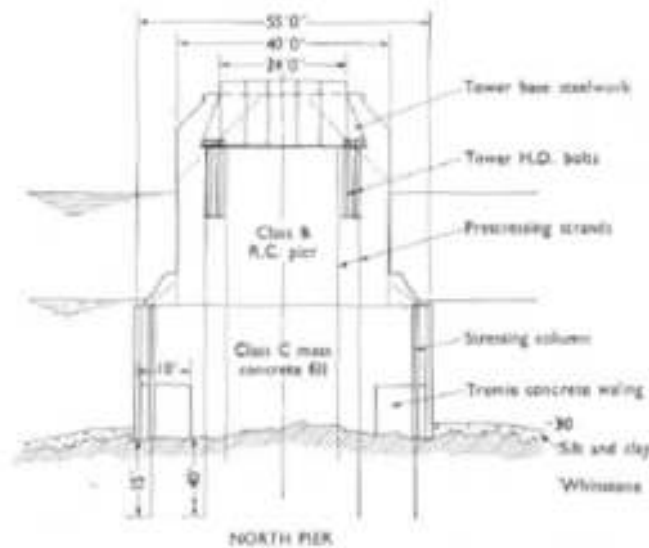


Figure 2.6: Cross section of north pier (ICE, 1967)

### 2.2.3 Main towers

All the towers were prefabricated in Glasgow where there was enough space to assemble the members. The towers are of welded cellular high tensile steel construction and rise some 150 metres above high water level. The section of each tower leg is composed of five cells formed by three fabricated boxes joined together by four connecting plates. The dimensions of the centre box are 3.6 x 1.5 metres and the spacing of 1.3 metres between boxes, are maintained for the full height of the tower. The boxes are 1.5 x 0.9 metres (ICE, 1967). The stiffened plates forming the sides of each box are of high tensile steel and the connexions are made with grip bolts.

The base section of each tower leg is in mild steel of similar construction to the main leg but splayed out to a greater width below the surface of the concrete pier. The tower legs are tapered because the sectional area required to carry the direct load decreases towards the top. In fact, the tower taper from 7.3 metres at the base to 5.5 metres at the summit, as we can see from the figure above.

The FRB main towers act as the primary structural support for the main cables. The main cable saddles are housed atop of the main towers as seen in Figure 2.7 By locating the saddles at the summit of the bridge towers, longitudinal displacements arise from the cable loads which in turn produce movement at the tower summits. The

towers provide bending resistance to the cable loads which can amount to 50 percent of the direct stress (this is the critical loading condition).

It can be noted that the tower base has been sized accordingly to ensure both bending resistance and that they can support themselves in the free standing orientation when subjected to high winds. With reference to Figure 2.7, it can be seen that the base size changed from tender to detailed design to accommodate this.

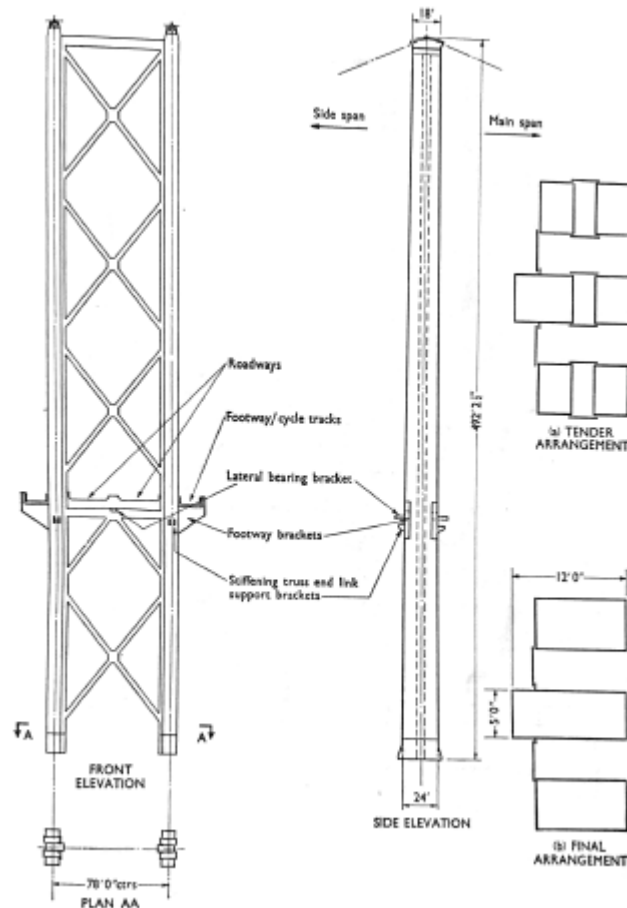


Figure 2.7: General arrangement of the main towers (ICE, 1967)

Both towers measure 150 by 24 metres in terms of height and width (centres to centres) (ICE, 1967). Figure 2.6 shows how the tower legs are strengthened throughout their length by the addition of welded angles (ICE, 1967). It should also be noted that the maximum steel thickness was 25 millimetres (ICE, 1967) in order to assist the welding processes adopted for construction. Furthermore, Figure 2.8 highlights the design for the main tower leg base.

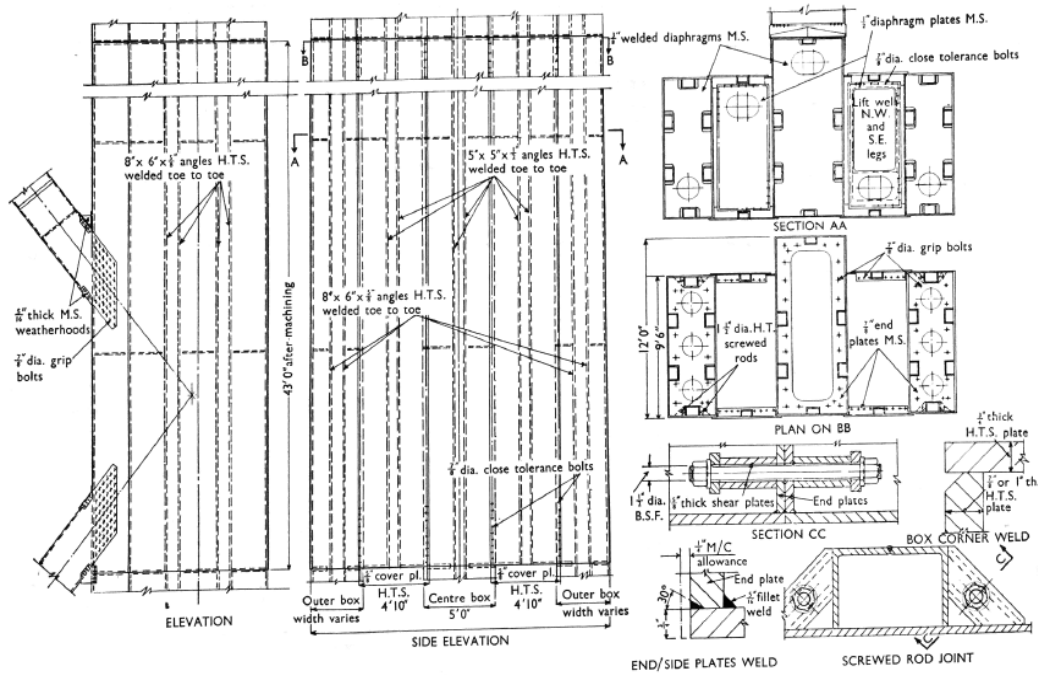


Figure 2.8: Main tower leg details (ICE, 1967)

## 2.2.4 Side towers

The side towers are 45 metres high and are required to support the rocker saddles over which the cables are deflected from the side spans down to the anchorages. In addition, they provide vertical, longitudinal and lateral supports for the side span superstructure as well as for the approach viaducts. The vertical loads from the viaducts are heavier than those from the side spans, and to counteract the overturning moment thus produced the bearings for the cable rockers are set about one metre forward of the leg centre line. Reinforced concrete construction was chosen for the side towers to match the design proposed for the approach viaducts (ICE, 1967).

Figure 2.8 illustrates the detailed design of both side towers, made of two reinforced concrete legs and a cross beam all of box section. The cable saddles are located at the tops of each leg. It can be noted from the figure that the reinforcement is provided with post-tensioned strands which extend from the summit of the tower to the tower base, then a further 13.7 metres into the foundation rock (ICE, 1967).

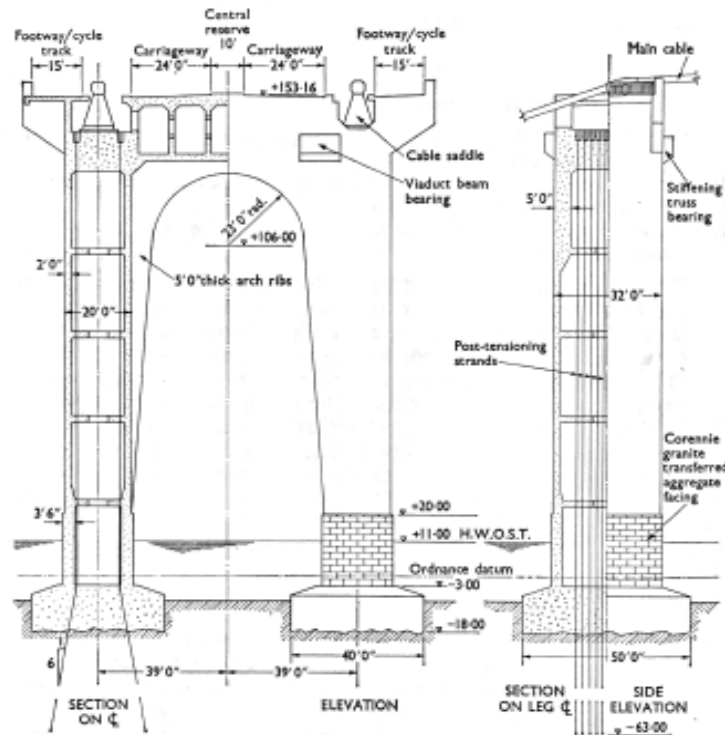
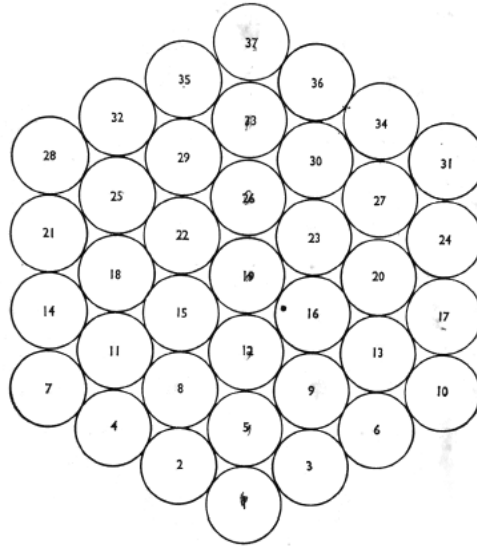


Figure 2.9: Elevation and sections of side towers (ICE, 1967)

## 2.2.5 Main cables

The FRB main cables play a crucial role within the structure. They support the load due to traffic and weather conditions (wind). The cables were designed and constructed using a technique known as spinning. The spinning process gives a uniform cross-sectional area from anchorage to anchorage, and according to the design, from one saddle to the other cross the length of the bridge, the horizontal component of cable tension is uniform for all condition of loading. The cable tension at any point is then proportional to the secant of the angle the cable makes with the horizontal at that point. The slope of the cable is greatest at the sides of the main tower, and there occurs the maximum cable tension.

According to (ICE, 1967) each cable required a cross sectional area of  $0.22 \text{ m}^2$  to cope with the stresses caused by loading. Therefore, it was decided to use 37 strands of 314 wires each as shown in figure 2.10. Every wire has a diameter of 4.98 millimetres. The cables are spun in a series of strands that are arranged in the form of a hexagon, in order to reach a circular form after been compacting.



*Figure 2.10: Pattern of strands in cable before compacting (ICE,1967)*

The saddles on the main and side towers support the FRB's main cable. The difference between the two is based on their support. The saddles located on the main tower are fixed. Whereas the saddles located on the side towers are on rocker bearings. The reasoning for this is to accommodate for changes in longitudinal displacement which are caused by load and temperature variations (ICE, 1967). Figure 2.11 and figure 2.12 illustrate the details for both the main and side tower saddles. It can be noted that both saddles feature spacers. These were incorporated into the design to assist the spinning process and ensure the hexagon shape was maintained.

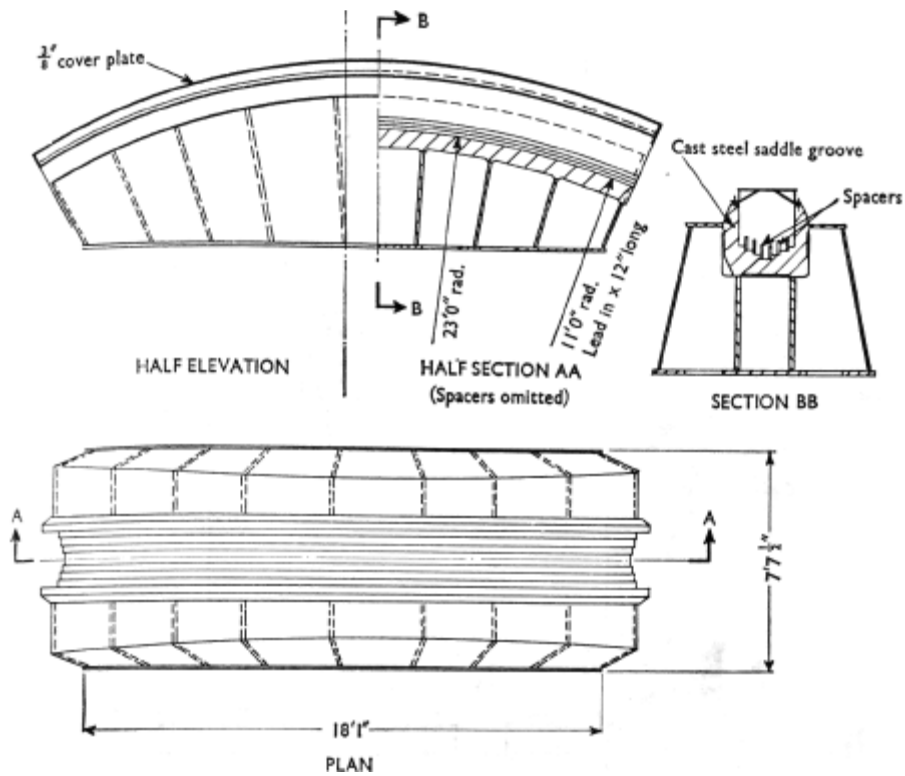


Figure 2.11: Main tower saddle details (ICE, 1967)

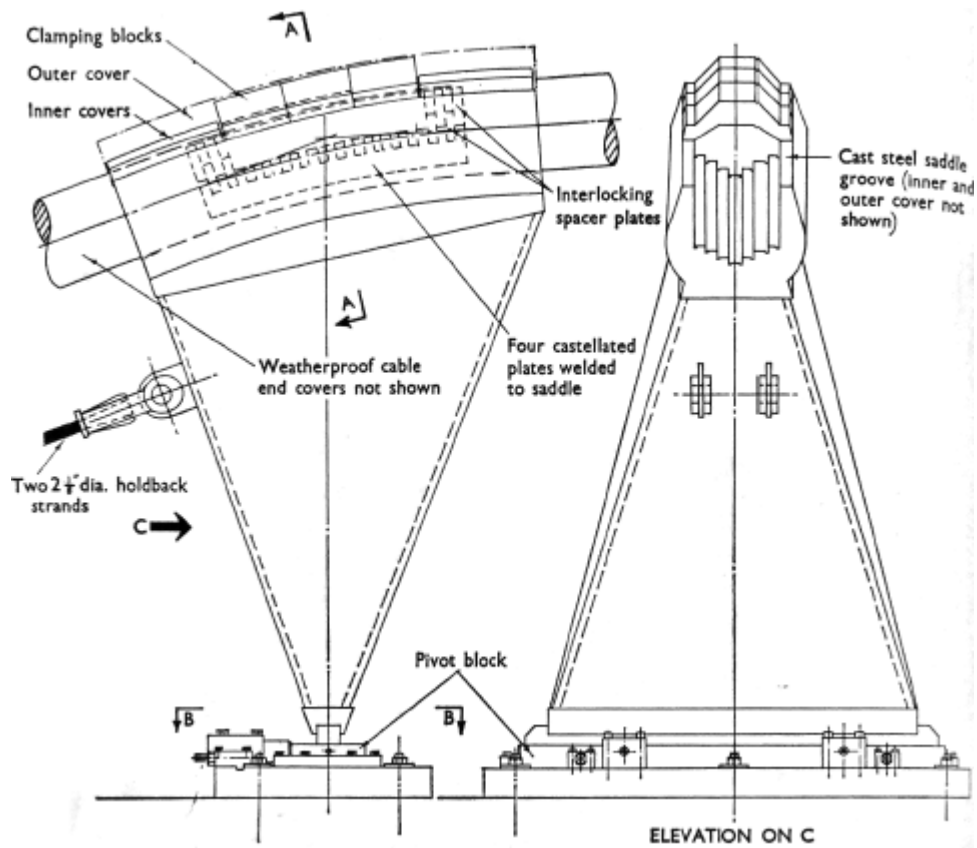


Figure 2.12: Side tower saddles (ICE, 1967)

Main cables support also the hanger ropes which are connected to the cable trough high tensile steel cable bands. The hanger rope varies dependent on its location. At the main span the rope has a diameter of 44.5 millimetres. By comparison the diameter at the side span is 54 millimetres (ICE, 1967). The difference in diameter results in varied breaking loads: 218 and 300 tons respectively (ICE, 1967).

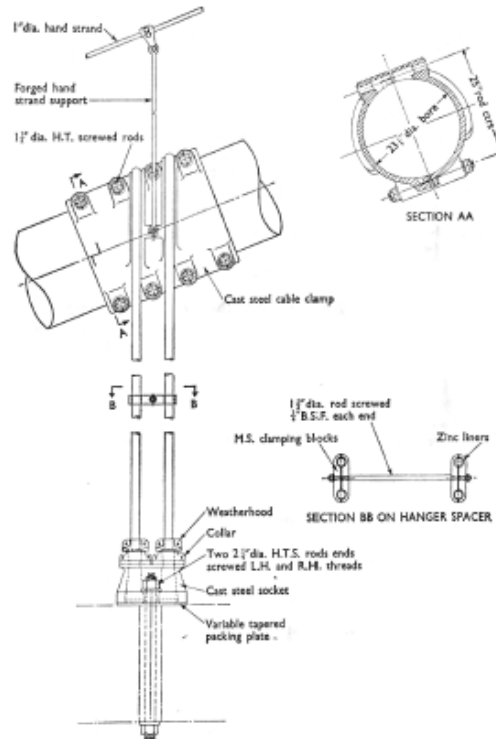


Figure 2.13: Cable band and hanger assembly (ICE, 1967)

The connexion to the top chord of the stiffening truss is realized with a common socket that takes the two rope ends and a pair of high tensile bolts. Where the rope enters the socket, which is the point most vulnerable to corrosion, a split cap and rubber gasket where fitted to exclude moisture. Figure 2.13 shows cable band and hanger assembly.

### 2.2.6 Anchorages

To anchor the cables, it was decided to take advantage of the natural rock configuration on either side and drive tunnels at a slope of 30° to the ground level. The lengths of the tunnels vary at both the North and South Queensferry locations: 56 and 79 metres respectively (ICE, 1967). Figure 2.14 highlights the detailed design of the South main cable anchorage tunnel.

There is one tunnel for each cable, filled with a mass of concrete and a overburden sufficient to resist the tendency of the cable to pull it up the slope against the friction on its base, friction that provides an additional factor of safety. The concrete block dimensions were 7.6 metres square and 52 metres long. The concrete is said to be tapered along its length to ensure a wedged connection with the foundation rock (ICE, 1967).

This arrangement required a prop at the end of the side span to take the vertical reaction from the deflection of the cable at this point as well as the vertical and horizontal reactions of the side span structure.

The slope of the cable between the side tower and the splay saddle does not exceed the slope of at the main tower so that no increase in the cable stress is involved.

The load from the cable is transferred to the concrete block via anchorage strands, connected to 19 crosshead steel slabs 203 millimetres thick (ICE, 1967). This was achieved by pairing the main cable strands to 6 anchorage strands per slab, which ensured the load (375 tons per main cable strand) was distributed equally (ICE, 1967). Figure 2.14 illustrates the detailed design for the FRB main cable anchorages.

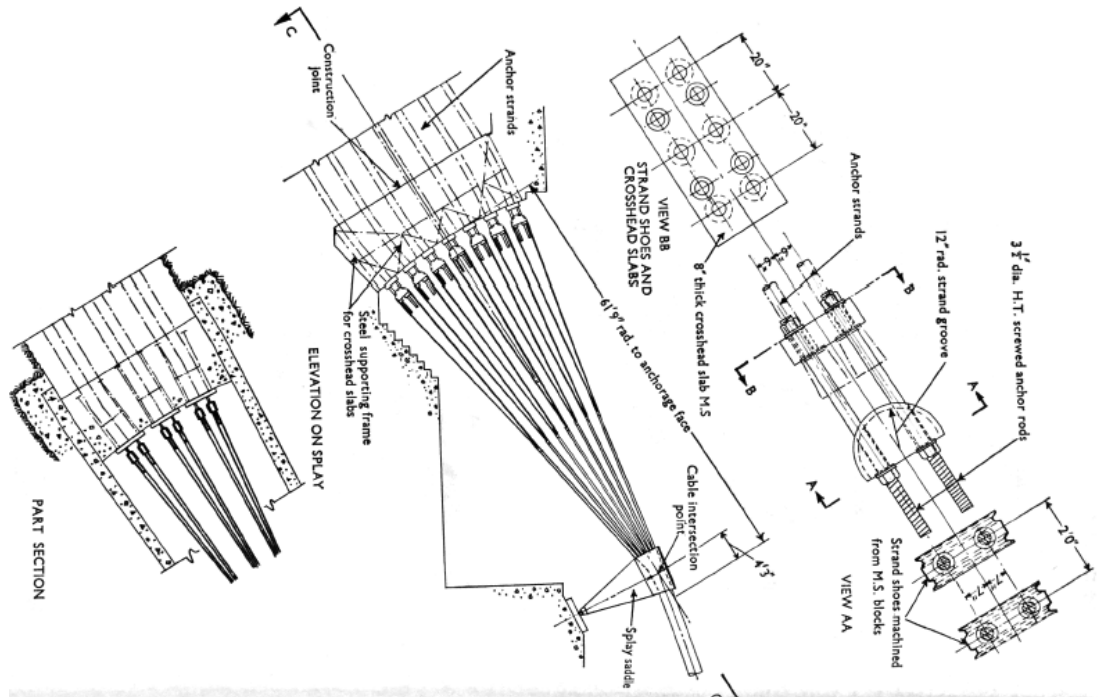


Figure 2.14: FRB main cable anchorage detailed design (ICE, 1967)

In order to provide access to the stressing chambers at the back of the anchor blocks, a vertical shaft with side adits was sunk. After the excavation the creation of the tunnel roof took place. The lining was made of steel plates curved in rings. The voids between the rock and the lining were then filled with fine aggregate by low pressure grouting.

When the ducting for the cables was finished concrete fill started from the surface. Threading of the cables in to the ducts was carried out from the top. The four strands in each cable were stressed simultaneously by four separate jacks. After all stressing works had been finished, the strands were grouted.

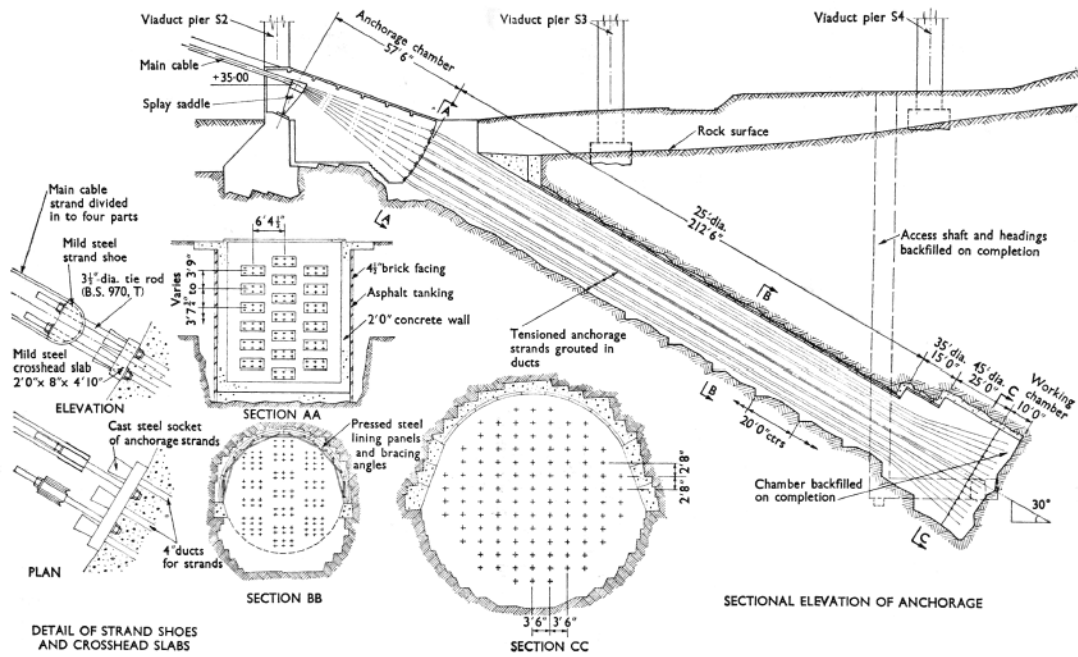


Figure 2.15: General sections of south anchorage tunnel (ICE, 1967)

### 2.2.7 Suspended structure

The design of the stiffening truss configuration took a lot of time and different proposals were taken into account. It was decided that an open rectangular framework would have been the best option to solve stability problems due to aerodynamic effects. The final arrangement consists of: cantilever footway/cycle tracks, with decks raised above the truss, as evident in Figure 2.16 (d), to introduce a plane of lateral bracing between the top chords to improve stiffness and torsional resistance.

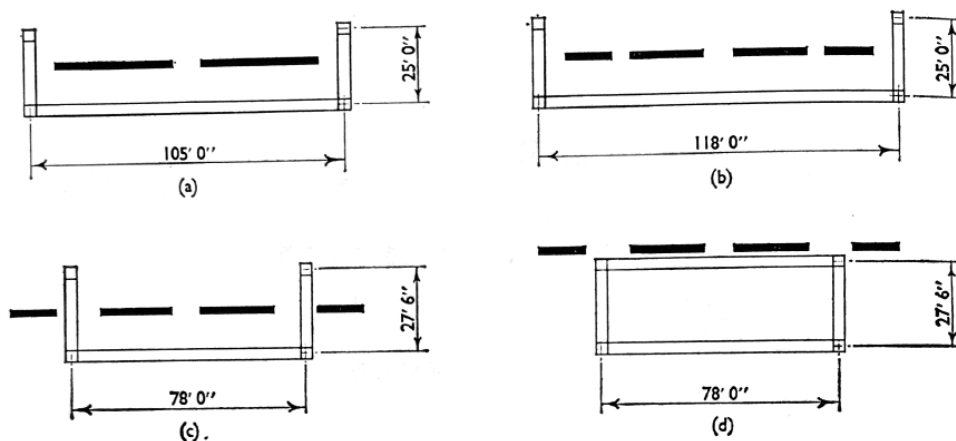


Figure 2.16: Evolution of stiffening truss and deck configuration (ICE, 1967)

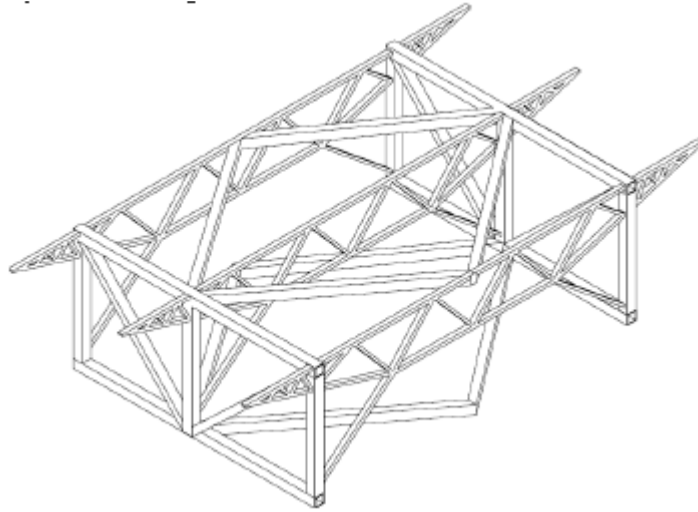


Figure 2.17: Deck truss arrangement

The trusses are 24 metres wide and 8.4 metres deep. The main span has an orthotropic deck made up of a 12.7 mm stiffened steel plate overlaid with 38mm thick mastic asphalt, on a waterproofing layer. The side span decks are 203mm thick reinforced concrete slab with a similar surfacing to the main span. The decks on both the main and side spans are supported on steel stringer beams that span between large steel cross girders spaced at 9.144 metre centres. These cross girders are supported by two longitudinal stiffening trusses, which are in turn attached to the main cables by rope hangers. Deck's panels are 18.29 metres long with expansion joint that were offset from the cross girders to obtain the continuity of the panel over the support.

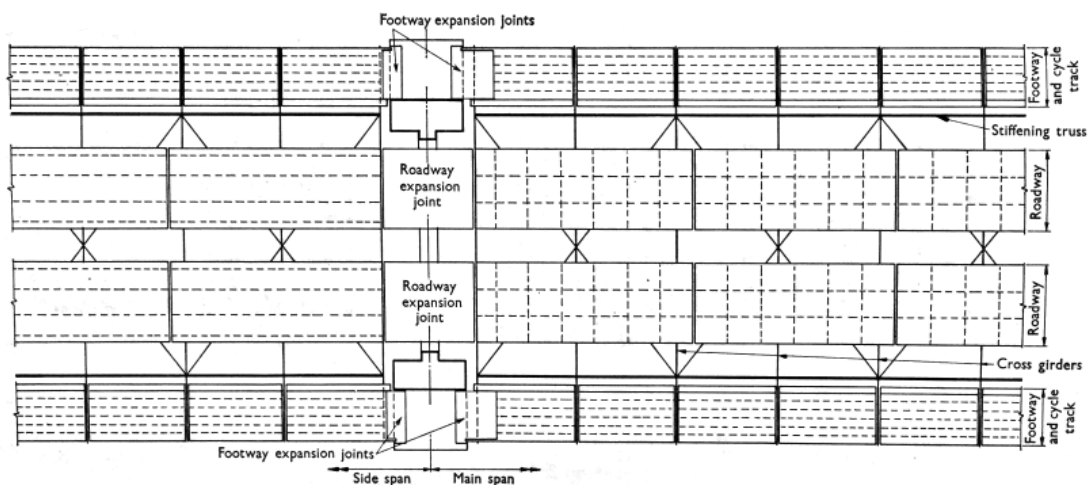


Figure 2.18: FRB deck arrangement (ICE, 1967)

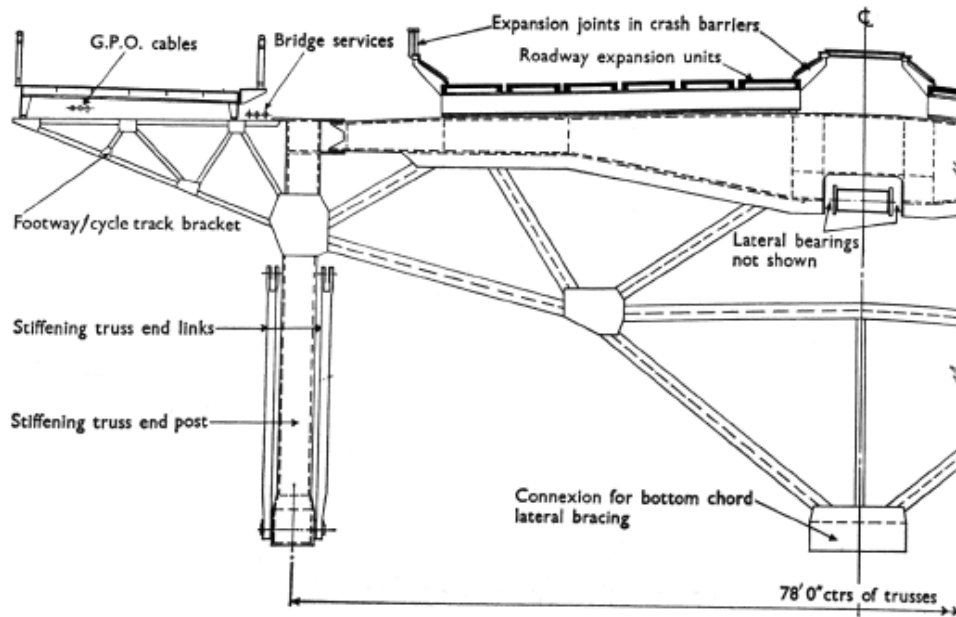


Figure 2.19: Cross girder of main span at main tower (ICE, 1967)

Figure 2.19 and Figure 2.20 highlight both the elevation and top chord bracing for the truss configuration. The (ICE, 1967) state that the truss has been designed to resist: torsional, vertical and horizontal bending. This is to accommodate: the vertical traffic loading, the horizontal loads attributed by the wind and the torsional loading attributed by aerodynamic effects, hence the open design of the cross girders.

Similar to the main tower, the truss members are made from high tensile steel in correspondence to the British Standard (BS) 968, this was to ensure that the specified welding procedure would not affect the base material properties (ICE, 1967). The vertical restraint to the truss at the main towers is provided by pendulum links, also attached to the side faces of the towers. These links are designed to carry both tension and compression forces (Rehfisch, 2016).

The links connecting the main towers to the ends of the stiffening trusses are formed from mild steel H sections. The link members are connected to the bottom chord of the truss and to a pair of cantilevered support brackets from the main towers. These connections are formed with pins made from high tensile steel (Forth Estuary Transport Authority, 2008). Details of the links are shown in Figure 2.22.

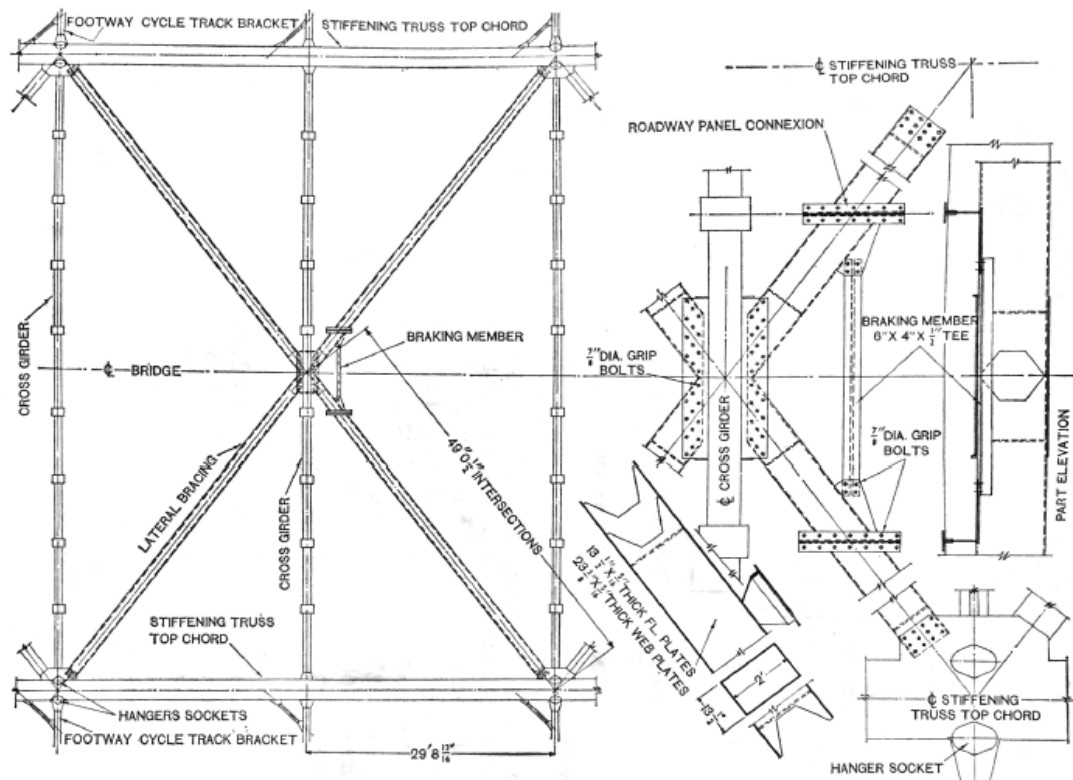


Figure 2.20: Top chord lateral bracing (ICE, 1967)

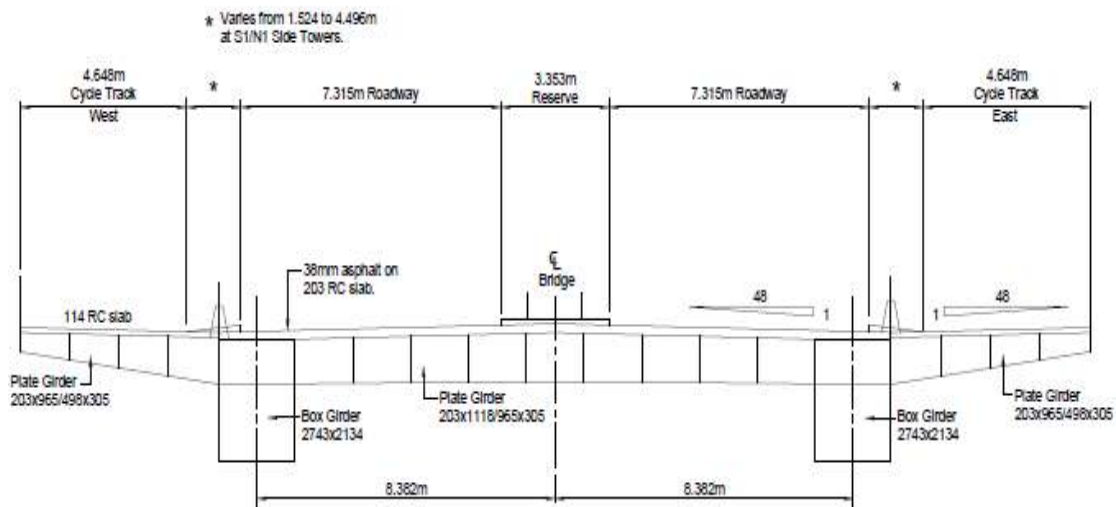


Figure 2.21: Typical viaduct section (facing North) (Jack, 2003)

Figure 2.22 highlights the end truss link and detailed design. The end link of the FRB provides the load path for the vertical loading, caused by the movement of vehicles and weather effects (temperature and wind), as well as, the dead load of the deck, and transfers this to the bridge tower via a bracket (Arndt M., 2017). In addition, the end link allows the deck to accommodate for longitudinal movement of up to 800 millimetres (Arndt M., 2017)

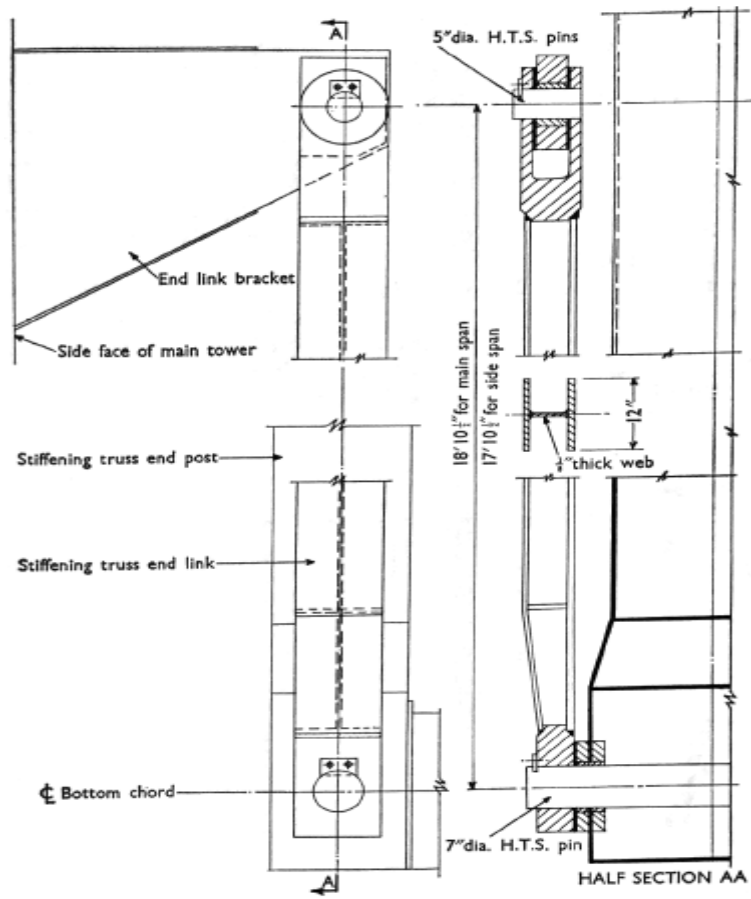


Figure 2.22: Stiffening truss end link (ICE, 1967)

### 3.0 Case study maintenance and repair work

The condition of the Forth Road Bridge has deteriorated over time, with the changes in traffic and the effects of climate accepted as the primary factors in this deterioration. Over its lifetime, the Forth Road Bridge has been subject to a continued increase in traffic volume and traffic intensity, the volume of traffic having increased from 4 million in 1964 to a level of more than 24 million vehicles per year. Heavy Goods Vehicle traffic has increased proportionally to the total volume of traffic being carried. Therefore, inspections and maintenance are a constant requirement in the operations of the bridge. Existing traffic conditions are summarised in figure 3.1 (Transport of Scotland, 2009).

Year	Vehicular Loading	Traffic Volume
1964	22t (BS-153)	<ul style="list-style-type: none"> <li>➤ 4 million veh/year at opening</li> <li>➤ Move from rigids to artics in 1960s</li> <li>➤ Max design traffic 30,000 vpd (10 million veh/year)</li> <li>➤ Currently 70,000 vpd (24 million veh/year)</li> <li>➤ 9% HGV – 6,300+ vpd</li> </ul>
Late 1960's	28t 4 axle rigid	
1964	32t articulated	
1983	38t articulated	
1999	40t articulated	
2001	44t articulated	
2016	150t Abnormal Load restriction	

Figure 3.1: Changes in traffic volume and loadings (Angus E. , 2017)

Beside traffic also the climate change plays a role in the bridge deterioration. The Forth Road Bridge is situated at relatively northern latitude and subjected to strong winds from the west. Furthermore, high humidity coupled with the cold water of the Firth of Forth leads to regular occurrences of fog during the spring and summer months. These effects and the presence of salt water contribute to the highly corrosive conditions experienced (Transport of Scotland, 2009).

Thus, during the life of a bridge maintenance works are strongly required to strength or replace some components that do not have the same design life as the bridge. The following chapter focuses on the reported maintenance, repair work and feasibility studies, available from literature, for the FRB, and in particular on the truss end links repair.

### 3.1 Truss end links repair

On the 1<sup>st</sup> of December 2015 a fracture was discovered at the truss end link at the north east main span during a routine inspection. On the 3<sup>rd</sup> of December the bridge was closed to all traffic. The closure of the forth bridge was an event of national significance, since it caused an economic impact of around 1£ million per day.

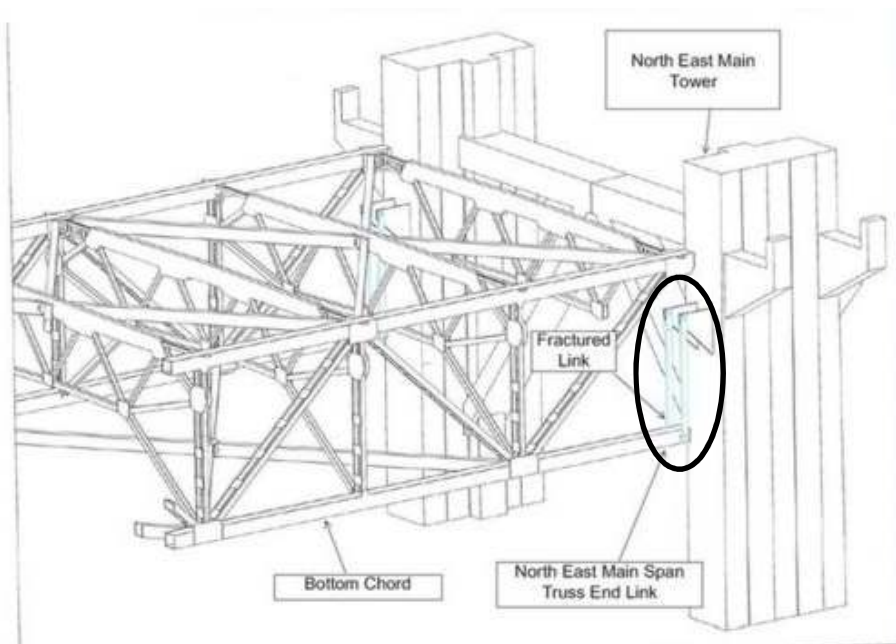


Figure 3.2: Location of the defective steel component (BBC, 2015)

After the fracture was found Mark Arndt, Operating Company Representative, Forth Bridges unit at Amey (contractor of the FRB project), explained in a conference what's happened to the bridge through a model. The model, showed in Fig 3.3, is made up of part of the main cables, North tower and the bridge deck. The deck is suspended on hangers but at the very end of the bridge near the tower there are not hangers. At this point the bridge is supported by the truss end links. These members are pinned at the top and at the bottom. The failure mechanism that has occurred in December 2015 was that the bottom pin of the inner link has seized up preventing link movement and causing the fracture of the truss end link. The vertical load that this member carried was subsequently transferred to the other element of the structure. The failure of both members could drop the bridge deck by up to 150 mm vertically; thus resulting in severe structural damage or even risk of injury to road users.

The project to repair and replace the truss end links on the Forth Road Bridge was under way since the fracture occurred. In fact, on the 4<sup>th</sup> of December the new design of the truss end link commenced, and a travel plan was implemented.

The repair work carried out on the truss end link was split into three phases, shown in the figures below.



Figure 3.4: End truss link movement diagram and fracture photos (Arndt,2015)

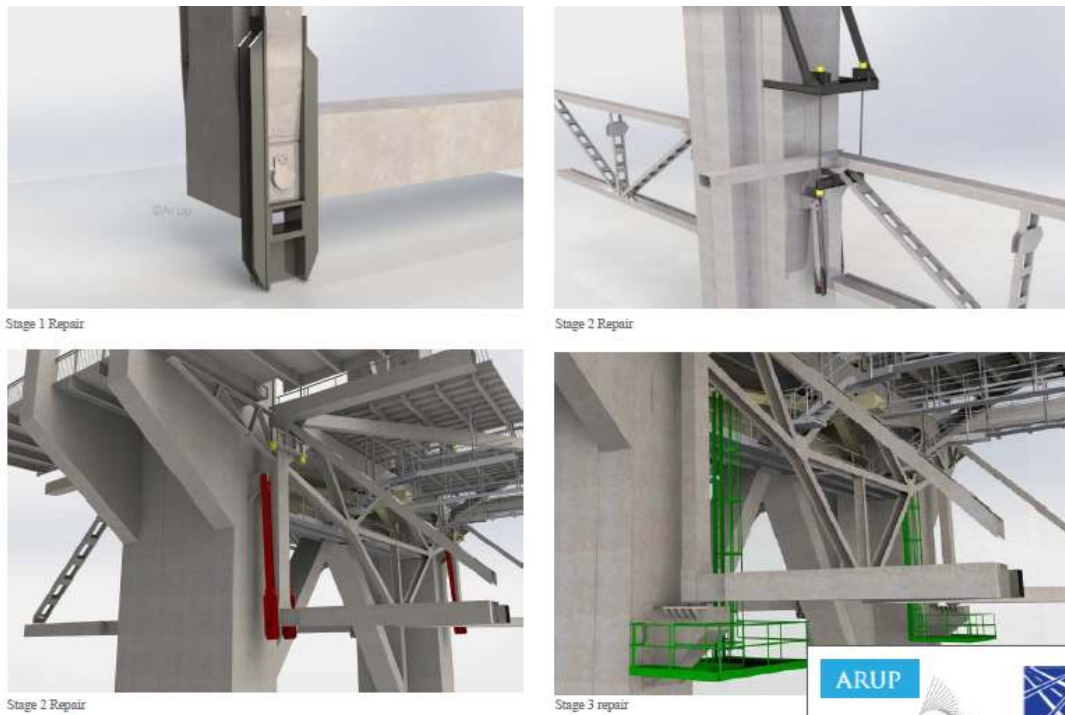


Figure 3.3: End link repair stages (Arndt M., 2017)

### 3.1.1 First phase

Phase one design was completed on the 9<sup>th</sup> of December. During the first phase stiffening bracket and jacked support were installed (Transport Scotland, 2017). This was initially carried out to the fractured end link before being installed to the other seven end links (Transport Scotland, 2017). It took only 21 days to design a solution and to construct and install the new device. (Transport Scotland, 2017).

At the same time during this phase a SHM system was commenced and installed to provide temperature, strain, stress and displacement at all eight end link positions. In addition, incremental load tests were conducted to observe real-time structural behaviour. (Transport Scotland, 2017). After twenty days following the successful completion of the load tests, the FRB was reopened to approximately 91 percent of traffic. HGVs and abnormal loads were still not allowed to cross the bridge because it was discovered that lower pin joints of the other links were partially seized, inducing high stresses (Transport Scotland, 2017). On the 23<sup>rd</sup> of December phase one was completed.

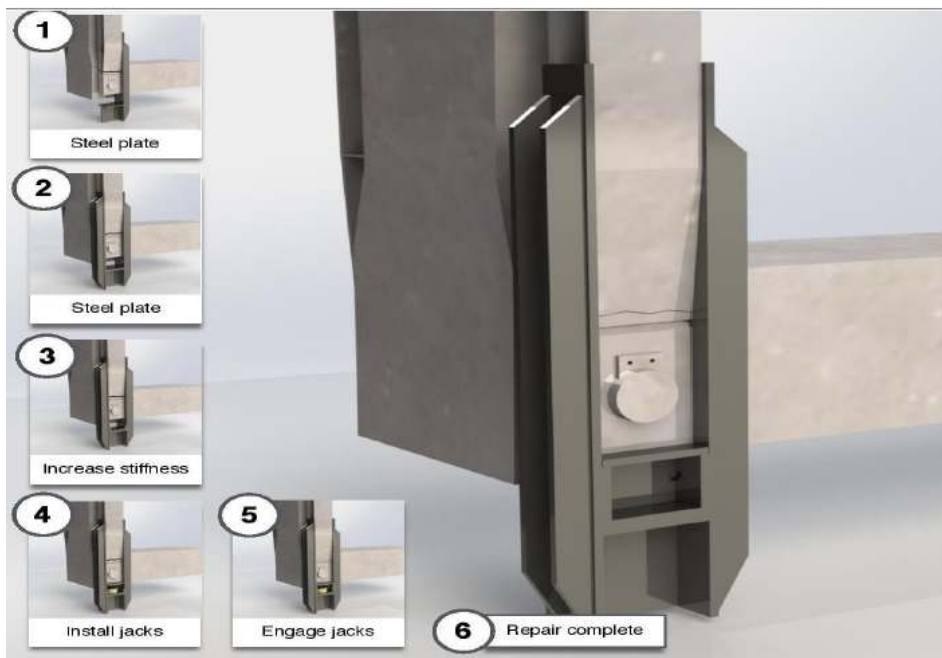


Figure 3.5: Truss end link repair: Phase one (Arndt M., 2017)

### 3.1.2 Second phase

Phase two design was completed on the 13<sup>th</sup> of January and by this time the SHM was in place at all eight links. Stage two involved constructing new steel brackets attached to the tower legs, from which the deck would be jacked and supported via steel cables. On the 20<sup>th</sup> of February 2016, phase two was completed and the bridge was fully reopened to all vehicles upon completion of load testing. The phased reintroduction of HGVs was trialled for safety during overnight load tests, with lorries merged into general traffic using a temporary ramp-metering system and the structural impact monitored in real-time using the SHM system.

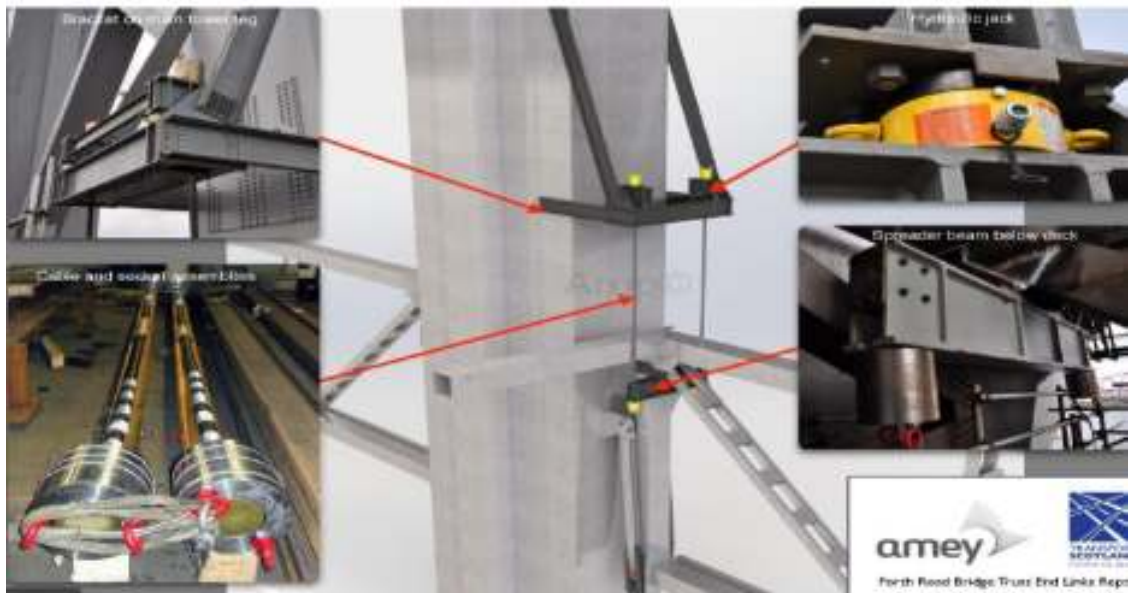


Figure 3.6: Truss end link repair: phase two (Arndt M., 2017)

### 3.1.3 Third phase

The final stage of the work programme involved installing a new sliding bearing design to replace the fractured end link (Transport Scotland, 2017). In springtime 2017, the new bearing was installed and supported on a new bracket below the bridge deck (Transport Scotland, 2017). The replacement work was carried out successfully without causing bridge closure. By springtime 2018 the remaining end links were replaced with the new design. Structural health monitoring was then incorporated to complete that installed during the initial emergency works.



*Figure 3.7: New sliding bearing (Arndt M., 2017)*

The project to repair the truss end links has demonstrated exemplar innovation and creativity in engineering, management and communication. Completed during challenging weather conditions, and under extreme scrutiny, the project successfully delivered immense social value by sustaining one of Scotland's arterial and iconic transport networks. The expertise and dedication shown enabled completion ahead of programme, alleviating prolonged economic, social and environmental impacts associated with diverting over 70,000 vehicles 33 miles each day, whilst ensuring public safety and the structural integrity of the bridge (Transport Scotland, 2017).

## 4.0 Structural Health Monitoring system

Due to the sudden fracture of the truss end link at the north main tower, a State-of-the-art structural monitoring system were promptly installed on all eight truss end links to provide as much data as possible about the behaviour of the bridge, such as how much strain is being put on it, and the effects of changing climatic and traffic conditions. In this section we will focus primarily on the system utilised on the end truss link and afterwards on the other sensors installed later. As a result, this will form the basis to understand the process of data analysis.

To look after and keep track of more than 30,000 critical elements on the Forth Road Bridge a large group of assets are necessary. The solution founded by Amey involves the use of an integrated technology system to ensure safety and efficiency on the Forth Road Bridge. With reference to (Angus E. , 2018), the basic components of a SHM system comprise of the following: bridge sensors, data storage and processing, web browser and report generation. The bridge sensors are responsible for recording the applied traffic loads, the weather effects (wind and temperature) and the bridge response (displacement, strain and position). With regard to the data storage and analysis, this requires inputs in terms of the bridge structural capacities and components before the sensor data can be processed and trigger alarms set (Angus E. , 2018). At the end reports are automatically generated by the web browser in which traffic loading, movements and component stress are written (Angus E. , 2018).

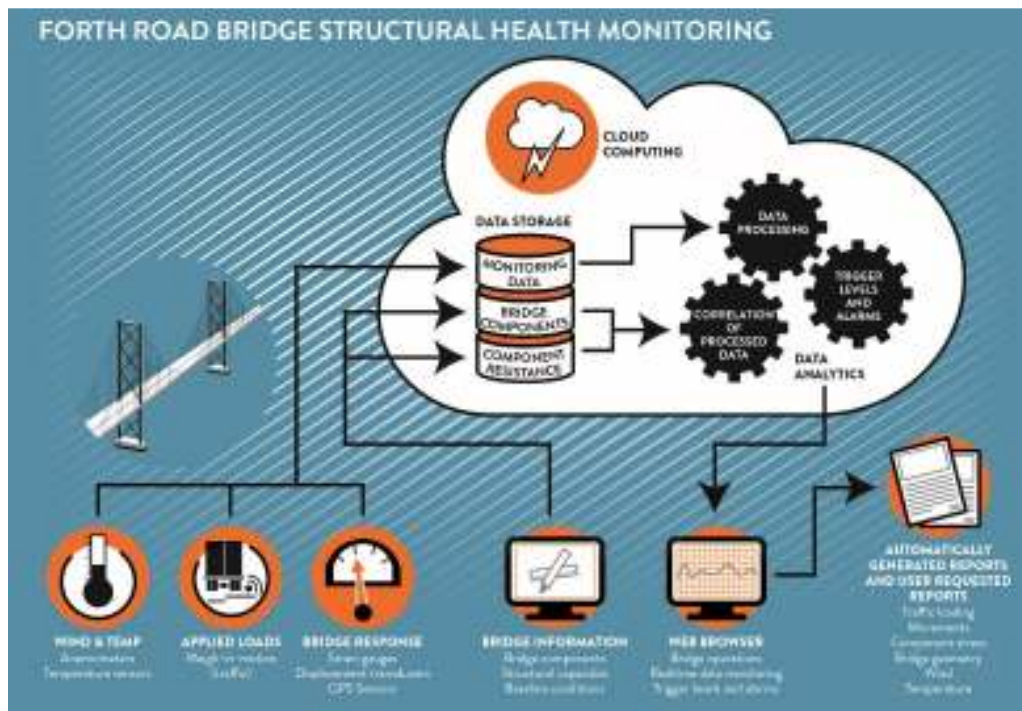


Figure 4.1: FRB structural health monitoring (Kitching, 2017)

#### 4.1 Integrated systems on FRB

To implement the SHM a bespoke integrated system has been created by Amey. The advance digital system is made of two software: “Mercury”, data analytics platform, and “Pearl” information and condition database (Angus E. M., 2018).

*Mercury* is the main system which contains remote sensor and maintenance record data. It uses machine learning algorithms to understand bridge behavior and actively monitors and reports on sensor and condition data. Moreover, the platform interprets data to provide rich custom visualizations of bridge behavior, intelligent alerts and lifecycle records. Intelligent alarms are specified (or even “learnt” from the data) to send SMS and email alerts, or notifications to other systems. Other data sources, such as analysis and modeling outputs can be included to provide a rich, integrated picture of the bridge (Angus E. M., 2018).

*Pearl* is a cloud storage of all records and data relating to each of 30,000 elements. This system allows managing the inspection programmes. Moreover, it records type and severity of all identified element defects. It generates automatic inspection report including online approvals. In addition, the database enables automatic update of bridge condition indices from inspection findings. Finally, in the storage there is a

document management module for storage of archive files and project records and a full description of the structure and key components, including maintenance project history (Angus E. M., 2018).

## 4.2 Sensors arrangement

Straininstall was appointed by Amey on behalf of Transport Scotland to install a structural health monitoring system on the Forth Road Bridge to monitor the failed inner truss end link and the cracked outer truss end link. The company provided and installed rapidly the sensors in response to sudden transport infrastructure closure in December 2015. A team of specialist engineers worked rapidly to provide specialist expertise and deploy the innovative structural health monitoring system. By quickly installing a few sensors, including strain, temperature and tilt, the system delivered crucial monitoring and engineering information to allow the reopening of the bridge in a short time (J. Fisher and Sons plc, 2015).

The work was carried out in two phases, Phase 1 once the above mentioned truss end links was been repaired but prior to opening the bridge to traffic and followed by Phase 2 installing monitoring on all the other end links on the bridge (Straininstall, 2016).

The system provided real-time information on the effects of wind and traffic loading on the integrity of the structure. These data, provided to the bridge's control room, supported the decision to open the bridge almost two weeks earlier than officials had originally stated (J. Fisher and Sons plc, 2015).

During the process of replacement of the links, 150 strain gauges and displacement sensors together with four data acquisition units (DAU) were installed first on the bridge (Angus E. , 2017). **Errore. L'origine riferimento non è stata trovata.**1 illustrates the first sensor arrangement utilised for the initial truss end link repair. This system was utilised to monitor the strains and displacements once the bridge was reopened to vehicles (excluding HGVs).

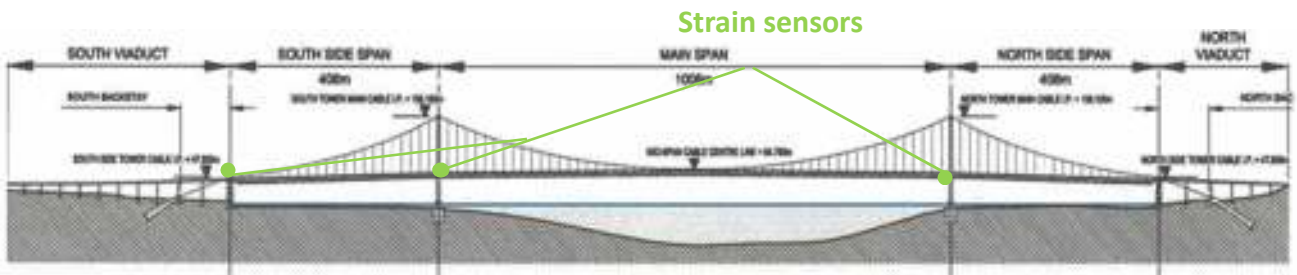


Figure 4.2: Sensors location (Angus,2017)

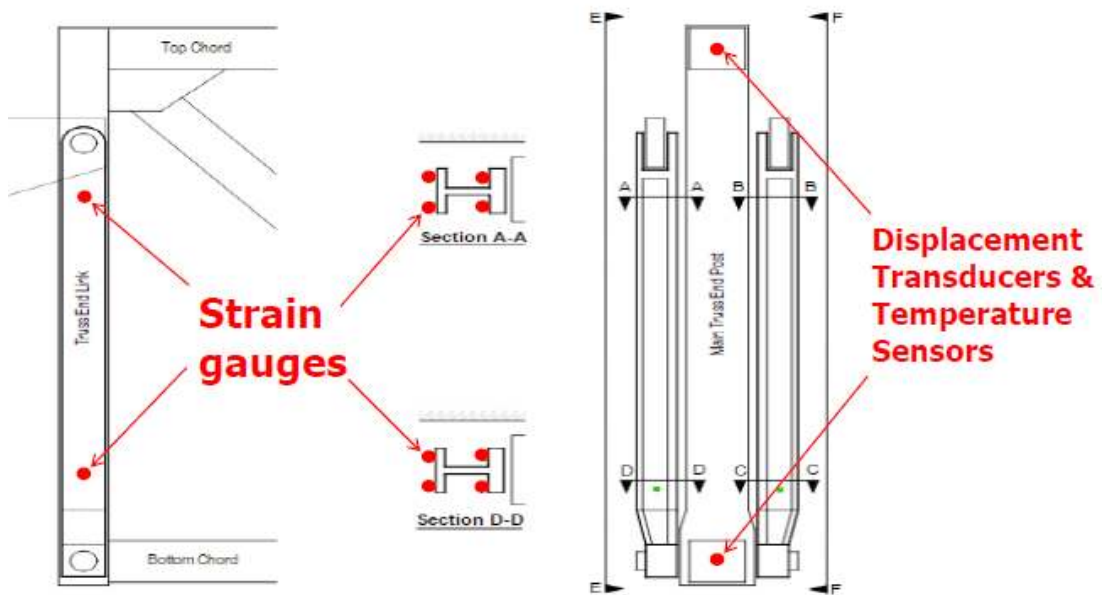


Figure 4.3: FRB truss end link original SHM system arrangement (Angus, 2018)

Besides the original sensors, that continued to provide monitoring data, then additional sensors were installed during a second phase to monitor other critical points of the bridge (Kitching, 2017).

Figure 4.4 and Figure 4.5 highlight the updated SHM system utilised when the temporary end link repair work was replaced with the current sliding bearing design. It should be noted that the bearing types differ for the truss end links at the side towers from the main towers, with the side towers utilising a rocker bearing configuration. It should be noted that in Figure 4.4 a change in the load acting on the bearing sensor indicates a potential failure in the end truss link.

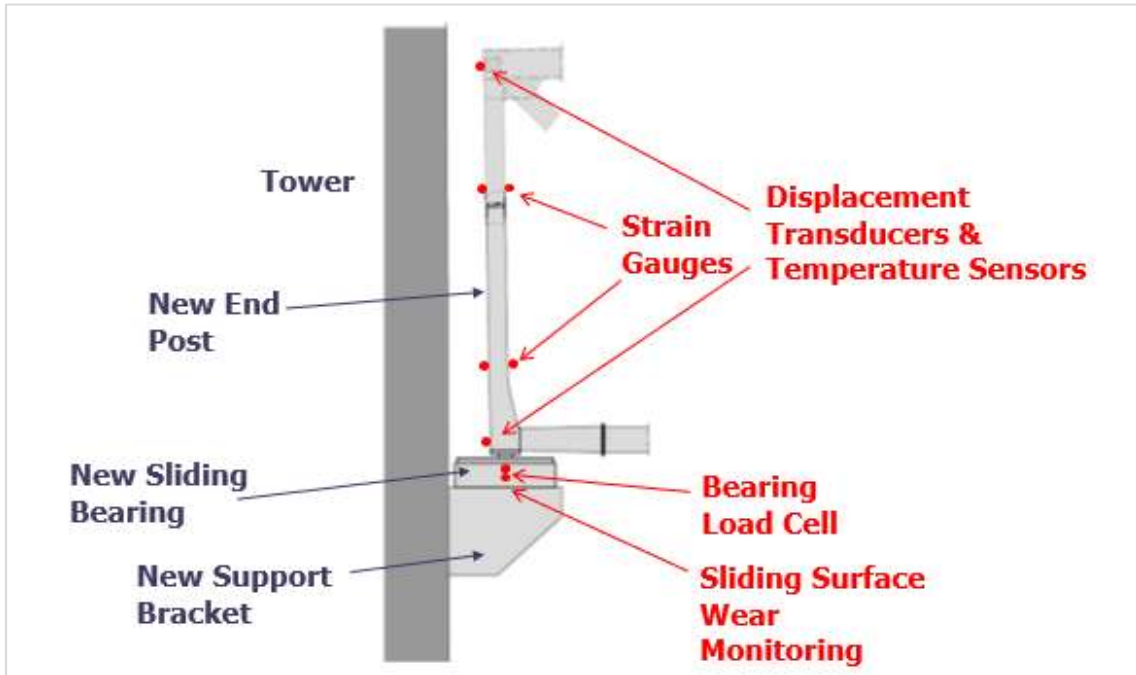


Figure 4.4: FRB new SHM system arrangement: main towers (Angus, 2018)

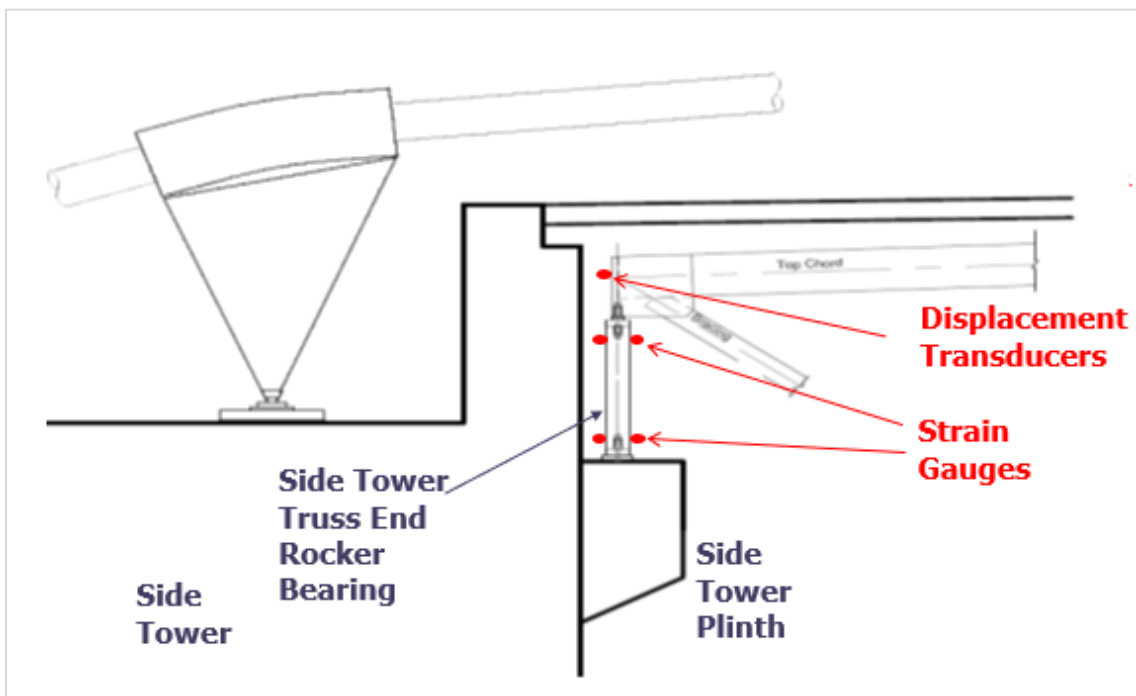


Figure 4.5: FRB new SHM system arrangement: side towers (Angus, 2018)

### 4.3 Sensor technology

The number of sensors used in monitoring is endless. Different applications with various techniques, like electrical, optical, acoustical, etc. are available. A variety of parameters like strain, displacement, inclination, stress, pressure, humidity, temperature, different chemical quantities and environmental parameters such as wind speed and direction can be monitored.

Currently the SHM system on the Forth Road Bridge consists of a network of DAU's distributed over the bridge structure. The SHM main system is made up of (Data Software) DS-DAU's, connected by a fibre-optic network to one server, which is located at the bridge office (Strainstall, 2016).

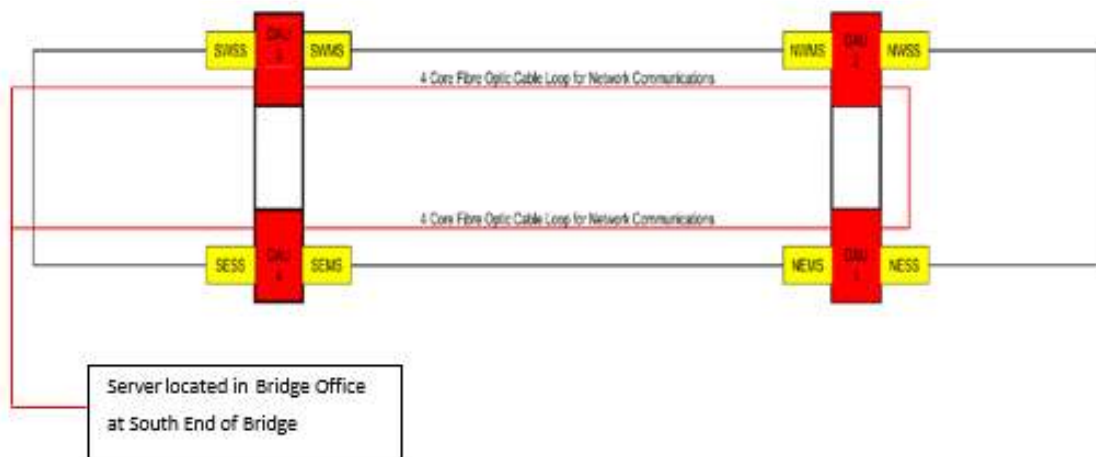


Figure 4.6: System overview (Strainstall, 2016)

Structural health monitoring of the bridge now incorporates 476 sensors, as we can see from *Table 1* (Kitching, 2017). From this table it is clear that providing the reader with the location of all these sensors and their functions would be time consuming and superfluous. Therefore, the author will provide the reader with a description of the characteristics of a selection of the sensors provided in this list and drawings showing some of their locations on the structure. The author will provide the reader with a more detailed description of the sensors from which the data for this thesis was obtained.

<b>SHM SENSOR TYPE</b>	<b>NUMBER OF SENSORS</b>
<i>Air Temperature sensors</i>	2
<i>Anemometer</i>	2
<i>Asphalt Temperature Sensors</i>	6
<i>Barometers</i>	1
<i>Bearing Gauges</i>	8
<i>Bearing Pressure Sensors</i>	8
<i>Displacement Transducers</i>	48
<i>Dynamic Weigh-in-Motion Sensors (DWIMS)</i>	64
<i>GPS Location</i>	10
<i>Rainfall Gauges</i>	1
<i>Relative Humidity Sensors</i>	34
<i>Strain Gauges</i>	128
<i>Steel Surface Temperature Sensors</i>	32
<i>Main Suspension Cable Acoustic Monitoring</i>	116
<i>Tiltmeters</i>	16

*Table 1: SHM sensor types and quantities (Kitching, 2017)*

#### 4.3.1 Strain gauges

The type of strain gauges used is a weldable linear strain gauge, which measures strain on the surface of the steel structure in one direction.

The gauge is made of polyimide and with an encapsulated constantan foil grid, with large, rugged, copper-coated tabs. It consists of two end blocks with a tensioned steel wire between them. The end blocks are attached to stainless steel tabs which are attached to the surface of the bridge structure by a micro-spot-welding technique.

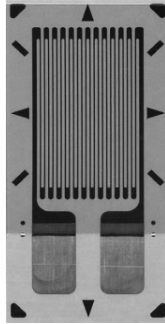


*Figure 4.7: Weldable strain gauge (Vishay Precision Group, 2016)*

This type of strain sensors was used during monitoring of the truss end links as well as nowadays with the new sliding bearing.

The strain gauges are located at the North Tower, North West and South West truss members. The original arrangement installed at the towers can be seen in figure 4.3, while the actual configuration is displayed in figure 4.4. Further on North East main tower strain data will be analysed in detail.



*Figure 4.8: Strain gauge at the NEMS bottom chord*

#### 4.3.2 Displacement transducers

These sensors are used to measure displacements of key structural elements due to live loads and temperature variations. There are 48 deployed on the bridge. The displacement transducer sensors are located at the North Tower main span truss members. Displacement sensors on the truss end link initially measured how much

links were moving in the longitudinal direction in order to take under control the suspended structure total displacement.

The 48 displacement transducers are now clustered in four deployments in four key sections of the bridge structure, in terms of movement. There are deployments at both main towers and at the side towers.

The deployments in the main towers are at the bottom of the end post next to the sliding bearings and at the top. The deployment in one of this section at the North Tower is shown in Figure 4.7. These areas have been selected as the design of the structure dictates that movement will be allowed at these locations. These movements should however be closely monitored to ensure there are within expected ranges and there is no unexpected structural behaviour, which may indicate damage.



*Figure 4.9: Displacement transducer at the bottom of the end post at NEMS*

### 4.3.3 Tiltmeter

Tiltmeter measures uniaxial or biaxial tilt, which is measured from the plane perpendicular to the base and bending of structural elements. The tilt sensors, based on Microelectromechanical Systems (MEMS) technology, are mounted within a rugged, heavy-duty waterproof die-cast metal enclosure suitable for the harsh environments. The integrated filter improves performance and allows using the sensor

in many noisy environments. Thermal effects of the MEMS sensor are minimal but in order to compensate for the effects of temperature on the enclosure, mountings and structure, the unit is fitted with an integral thermistor. The tilt meter sensors are located at both North and South main span truss members.



*Figure 4.10: Tiltmeter on truss end link NEMS (Kitching, 2017)*

#### 4.3.4 GPS

GPS technology has been employed to monitor civil engineering infrastructures, including bridges for more than 20 years. GNSS technology provides continuous and automated measurements and helps understanding the static profiles and dynamic behaviour of monitored structures. It is very useful specially to monitor deformation of bridges (X. Meng, 2018).

Figure 4.11 describes the status (update July 2018) of GPS sensor system installed on the FRB. Three pairs of Leica GNSS receivers are installed along the main span; one is at the mid span while the other two are at the navigation points. There are two other Leica GNSS receivers located at the top of the North-East and South-West tower legs to monitor deformation of the main tower ( Nguyen, et al., 2018). At the top of each tower there are also tri-axial accelerometers which provide additional data to identify modal frequencies and vibrational mode shapes of the FRB (X. Meng, 2018).

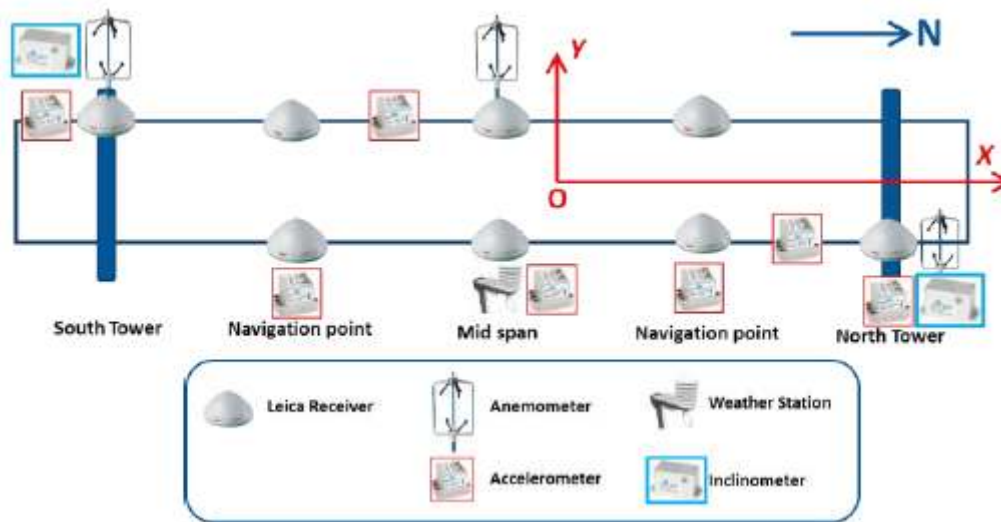


Figure 4.11: Locations of GNSS receivers ( Nguyen, et al., 2018)

#### 4.3.5 Temperature sensors

Ideally, we would prefer the strain gage to change resistance only in response to stress-induced strain in the sensor, but the resistivity and strain sensitivity vary also with temperature. For this reason, we need temperature sensors on the bridge together with strain gauges, in this way we can compare the strain results with the temperature at that moment and do a correct assessment. In this case study we have three types of temperature sensors: the strain gauge temperature sensor, the internal temperature sensor and the air temperature sensor.

The strain gauge temperature sensors (PT100 TMP) are located adjacent to the strain gauges attached to the trusses. In this way all gauges are self-temperature compensated for use on stainless steel with a specific thermal expansion coefficient. The internal temperature sensor is located inside the DS-DAU to measure the internal temperature.

Other environmental conditions are determined by the meteorological station installed at the mid span.

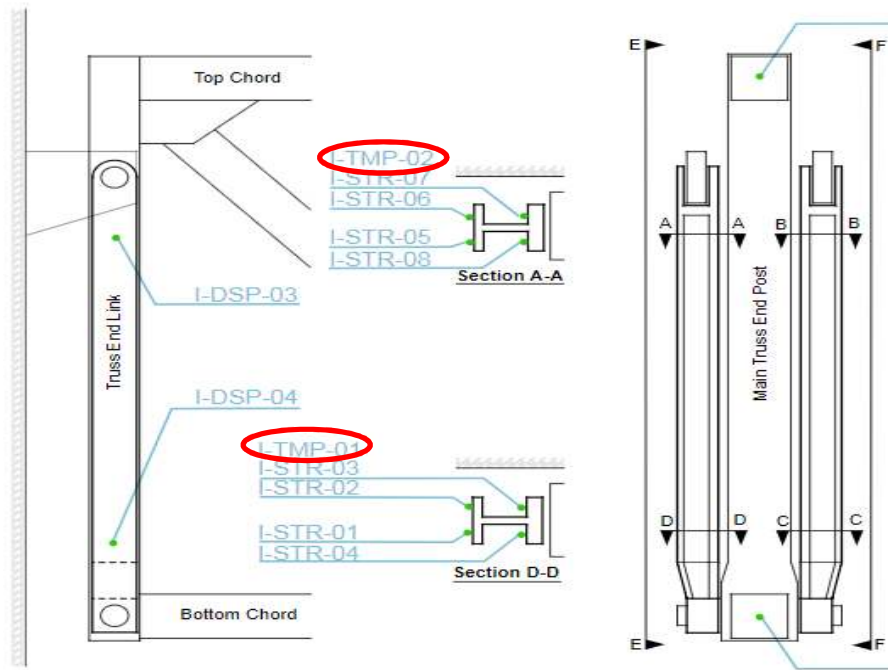


Figure 4.12: Strain gauge temperature sensor at NEMS truss (Arndt M., 2017)

#### 4.3.6 Anemometers

An anemometer is a device used for measuring wind speed and is also a common weather station instrument. On the Forth Road Bridge there are ultrasonic anemometers, which use ultrasonic sound waves to measure wind velocity. They measure wind speed based on the time of flight of sonic pulses between pairs of transducers.

Two-dimensional sonic anemometers are capable of monitoring high wind speeds and wind direction and are used in applications such as weather stations. In addition, the wind measurement is facilitated by using three-dimensional sonic anemometers, which are ideal for monitoring turbulent airflow around bridges, with data provided for wind speed, wind direction and Sonic Temperature.

Two-dimensional wind sensors on the bridge are of three ultrasounds paths type. These sensors have three arms. They give one path redundancy of the measurement which improves the sensor accuracy and reduces aerodynamic turbulence. Three Wind Master 3D sonic anemometers are placed at the mid span and at the top of the two main towers ( Nguyen, et al., 2018).



*Figure 4.12: 3D sonic anemometer at midspan*

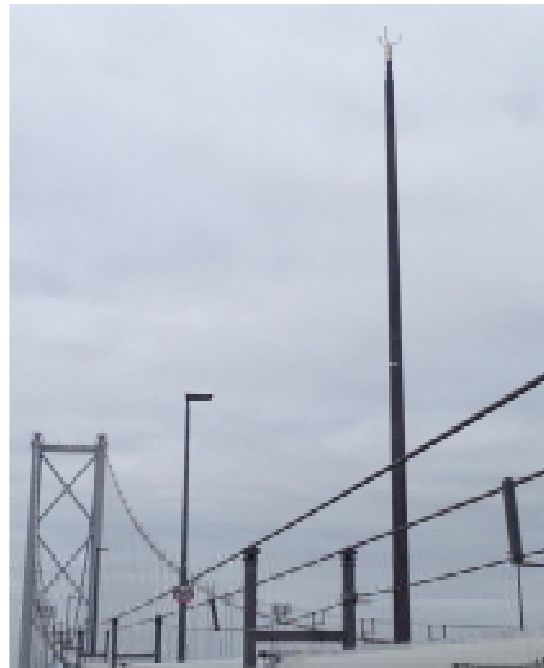


*Figure 4.13: 2d ultrasonic anemometer with 3 paths*

## 5.0 Methodology

This chapter focuses on outlining the dissertation methodology which has been used to determine if monitoring data from the SHM deployment on the Forth Road Bridge could be a valid support to understand the behaviour of the structure.

The research methodology applied throughout this thesis has been both qualitative and quantitative in nature.

The qualitative research undertaken for this thesis included a review of selected SHM literature. This provided the author with a grounding in the subject area and allowed for suitable introduction to this topic in order to let the reader familiarise with the concepts.

Following, a case study with a SHM system was selected. Detailed review of the Forth Road Bridge was carried out, focusing on the development of the design, the structural scheme, the construction phases of the project and finally the SHM deployment.

In addition, a detailed description of maintenance and repair work was carried out to understand the change in the structural behaviour of the bridge before and after this event.

This allowed the author to achieve the required level of understanding of the structural behaviour of the bridge, the construction process and the SHM deployment to discuss and describe the monitoring data and offer qualitative comments on the results of data analysis.

The quantitative process of this research involved analysing and processing data from selected sensors of the SHM system deployed on the Forth Road Bridge. All data analysis was carried out using Matlab and Excel.

After a qualitative analysis of the data, the second step was to evaluate quantitatively if the sensor data trend matches with the theoretical results.

The sensors selected to be analysed were located at the main span. Where it was possible the four main span sides were analysed and compared. Data analysis procedures used will be detailed and justified in the second section of this chapter.

## 5.1 Data acquisition

The structural health monitoring system transfers data from sensors via fibre optic cables to a cloud server where it is sorted and stored and where analytics process it into more relevant information.

The data employed for this project were transferred by selected sensors on the Forth Road Bridge via fibre optic cables to the cloud server at Amey Administration Office. The data acquisition started right after the fracture at the truss end link was found and then they were collected by Amey.

These data were then acquired by the author during a visit at Amey Administration office. This was the only method available to allow the author access to the required data because of the big amount of data and the impossibility to send them by other means.

The data received was all in Excel format, in addition to this technical drawings and functional test reports were also provided. All the selected data was recorded from sensors located at the North and South main towers and each spreadsheet contained data from one side of the span only.

The first data acquired for this thesis refer to North East main span because this was the location where the fractured link was found. Following this North West side and South side were also taken in to account to enable the author to have a general view of the truss system structural behaviour.

The data received was from dynamic strain gauges and displacement transducers, applied to the truss end links at the four corners of the main span. The same types of sensors applied to the sliding bearing were also included, due to the recent substitution of the truss end links there were less data regarding the new configuration to analyse. These data concern only the North East main span.

Starting from the data of the strain gauges at the NE main span was deemed to be best suited for analysis, to achieve the aims of the thesis. This judgment was made due to knowledge of the maintenance process.

The sampling frequency of the sensors was one per hour. For each sample from each sensor location, the temperature and the time and date of the sample was recorded. In addition, the author was provided with displacement and wind data for the same period of time.

There is a total of eight strain sensors per link located at each side of the towers, see Figure 5.1. Strain sensors 01,02,03 and 04 together with displacement transducers 02 have been analysed in this thesis.

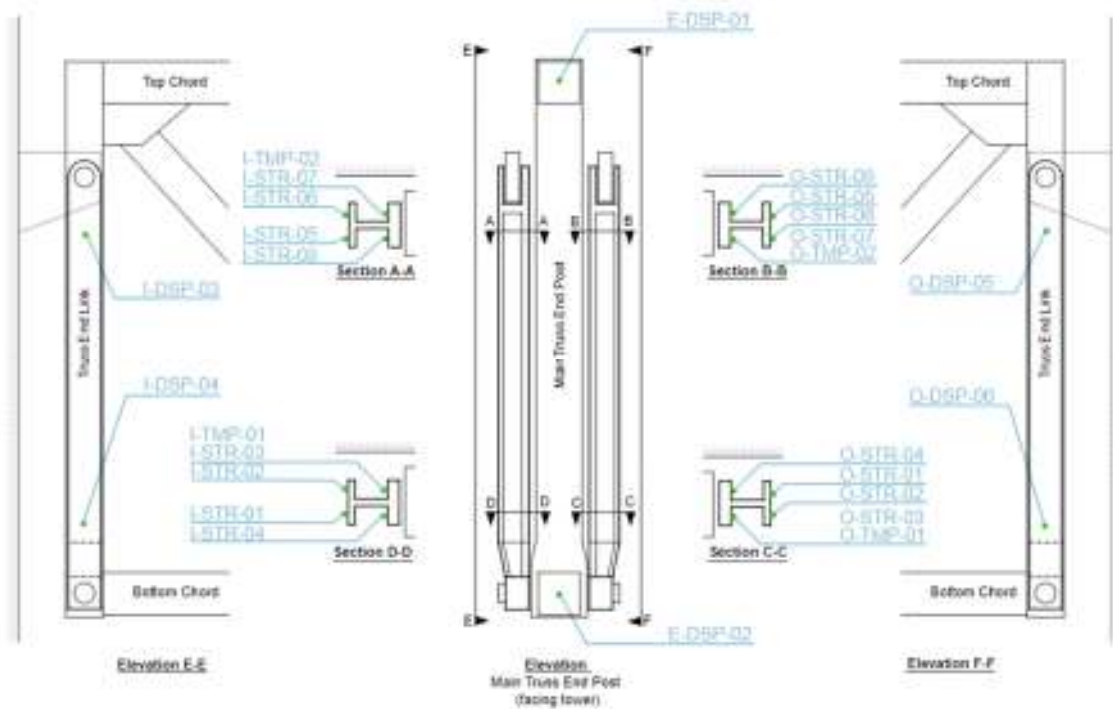


Figure 5.1: Strain gauges positions (Arndt M., 2017)

## 5.2 Data analysis

The purpose of analysis the data is to continuously monitor the bridge performance through comparisons of measured results such as bridge responses, bridge characteristics, bridge loads and environmental conditions to design values.

All data analysis has been carried out using Matlab and Excel. Matlab was selected due to the vast amount of data and the ability to create a code that would perform all the data analysis steps required.

### 5.2.1 Sensor specifications

Prior to the start of the analysis, the measuring units of the strain gauges were transformed, as they were given to the author in the form of Volts. The transformation from Volts to microstrain was done according to the functional and assembly test's report of Strainstall (Strainstall, 2016). Strain gauges calibration test results are recorded in table 2.

Sensor tag n°	Initial Reading of strain gauge channel		Amplifier shunt calibration applied $\mu\epsilon$		Amplifier shunt calibration removed $\mu\epsilon$		Resistor shunt calibration applied	
	Volt	$\mu\epsilon$	Volt	$\mu\epsilon$	Volt	$\mu\epsilon$	Volt	$\mu\epsilon$
NEMS-I-STR-01	-1.49	-564	0.497	188	-1.49	-564	1.152	436
NEMS-I-STR-02	1.691	640	3.678	1392	1.691	640	4.331	1639
NEMS-I-STR-03	1.511	572	3.498	1324	1.511	572	4.156	1573
NEMS-I-STR-04	1.403	531	3.39	1283	1.403	531	4.072	1541
NEMS-I-STR-05	3.913	1481	5.9	2223	3.913	1481	6.598	2497
NEMS-I-STR-06	1.855	702	3.842	1454	1.855	702	4.524	1712
NEMS-I-STR-07	2.463	932	4.45	1684	2.463	932	5.168	1956
NEMS-I-STR-08	2.016	763	4.003	1515	2.016	763	4.711	1783

Table 2: Strain gauges measurements calibrations

The calibration test results were then plotted to look for correlation between measuring units. From Figure 5.2 it can be seen that there is a linear relationship between V and microstrain shown in the following formula:

$$V = 384.6 \mu\epsilon \rightarrow \mu\epsilon = 0.0026 V$$

Therefore, every strain gauge measurement before being processed was multiplied by 384.6 to transform it into microstrain.

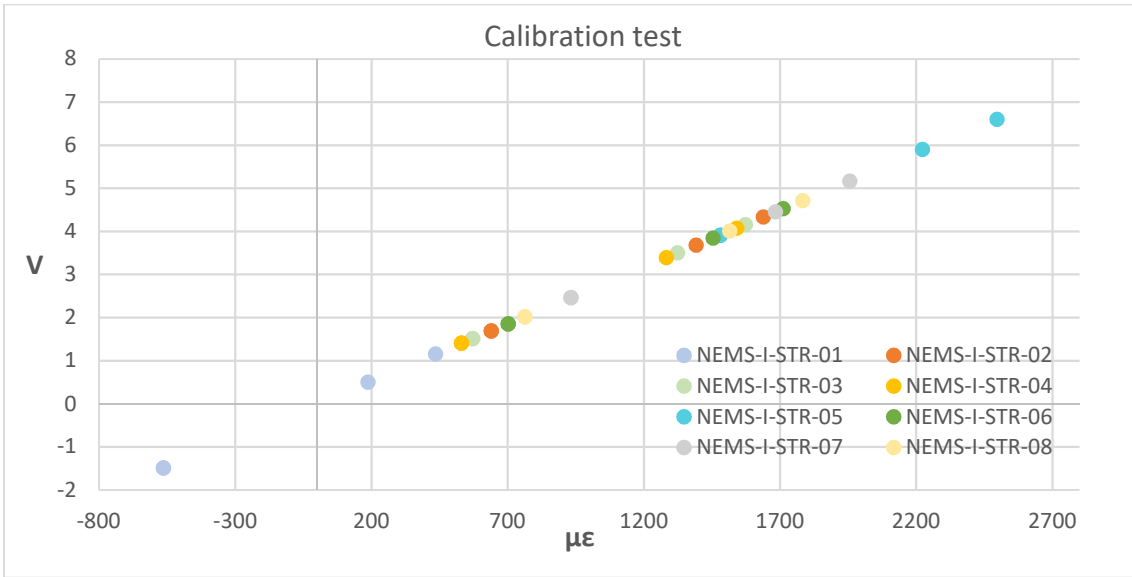


Figure 5.2: V- $\mu\epsilon$  correlation

The same operation has been done for the displacement transducers transforming Volts in mm. Unfortunately, the only data available were those regarding DSP-01 (End Post top displacement) and DSP-02 (End Post bottom displacement). However, as we can see from Table 3, the displacement transducer number two was not operational. In fact, the data concerning this sensor were proven to be not consistent.

Sensor tag n°	Istalled datum		Fully retracted		Fully extended	
	mm	V	mm	V	mm	V
NEMS-E-DSP-01	482	3.21	0.003	0.002	1500	10.001
NEMS-E-DSP-02						
NEMS-I-DSP-03	782	5.21	0.004	0.003	1500	10.001
NEMS-I-DSP-04	1013	6.75	0.005	0.006	1500	10.001

Table 3: Displacement measurements calibrations

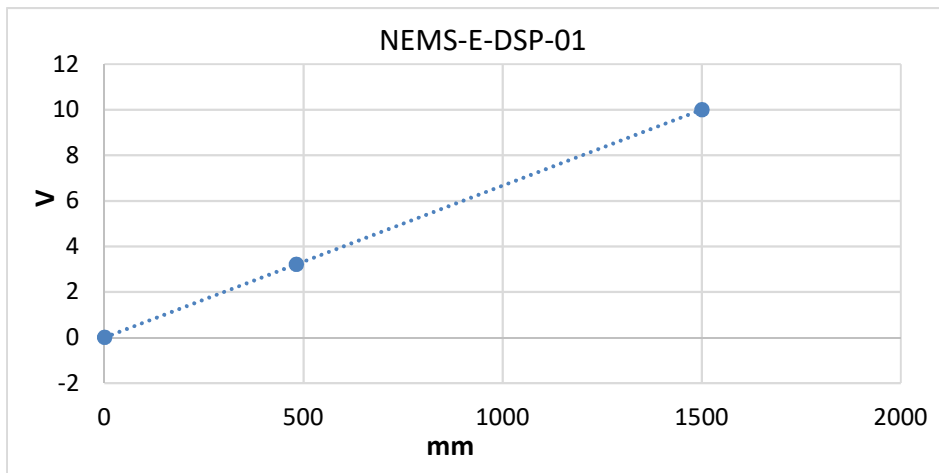


Figure 5.3: V-mm correlation

The linear relationship between V and mm (Figure 5.3) is explained in the following formula:

$$V = 150 \text{ mm} \rightarrow 1 \text{ mm} = 0.0067 \text{ V}$$

Therefore, every displacement measurement in Volt, before being processed was multiplied by 150 to transform it into millimetres.

### 5.3 Data processing

After the selection of what data would have been used, the methodology to process the data had to be developed. As mentioned previously the data is in the form of strain and temperature signals.

The aim of this thesis was to assess the structural behaviour of the truss end link and compare it with the behaviour of the new sliding bearing.

The structural behaviour can be identified by the changes in the signals from the sensors. Thus, the objective of the data processing methodology is to enhance understanding of the bridge structural behaviour and to provide a critical perspective of the assigned data; to develop a process that will allow the author to plot the signals from the sensors, which would enable identification of changes in signal and be repeatable for multiple data sets.

The data processing carried out by the script before plotting the resultant data was a step process. The first step was to plot all the data using Excel to have a general view and check the quality of the data. It is not unusual that there are issues with the DAU on site that required to reset the sensors. For this reason, it is preferable to make sure that the data are reliable.

The second step was to write a script in Matlab which could accomplish the objective of data processing. To process the data so that they could be easily analysed, the author has chosen to plot strain, temperature and displacement signals as change in strain temperature and displacement relative to the start of the time period being analysed.

To achieve this the first strain/ temperature/ displacement signal, from the time period being analysed would be subtracted from all subsequent signals before they were

plotted. The author believed this would provide the clearest method of plotting the data to enable the comparison between all the sensors analysed.

The third step of the data processing that was carried out was data normalisation. The objective of this data normalisation; separating the changes in signals received from sensors caused by environmental and traffic conditions from those caused by damage in the system. However only changes in the signal from environmental conditions were available.

The environmental condition that will be taken into account is temperature. This is the only environmental condition that will be considered, although wind speed and direction was also available. This judgement was made because it was assumed that temperature will have the biggest impact on the signal from the sensors above all the environmental conditions.

Moreover, it was seen that the influence of wind on stresses in the truss system doesn't have a large impact. The explanation to this lies in the shape of the suspended structure, which is an open rectangular framework. Thus, the impact of wind on the stresses in the truss system will not be accounted for in the data normalisation.

The temperature effect on the strain signals can be daily and seasonal. The daily effect is due to the temperature variations through the day and the seasonal is the temperature variations through the year. The effect of these variations in temperature is that when the temperature increases, the steel will elongate and as the temperature decrease it will compress.

These variations can complicate analysis of strain readings, especially the daily temperature effect, which can cause the strain signal to be noisy (signal changes frequently). This makes detecting the effect of operational conditions on the strain signal difficult. To eliminate the effect of daily temperature variations a simple solution has been selected.

Only one signal measurement from both the strain and temperature sensors will be considered, each day. Therefore, there will be no variations in strain signal through the day. The data used will be from 5am just before sunrise on average. The reason for appointing 5 am as the time during the day when the samples will be picked is that at

this time the surface of the structure will have been for as many hours as possible under absence of light. This absence of sunlight will therefore lead to lower structure surface temperature and lower stress because of it. The 5 am temperature will not vary much day to day. However, it will vary seasonally.

The last step of data processing that was carried out was the definition of a model which considered long-term effects to eliminate the seasonal temperature variation from the measurements. The model employed is a linear parametric model which is explained in detail in the next section.

### 5.3.1 Linear parametric model

A regression model is a formal means of expressing the two essential ingredients of a statistical relation:

1. A tendency of the response variable Y to vary with the predictor variable X in a systematic way.
2. A scattering of points around the curve of statistical relationship.

These two characteristics are embodied in a regression model by postulating that:

1. There is a probability distribution of Y for each level of X.
2. The means of these probability distributions vary in some systematic way with X.

A central problem is therefore that of choosing, for a regression model, a set of predictor variables that is "good" in some sense for the purposes of the analysis. A major consideration in making this choice is the extent to which a chosen variable contributes to reduce the remaining variation in Y after allowance is made for the contributions of other predictor variables that have tentatively been included in the regression model.

The model employed for the interpretation of the dependence between the measured strain  $\epsilon$ , the measured temperature T and the time  $t$  is the linear parametric model

$$\epsilon = \epsilon_0 + \alpha\Delta T + mt$$

where

- $\epsilon$  = Total deformation of the truss end link;
- $\epsilon_0$  = Strain value when  $T=0$  and  $t=0$ , i.e. before the installation of the monitoring system;
- $\alpha$  = Apparent thermal expansion coefficient. It is not the real thermal expansion coefficient of the material, but it takes into account how strain changes due to temperature  $T$ ;
- $m$  = Takes into account all deformations over time  $t$ , e.g. steel relaxation or viscosity and shrinkage for concrete.

Regression model is said to be *linear in the parameters* ( $\epsilon_0, \alpha, m$ ) and *linear in the predictor variables* ( $\Delta T, t$ ). It is "linear in the parameters," because no parameter appears as an exponent or is multiplied or divided by another parameter, and "linear in the predictor variables," because these variables appear only in the first power. A model that is linear in the parameters and in the predictor variables is also called *first-order model* (Kutner, Nachtsheim, Neter, & Li, 2005).

The parameters  $\epsilon_0, \alpha$  and  $m$ , in the regression model are called *regression coefficients*.  $m$  is the slope of the regression line. It indicates the change in the mean of the probability distribution of  $Y$  per unit increase in  $X$ .

### 5.3.2 Parameter estimation using least squares analysis

To find good estimators of the regression parameters the author employed the method of least square. The mathematical procedure of Least Squares Analysis (LSA) was performed for the full data set trying to find the best-fitting curve to the corresponding set of data. This was achieved by minimizing the sum of the squares of the offsets ("the residuals") of the points from the curve. This procedure is embedded in the least squares formula:

$$Q = \sum_{i=1}^N [y_i - f(x_i, \theta)]^2$$

Where

$Q$ : Least squares vector

$y_i$ : observation from sensors

f: parametric model

$x_i$ : variables of the model

$\theta$ : real unknown parameter

The objective of the method is to estimate the values of real unknown parameters  $\epsilon_0$ ,  $\alpha$ ,  $m$  for which the least square criterion is minimized. This can be done in two basic ways:

1. Numerical search procedures can be used that evaluate in a systematic way the least squares criterion  $Q$  for different estimates  $\epsilon_0$ ,  $\alpha$  and  $m$  and until the ones that minimize  $Q$  are found.
2. Analytical procedures can often be used to find the values of  $\epsilon_0$ ,  $\alpha$  and  $m$  that minimize  $Q$ . The analytical approach is feasible when the regression model is not mathematically complex.

In this case the analytical procedure was used, and it is outlined below:

1. State the observation vector

$$\epsilon = \begin{bmatrix} \epsilon_1 \\ \vdots \\ \epsilon_n \end{bmatrix}$$

2. State the interpretation model

$$\epsilon_i = \epsilon_0 + \alpha T_i + m t_i$$

3. Calculate the matrix

$$D = \begin{bmatrix} 1 & T_1 & t_1 \\ \vdots & \vdots & \vdots \\ 1 & T_n & t_n \end{bmatrix}$$

4. Calculate  $\theta$

$$\epsilon = D * \theta \rightarrow \theta = [D^T * D]^{-1} * D^T * \epsilon$$

5. Calculate the variance of the error

$$\sigma_y^2 = \frac{[\epsilon - D\theta]^T}{N-p} * [\epsilon - D\theta]$$

6. Calculate the parameter's covariance

$$\Sigma = \frac{Y^T Y}{N-3} (D^T * D)^{-1}$$

The parameters formulate the parametric model of:

$$\Delta \varepsilon_i = \varepsilon_0 + \alpha \Delta T_i + m \Delta t_i$$

and their estimation lies in the subtraction of the first value measured, e.g.  $\varepsilon_1$ ,  $T_1$  and  $t_1$ , to each quantity/variation measured in respect to an unknown offset.

The results of data analysis are provided in the next section.

## 6.0 Results and Discussion

The results of data analysis from the dynamic strain gauges and displacement transducers are presented in this part of the report. The data analysis process detailed in the methodology section has been applied to produce the results contained in this chapter.

The data analysis concerning the truss end links are exposed first, respecting the chronological order of the events.

Afterwards the results regarding the current structural configuration, with the sliding bearing, will be provided.

It is important to point out that the only temperature measurements available at the time of data collection were those relating to the North tower (TMP-01, see Figure 4.12). As a consequence, since the air temperature does not vary much from one side to the other, these data were also used for the analysis of the links on the south tower, where temperature data were not available.

### 6.1 Full time history of strain and temperature

Strain and temperature measurements at NEMS were collected for the period from 06/01/2016 to 09/02/2017. However, the plot starts on 20/02/2016, time in which the bridge was reopened to traffic after the closure to repair the links, because, prior to this time, data were fluctuating and did not follow a precise trend. This consideration was applied to all data collected concerning the links.

The strain measurements plotted in the graph below refer to the inner link strain gauge 03 and outer link 04 (I-STR-03/O-STR-04, see Figure 5.1).

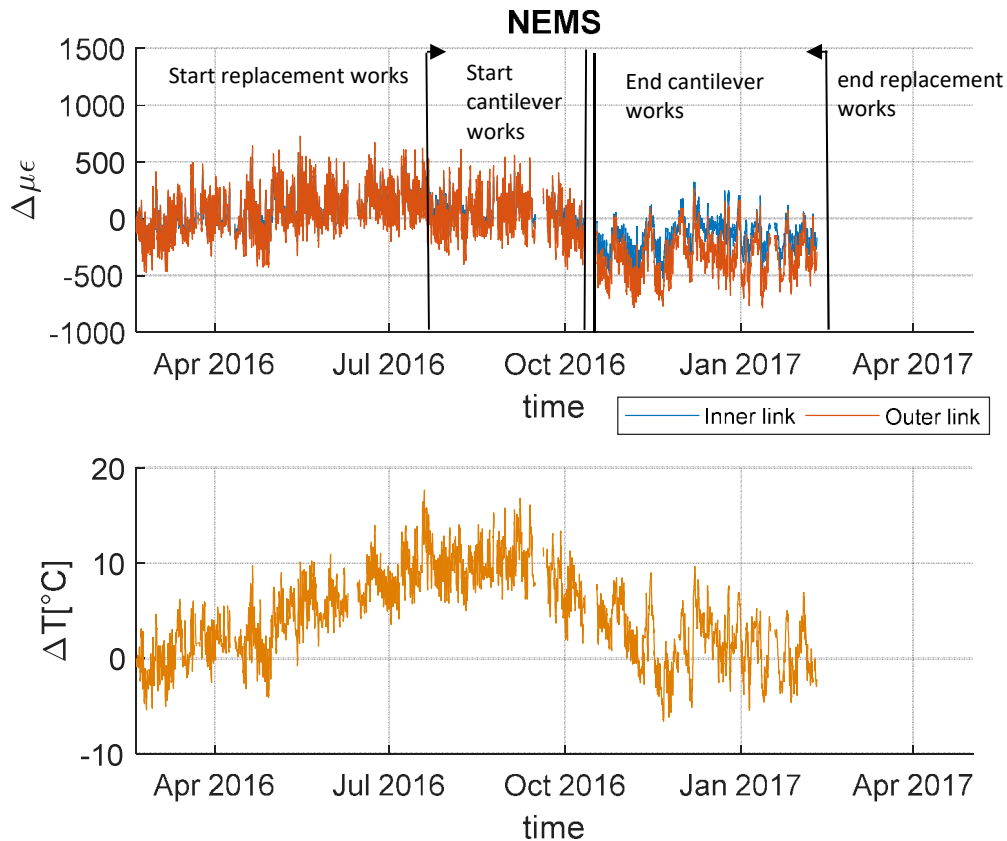


Figure 6.1: NEMS full-time history uncompensated strain and temperature

Looking at the graph it can be seen a qualitative change in the strain trend at the end of October 2016. On the 11<sup>th</sup> of October the sensors were disconnected for 6 days, after that date the trend is altered. This change can be explained with the replacement works at NEMS on the truss end links, going on from August 2016 until Spring 2017. The operations were carried on in steps, thus it is assumed that during October 2016 the cantilever at the bottom of the End Post was build, changing part of the initial configuration.

Finally, it can be easily observed that the two plots follow identical patterns, meaning that the fluctuations observed in one plot match those of the other. This dictates that changes in strain of the link are directly affected by changes in the temperature.

Strain and temperature measurements at NWMS were collected for the period from 12/01/2016 to 02/05/2017. On this side there are three months more of data compared to before, because the new bearing was placed first on the NE side disconnecting the strain sensors attached to the links.

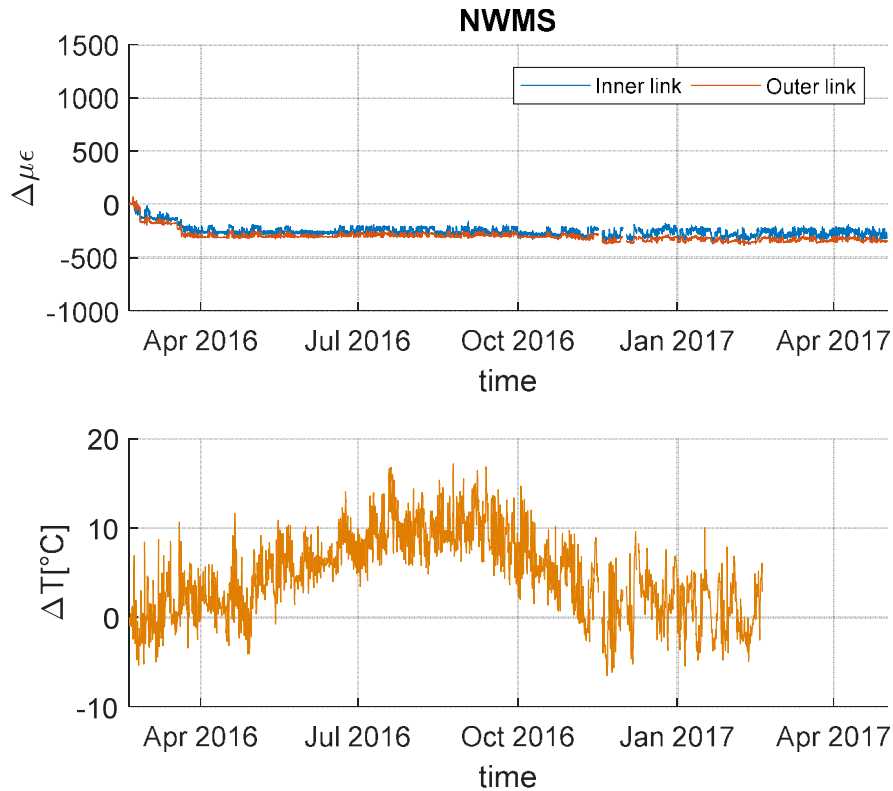


Figure 6.2: NWMS full-time history uncompensated strain and temperature

Having a look at the graph it can be seen that the measurements don't follow the same pattern as the temperature and compared to the previous graph the values are much lower. Therefore, data can't be compared to the others and are not reliable because probably there were issues with the sensors or the DAU.

To have a general overview of the main span links behaviour, the data concerning the South tower were collected and analysed. The plots are provided in Figure 6.3 and 6.4. The measurements for both SEMS and SWMS begin on the 20/02/2016 and finish on the 02/05/2017.

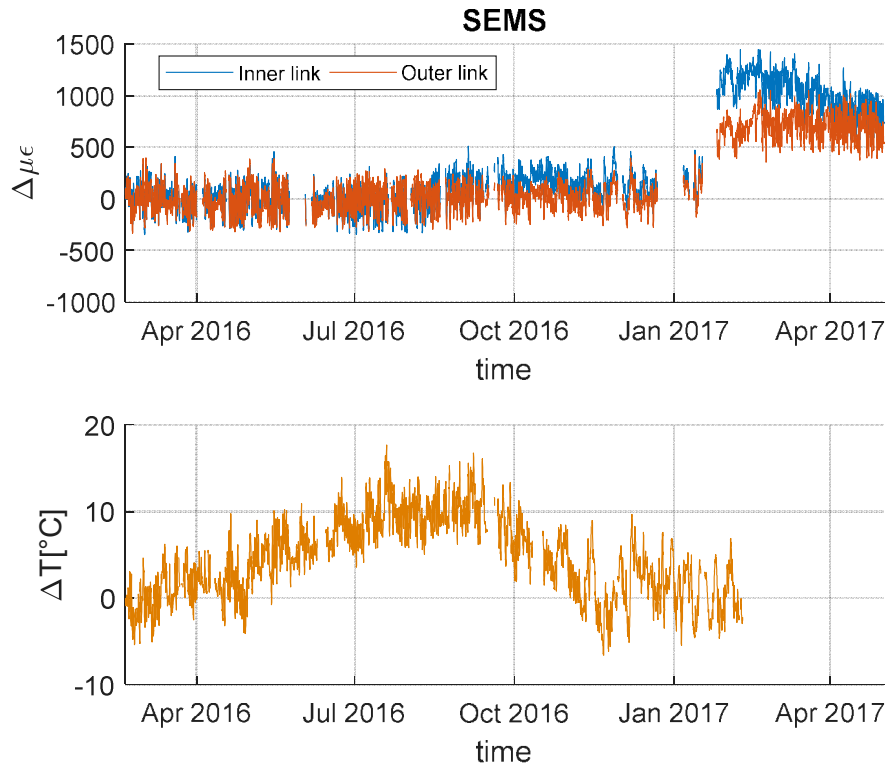


Figure 6.3: SEMS full-time history uncompensated strain and temperature

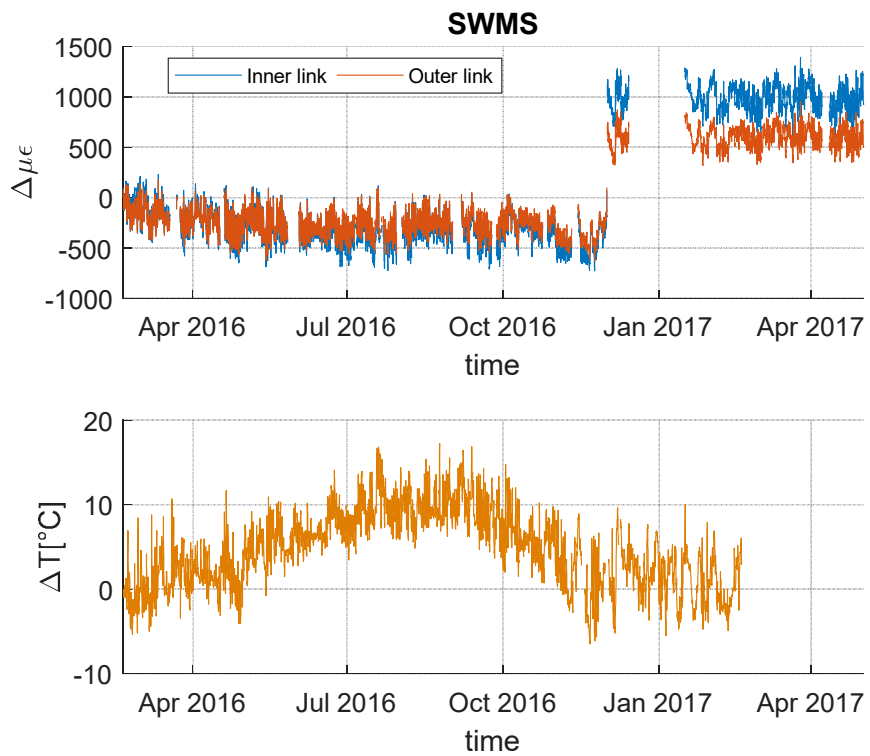


Figure 6.4: SWMS full-time history uncompensated strain and temperature

Observing the SEMS plot it can be noticed that sometimes data are missing and because of that there are holes in the plot. However, despite the lack of data, the overall trend does not change until January 2017. In fact, after a week's gap there is an evident trend jump.

The same observations can be applied to the SWMS measurements. The only difference is that the trend jump occurs on the 16/01/2017 after a month of lack of data.

Nevertheless, because even after the jump in both cases the qualitative trend does not change, it is not due to a sensor operation problem. It is more likely that after having disconnected the sensor when it was put back in operation the measurements were taken in respect of a different initial value. This would explain the shift visible when all the signals are plotted together. Considering this, the data have been shifted to obtain a real strain trend.

## 6.2 Strain data shifted

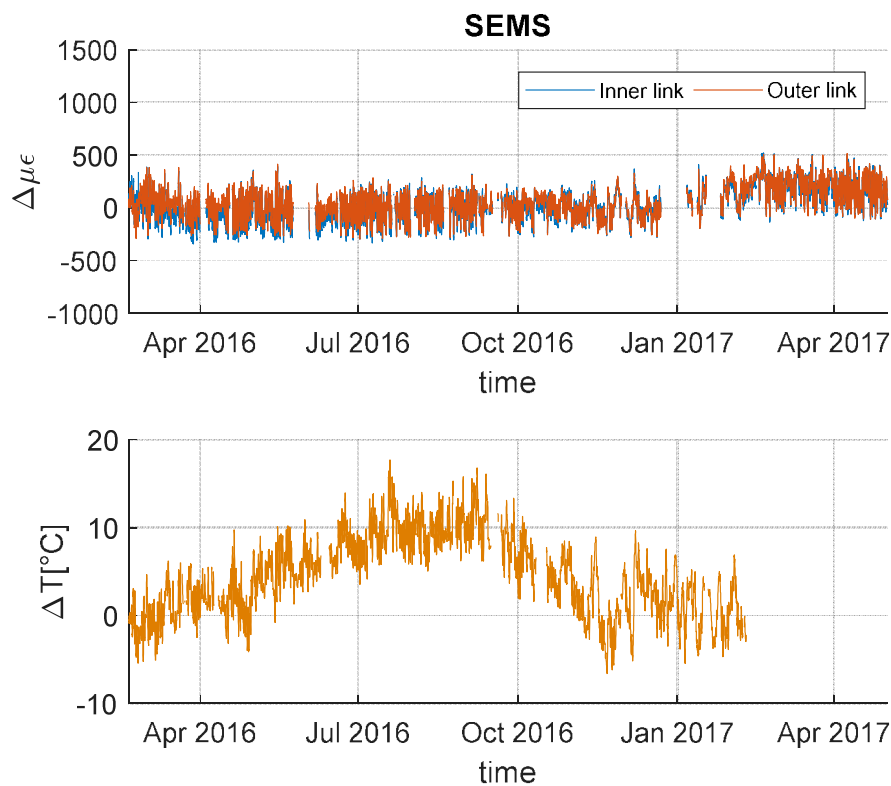


Figure 6.5: SEMS full-time history shifted data

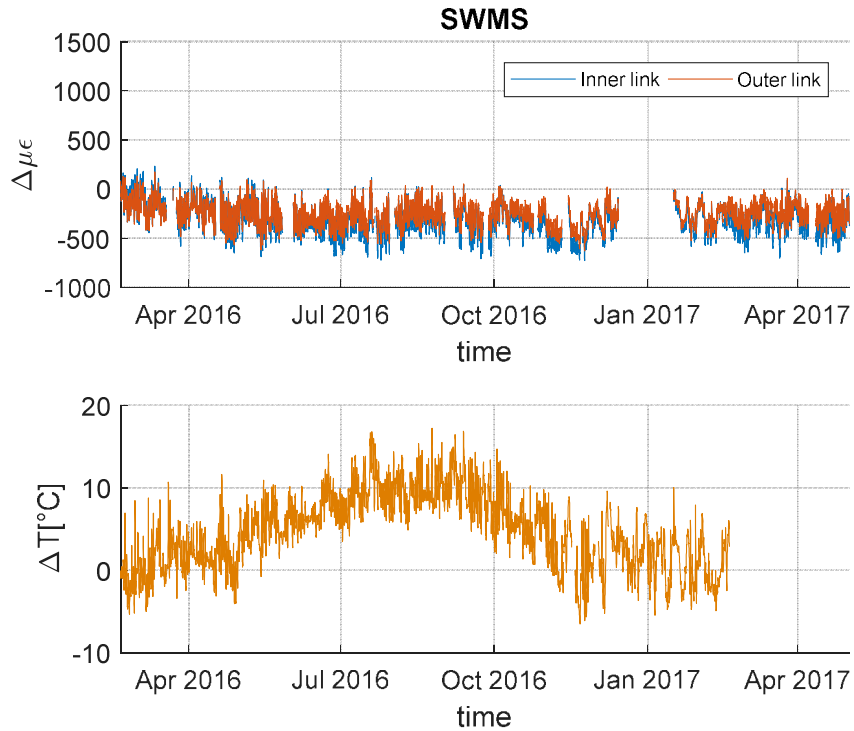


Figure 6.6: SWMS full-time history shifted data

### 6.3 Different period within the year

In this section, the graphs for uncompensated strain and temperature are presented for a span of three consecutive days, for two different and characteristic periods within the year. These graphs allow to see the daily behaviour of the truss end link and the strict dependence of stress on temperature. Those time periods, with their respective 3-day graphs are hereby presented.

#### 6.3.1 Summer solstice

The graphs for uncompensated strain and temperature for the summer period, for the full days of 20, 21 and 22 of June 2016 for North side are presented in Figures 6.7 and 6.8. As concerns the South side the measurements of the 21<sup>st</sup> of June were missing, thus the period plotted starts on the 22<sup>nd</sup> of June and stops on the 24<sup>th</sup>.

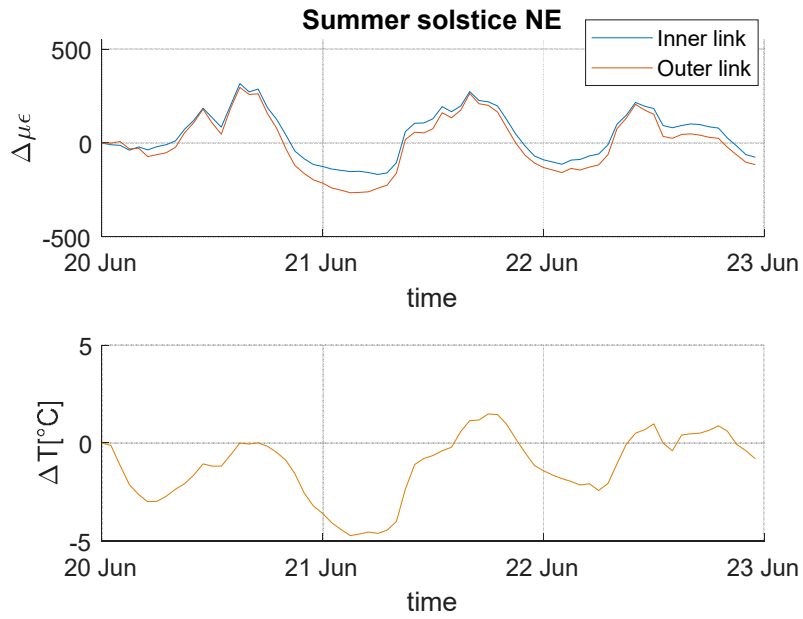


Figure 6.7: NEMS Summer solstice uncompensated strain and temperature

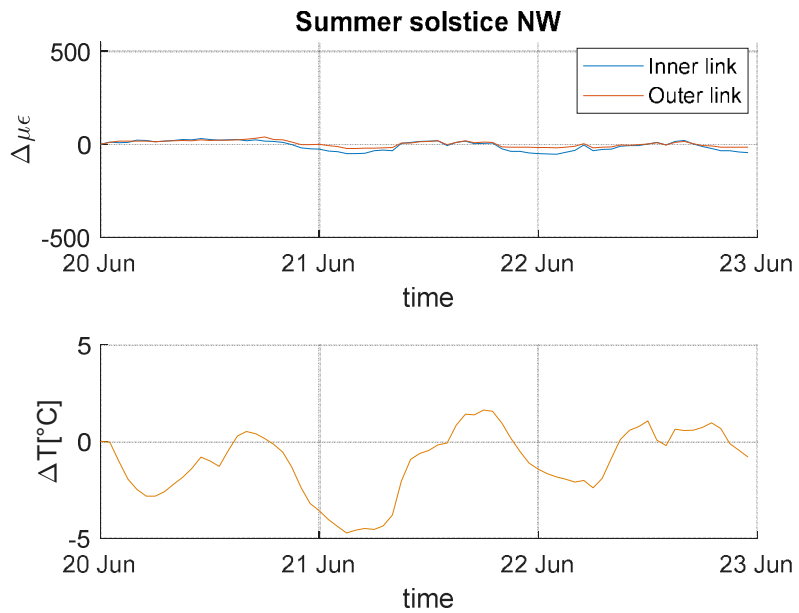


Figure 6.8: NWMS Summer solstice uncompensated strain and temperature

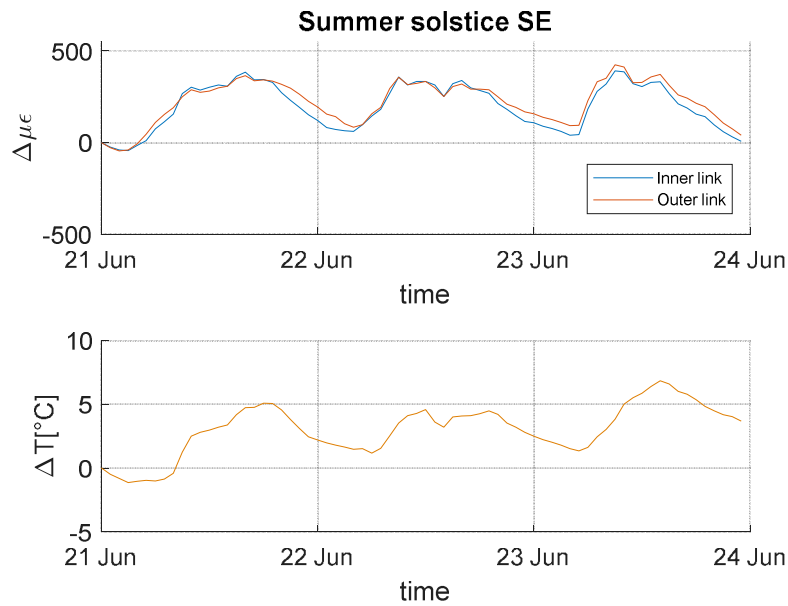


Figure 6.9: SEMS Summer solstice uncompensated strain and temperature

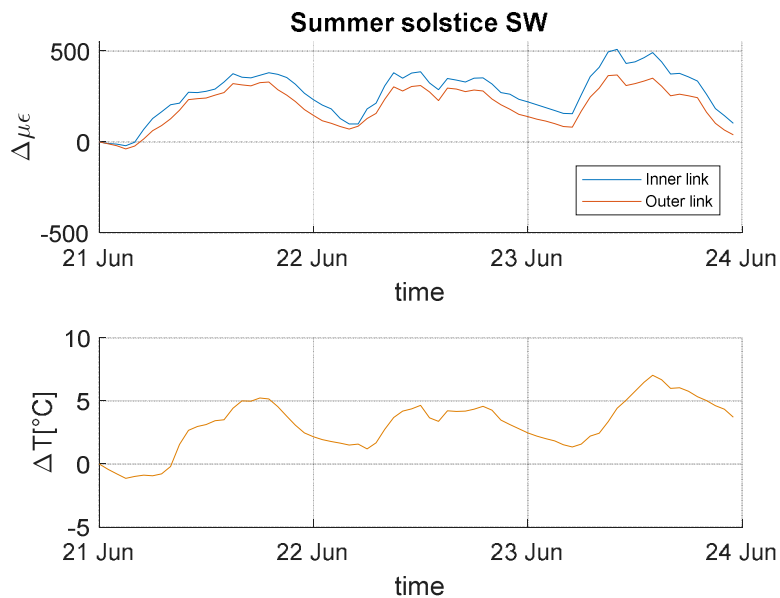


Figure 6.10: SWMS Summer solstice uncompensated strain and temperature

According to Timeanddate.com (2016), the time for sunrise and sunset for South Queensferry, for 20, 21 and 22 of June, are approximately 4:30 and 22:00 respectively. As observed in the graphs, the daily minimum values for strain and temperature appear at around 3:30, about one hour before sunrise. Moreover, the maximum values for strain and temperature are presented between 12:00 and 16:00.

Looking at Figure 6.8 it is even more evident that there has been a problem with the functioning of the sensor, which does not detect any strain change during the day.

### 6.3.2 Winter solstice

In this section the graphs for uncompensated strain and temperature for the winter period, for the full days of 20, 21 and 22 of December 2016 are presented.

The time for sunrise and sunset for 20, 21 and 22 of December are about 08:30 and 15:30 respectively. The daily minimum value for strain and temperature falls between 6:00 and 8:00 am approximately one hour before sunrise. Furthermore, the daily maximum value for strain and temperature appears at around 12:00 pm.

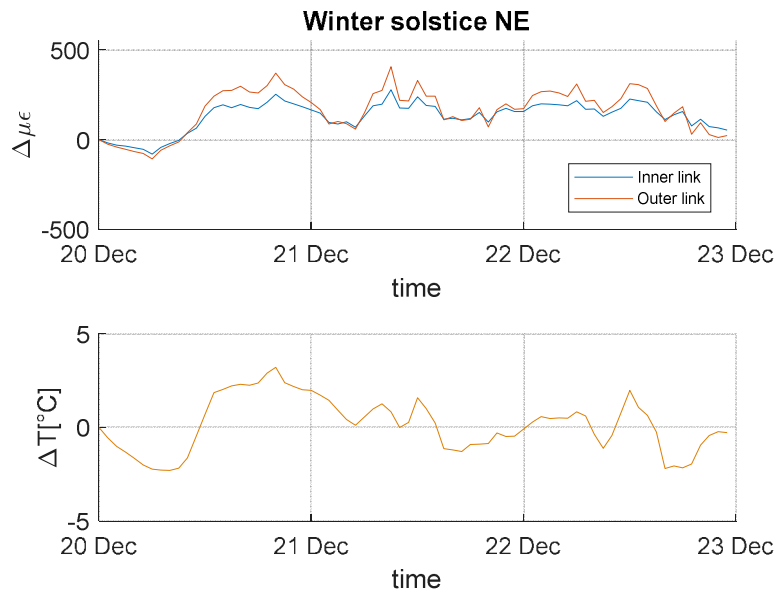


Figure 6.11: NEMS Winter solstice uncompensated strain and temperature

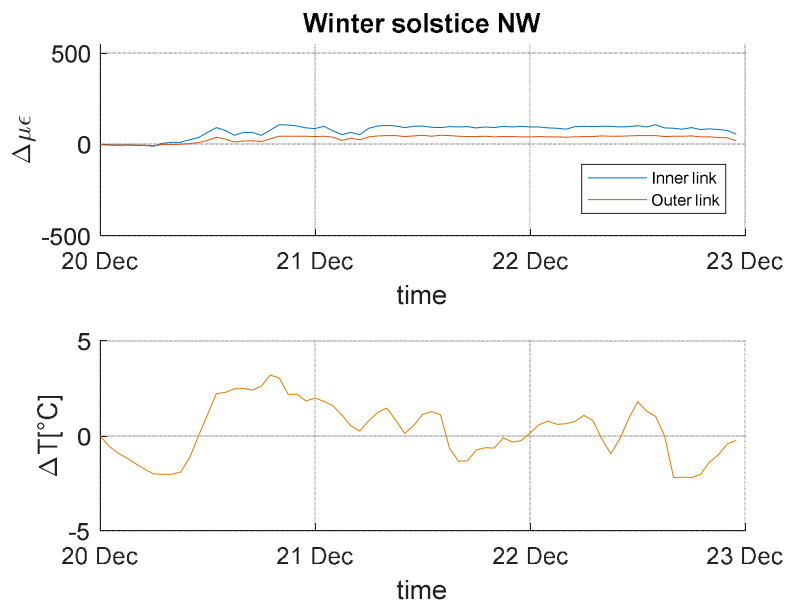


Figure 6.12: NWMS Winter solstice uncompensated strain and temperature

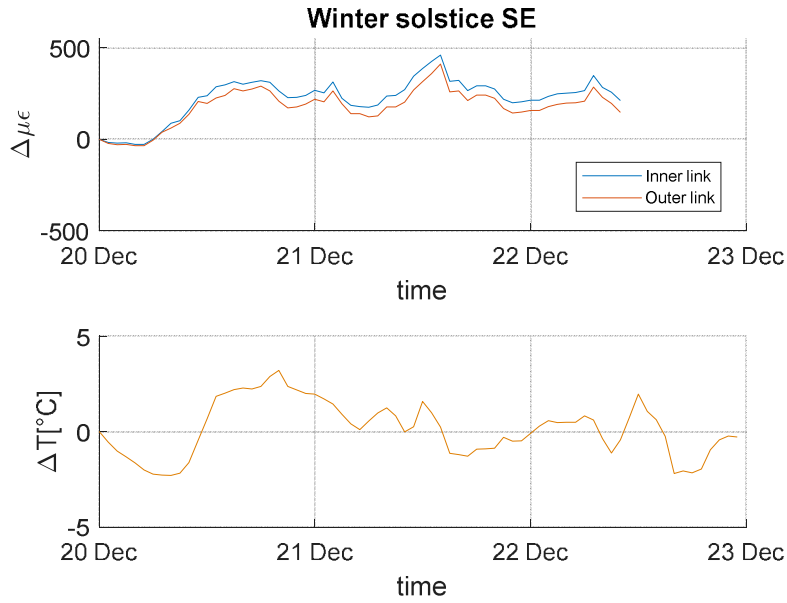


Figure 6.13: SEMS Winter solstice uncompensated strain and temperature

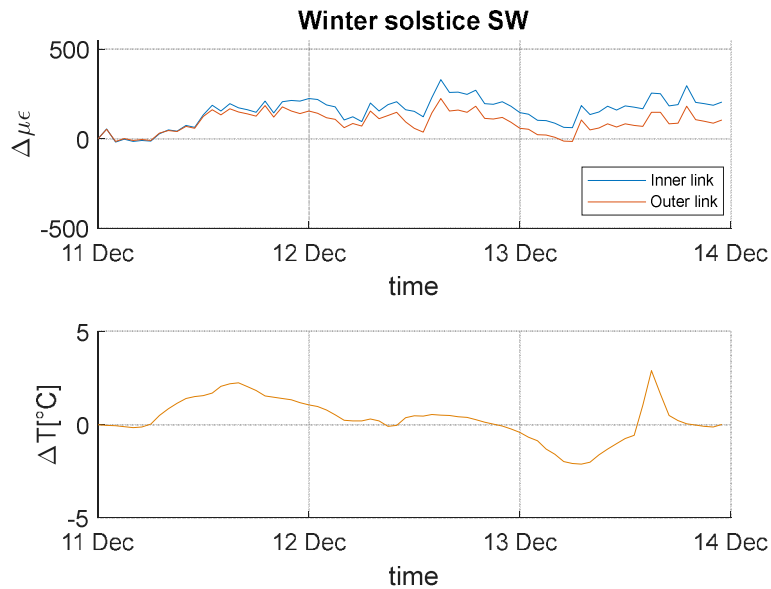


Figure 6.14: SWMS Winter time uncompensated strain and temperature

## 6.4 Daily temperature effect

What is being observed from the 3-day graphs, plotted for two characteristic yearly periods, is that the strain signals recorded for the various times within the day, are directly related to the temperature measurements taken for the same timestamps.

The truss end link behaviour is directly affected by the fluctuations in temperature that are expected within the different times of the day, with the most characteristic times being those around the sunset and the sunrise.

It has been observed that the minimum values for temperature, and therefore for strain, are recorded around the time of the sunrise, when the steel structure have 'cooled down' during the night-time and returns to its initial position, therefore the truss end link is less stressed.

Regarding the maximum values of temperature and strain, it was observed that they were recorded in the timestamps in early afternoon. In fact, at that time the steel structure has been exposed for hours to the sun and to higher daily temperatures, thus the truss temperature has risen causing an elongation of the steel and consequently the deformation in the link increase.

## 6.5 Strain and temperature trend with reduced data set

According to the results of the previous section the strain in the truss end link is subject to daily temperature variation. Therefore, the dataset was reduced to one significant sample per day, so that the daily temperature effect on the truss end link could be removed.

The reduced plots were produced selecting a daily sample at 5 am, just before sunrise on average. The reason for appointing 5 am as the time during the day when the samples will be picked is that at this time the surface of the link will have been for as many hours as possible under absence of light. Therefore, the surface temperature of the link will be as lower as possible and will not cause further stress in the link.

Isolating the daily sample to a time when the temperature effect is minimal will help measure strain in the link that derive from all the other factors that can cause it. To be more precise, this way we can observe the strain for reasons of loading of the suspended structure.

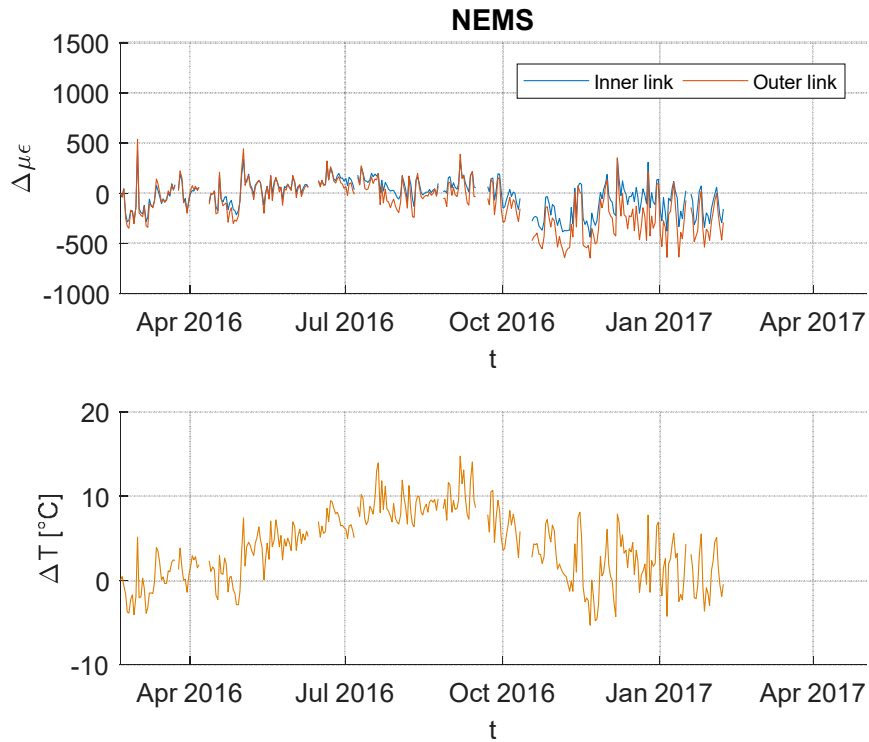


Figure 6.15: NEMS full-time history of reduced strain and temperature

Comparing the full-time history with uncompensated data set to the fulltime history with reduced data it can be observed that in the latter case the plots present less fluctuations, hence the graphs appear to be clearer. Anyway, they follow always the same pattern during the year. It appears that the strain is directly related to the temperature variation as before.

This similarity in the patterns can be explained by the overall temperature of each season that dominates in the creation of the trend plot, even in the reduced data set graph, where the temperature effect was attempted to be scaled down.

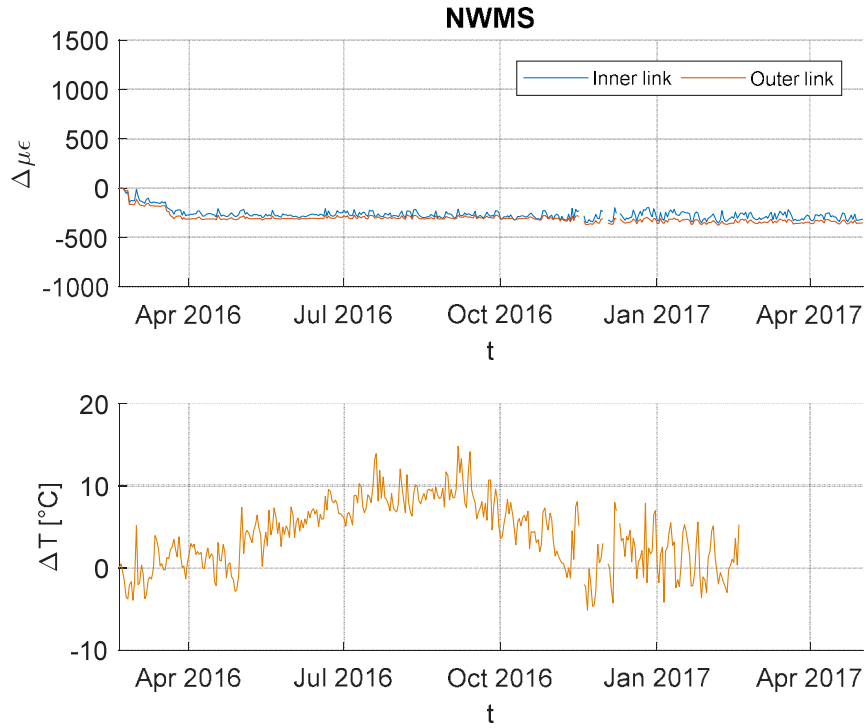


Figure 6.16: NWMS full time history of reduced strain and temperature

As stated before in the case of NWMS it is not possible to make any consideration, however, the graph has been reported for completeness.

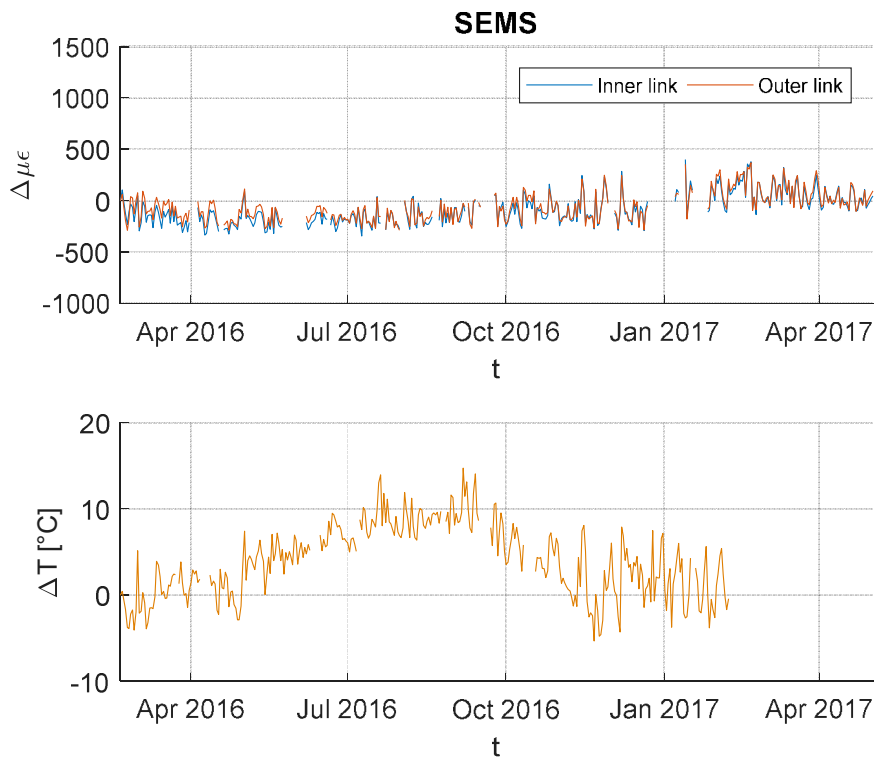


Figure 6.17: SEMS full-time history of reduced strain and temperature

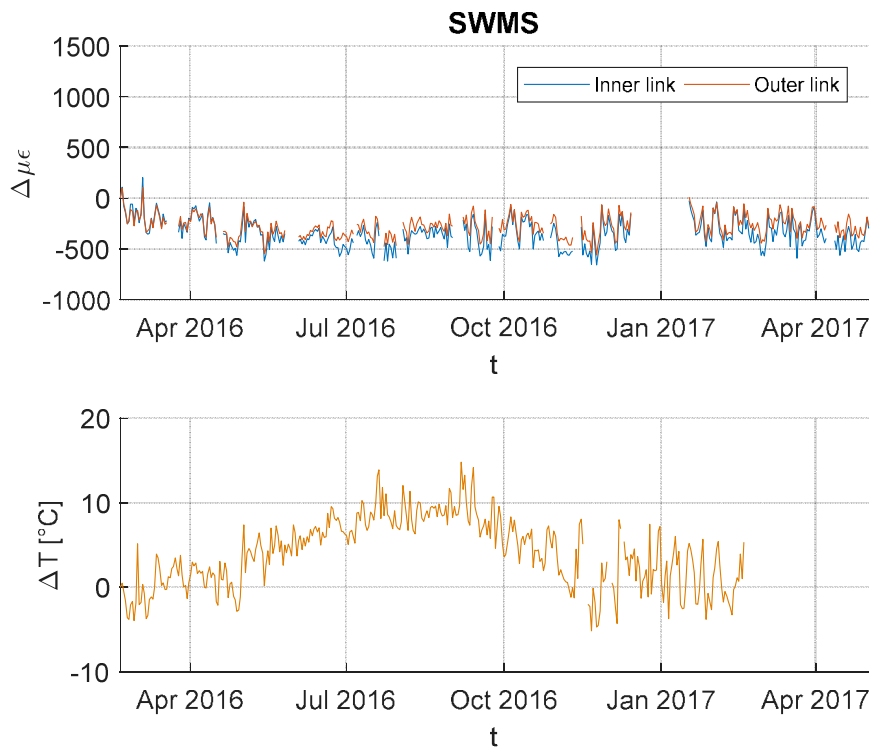


Figure 6.18: SWMS full-time history of reduced strain and temperature

Looking at the trend of the signals coming from the south, it can be noticed that they seem not to follow the same outline of temperature. Moreover, even if, as we have seen previously, the daily temperature effect on the measurements was evident, the influence of the seasonal temperature on the reduced data set does not seem so clear.

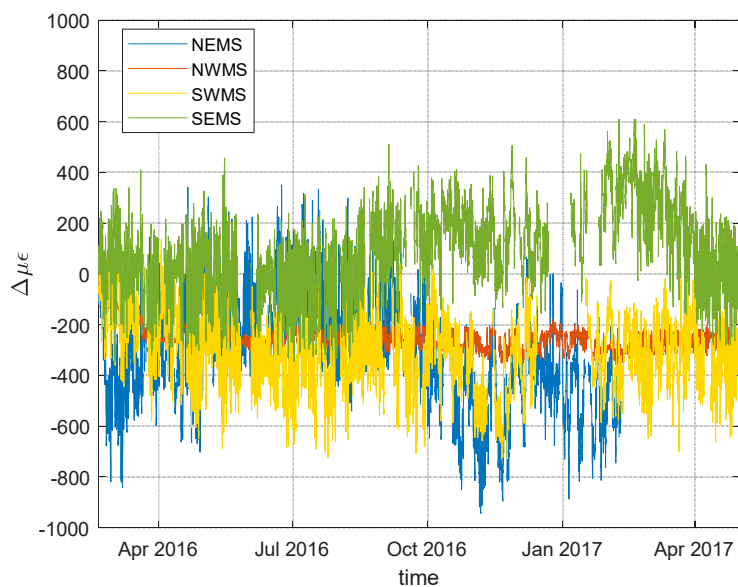


Figure 6.19 Comparison of the four cases

Comparing the values of the strain in the four cases, it can be seen clearly that the measurements coming from the NW side are not accurate. On the other hand, the other data have the same order of magnitude and they vary between the same range; therefore, the main span is loaded everywhere the same way.

Furthermore, in order to assess the temperature dependence, the graphs correlating strain and temperature have been plotted.

## 6.6 Strain-temperature correlation

A significant step for the evaluation of the existence of a correlation between the recorded signals, consists in drawing a dispersion diagram, that is to represent in the Cartesian plane the observations with points.

If the dispersion diagram suggests a linear relationship between parameters and the Pearson correlation coefficient is close to one the two variables are strongly correlated.

Pearson coefficient is calculated as follow:

$$\rho = \frac{\sigma_{xy}}{\sigma_x \sigma_y}$$

where  $\sigma_{xy}$  is the covariance and  $\sigma_x \sigma_y$  are the standard deviations.

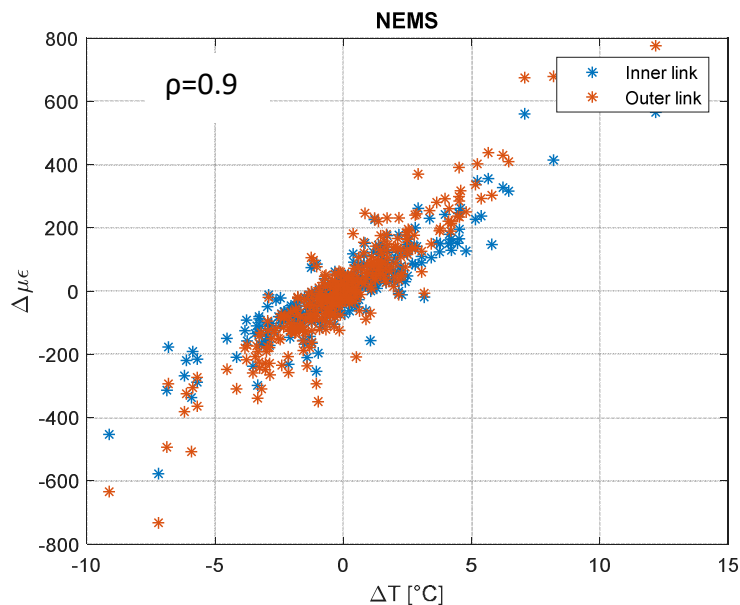


Figure 6.20: NEMS strain temperature correlation

From NEMS plot it can be observed that there is a positive correlation between strain and temperature and the correlation coefficient is 0.9. Moreover, it can be seen that for an increase of 1°C there is an increase of 45 microstrain. This ratio is unexpected, because usually for steel with a temperature variation of 1°C corresponds a variation of about 10  $\mu\epsilon$ , as the linear thermal expansion coefficient is equal to  $12.2 \times 10^{-6} \text{ }^\circ\text{C}^{-1}$ .

$$\epsilon = \alpha \Delta T = 12.2 \times 10^{-6} \times 1 = 12.2 \mu\epsilon$$

Taking this into account, a finite element model has been realized to deepen the correlation between strain and temperature and to assess the consistency of the sensor data. The result of the finite element model is presented in the next section.

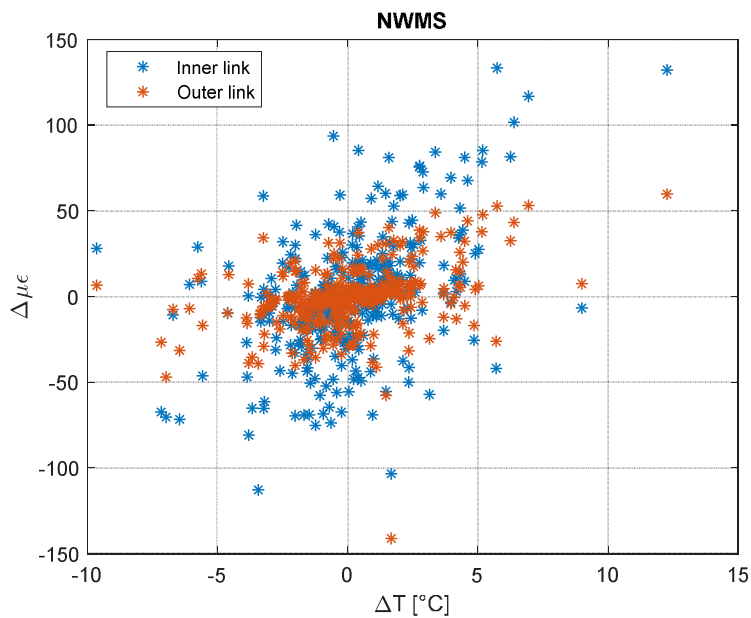


Figure 6.21: NWMS strain temperature correlation

As expected there is no correlation between strain and temperature at NWMS, in fact Pearson coefficient is -0,1.

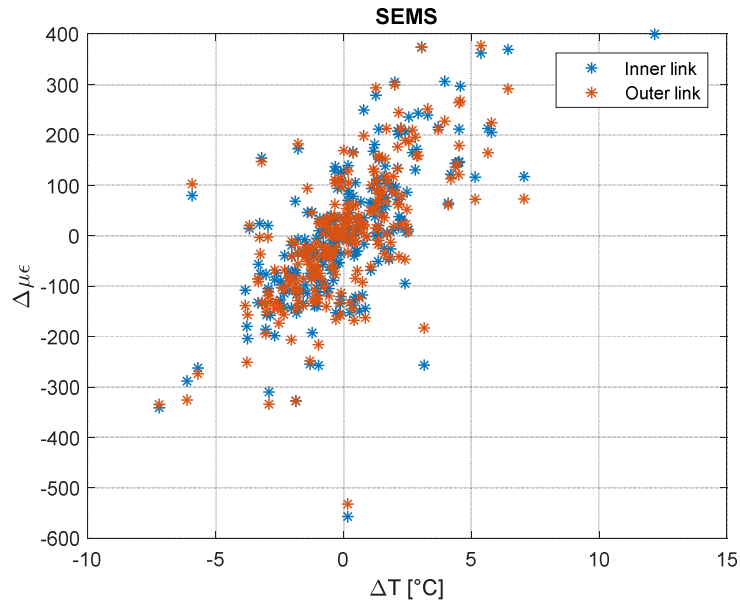


Figure 6.22: SEMS strain temperature correlation

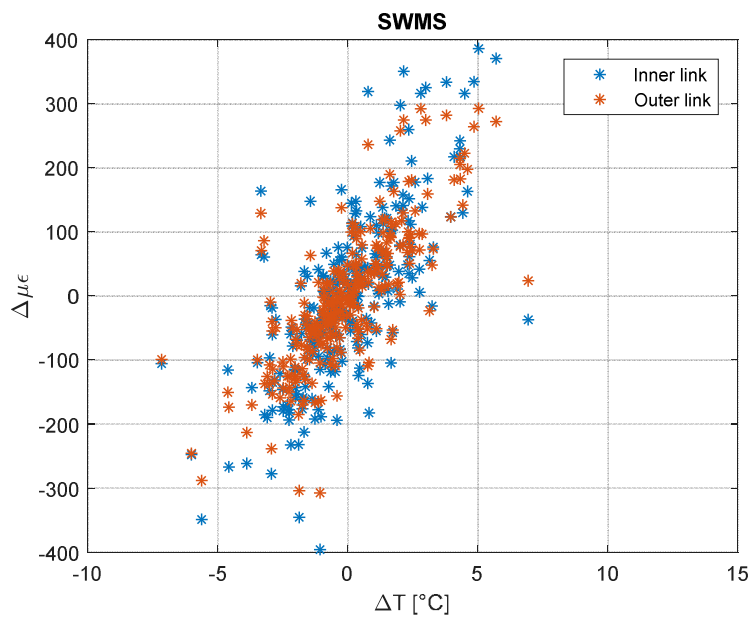


Figure 6.23: SWMS strain temperature correlation

As regard SEMS and SWMS, the Pearson correlation coefficient are respectively 0.6 and 0.7. Therefore, the variables correlation is less strong than in the NEMS case. Moreover, it can be seen that an increase of 1°C there corresponds to a variation of 40 microstrain, which is similar to the result obtained for the North East side.

### 6.6.1 Other studies supporting the monitoring

Temperature has a significant effect on the loading capacity of the bridge. The major structural elements in which temperature effects are significant are the deck trusses and the hanger cables.

To support the monitoring studies, finite element model of the bridge has been created. The model of the bridge, shown in Fig. 6.21, has been developed in SAP2000 and used for simulation of thermal loading effects on the bridge.

This simulation allowed to calculate the elongation of the truss end link caused by the increase in temperature and to trace the deformation of the element.

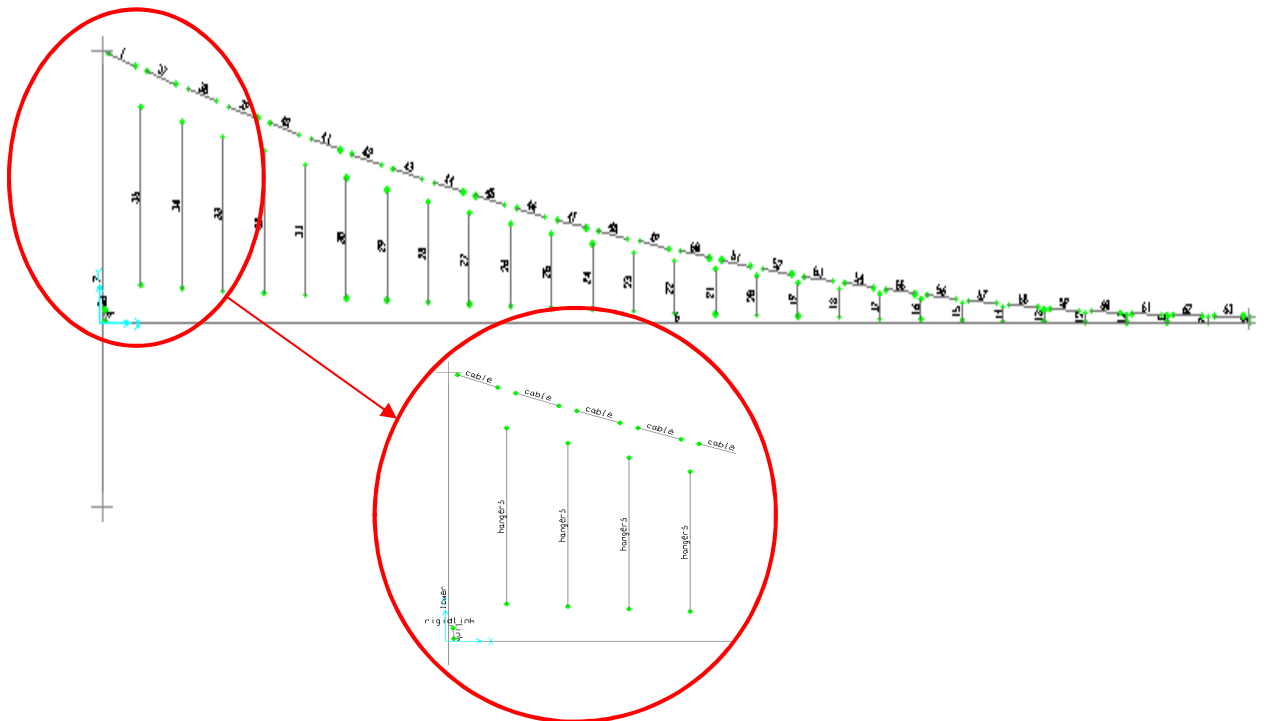


Figure 6.24: Finite element model

When the temperature increases uniformly on the bridge the main cables, as well as the hangers, elongate. Therefore, also the suspended structure expands, and the deck's height location is lowered. The deformed shape is presented in Figure 6.25.

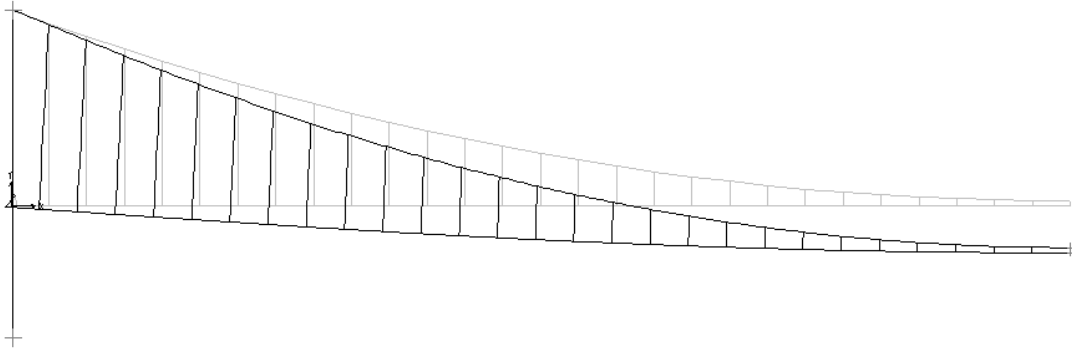


Figure 6.25: FRB Deformed shape due to temperature load

If all the structural elements were to elongate of the same quantity nothing would change in the behaviour of the links. Thus, we would only see the effect of temperature on the links due to the thermal expansion coefficient and not an additional deformation.

The model has been created assuming that the tower does not move and modelling the cables and the link like connecting rods. Following the application of a uniform temperature load of 10°C, the link elongation and the resulting deformation has been calculated.

The material and sections properties are described in the tables below. To calculate the bending stiffness of the truss system the following formula has been used:

$$EI = E A_{\text{chord}} b^2 / 2$$

Where E is the modulus of elasticity, A is the area of one chord that forms the cross section and b is the height of the section.

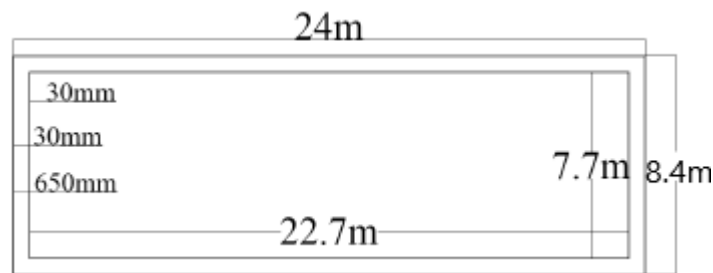


Figure 6.26: Simplified section

	Area [m <sup>2</sup> ]	E [KN/m <sup>2</sup> ]
hangers	0.0060821	193.0532
cables	0.226	193.0532
link	0.014	200.00

	A <sub>chord</sub> [m <sup>2</sup> ]	b[m]	E[KN/m <sup>2</sup> ]	EI	I[m <sup>4</sup> ]
Deck truss	0.0155	8.4	200	109.368	0.54684

Condition	L [m]	Δl [m]	Δε	Vertical deflexion in main span [m]
Temperature +10°C	5.4485	1.7E-3	310 με	0.3

From the model it can be seen that the temperature causes an expansion of the cables and the hangers greater than that of the link and of the deck. That part of the load first brought by the hangers is now transferred to the link which is therefore more stressed. Looking at the result obtained, it can be asserted that the sensors data are reliable. Indeed, from the model it was obtained a strain value of 310 με close to the experimental value of 400 με, which we would expect considering the data correlation found previously.

## 6.7 Full time history of displacement and temperature

In addition to strain and temperature data, displacement measurements were also collected from the sensors attached to NE and NW End Posts. Unfortunately, data regarding the South side were unavailable.

The NEMS end post displacement monitoring started on 20/02/2016 and ended on 25/09/2016. While, regarding the NW side there are about one year of data from 24/02/2016 to 19/02/2017.

The plots are provided in figures 6.20 and 6.21. The signals plotted come only from the displacement transducers at the top of the end posts (E-DSP-01, see figure 5.1), because the bottom transducers data (E\_DSP-02) didn't follow a regular pattern, hence they have been neglected.

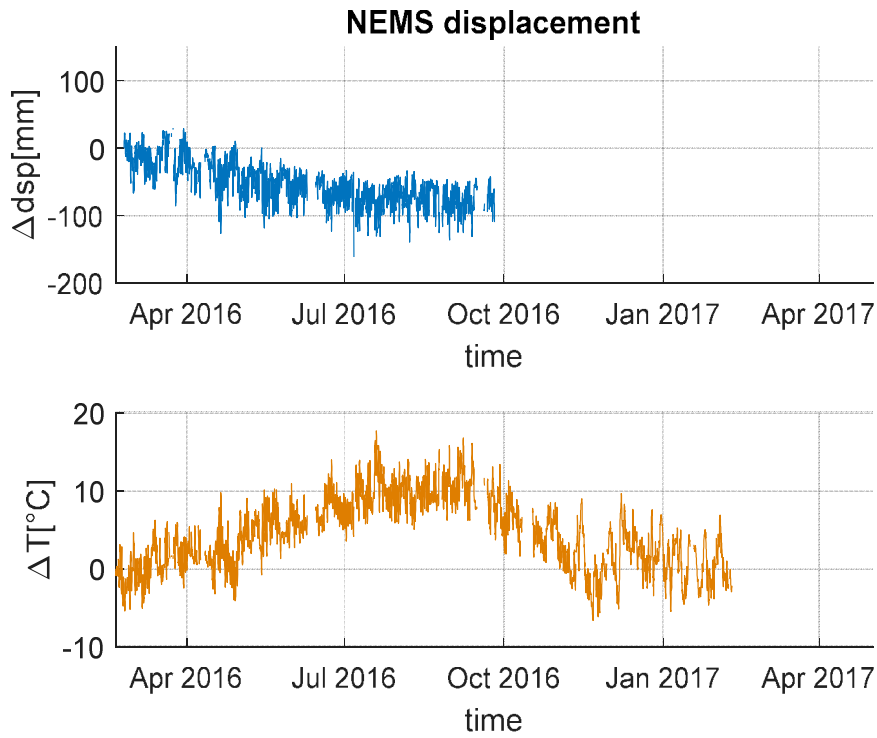


Figure 6.27: NEMS full-time history uncompensated displacement

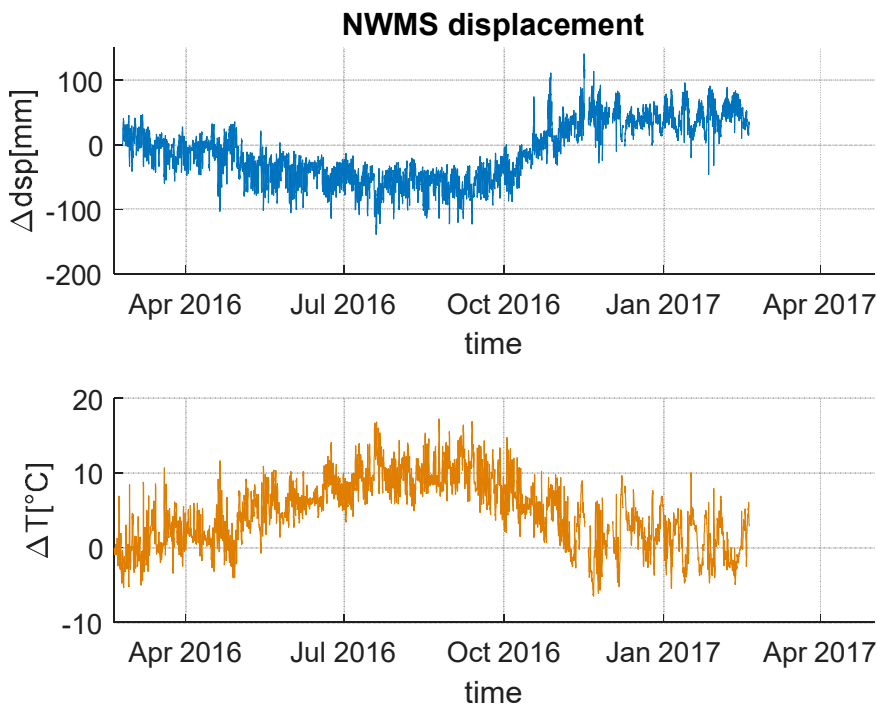


Figure 6.28: NWMS full-time history uncompensated displacement

It can be observed that the end post displacement trend tends to decrease from March to October. This can be explained with the seasonal temperature effect. In fact, during the warmer months of the year the suspended structure heats up and elongates

towards the towers, in this case the sensor records a negative displacement respect to the initial position. While during winter the truss system releases the heat and contracts. Therefore, we see a descendent trend when the temperature rises and an ascendant trend, only visible in the second graph, when the temperature decreases during the winter months.

## 6.8 Displacement trend with reduced data set

The second step, as has been done before, was to reduce the displacement data to one significant sample per day, to remove the daily temperature effect.

The reduced plots were realized by picking one daily sample at 5 am, when the truss system is less subjected to elongation due to the air temperature.

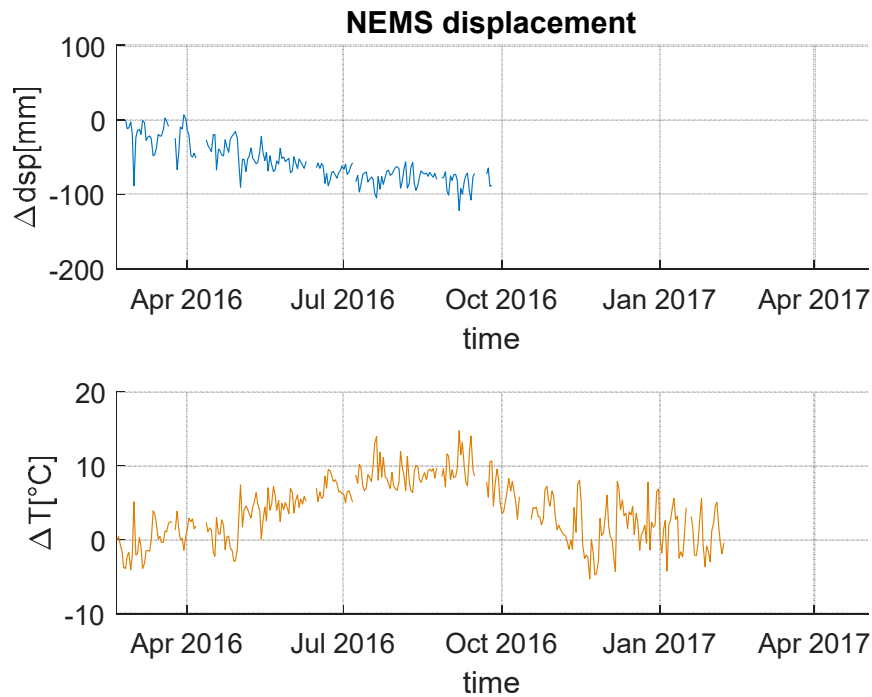


Figure 6.29: NEMS full-time history reduced displacement

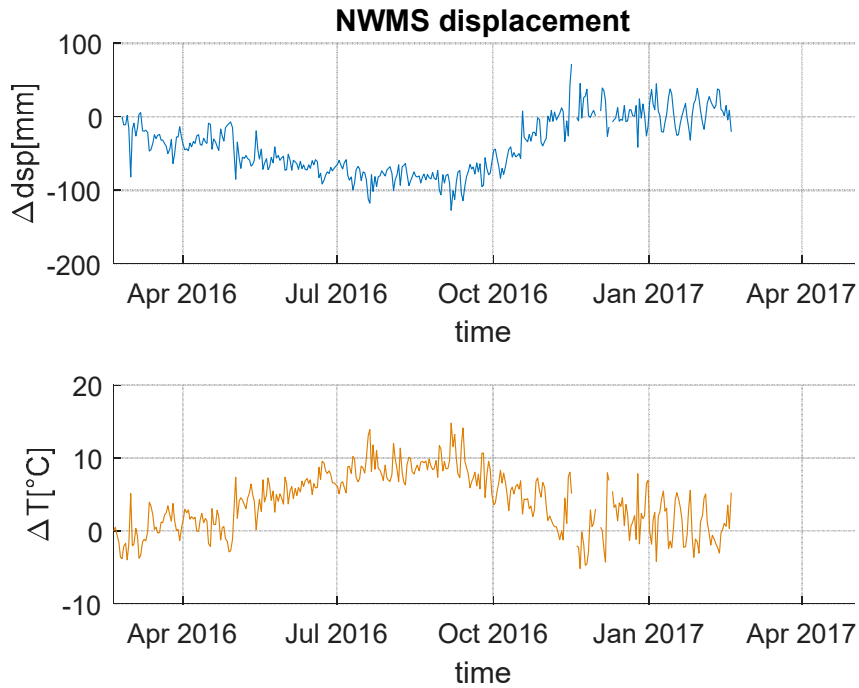


Figure 6.30: NEMS full-time history reduced displacement

Comparing the full-time history uncompensated displacement to the plots with reduced data set we can observe that the overall trend doesn't change, there are only less fluctuations. This can be attributed to the direct influence of temperature on the truss movement. Therefore, the similarity in the temperature plots determines the similarity observed in the two displacement plots.

## 6.9 Displacement-temperature correlation

In the temperature-displacement correlation diagram we can find the proof of the displacement dependence on temperature.

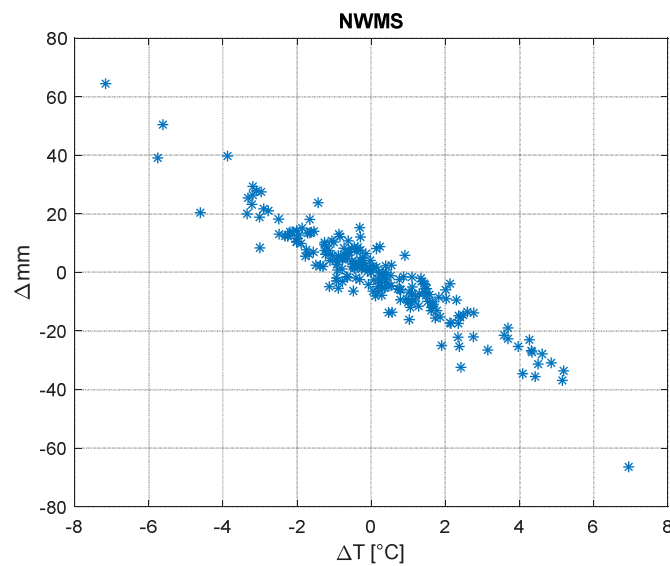
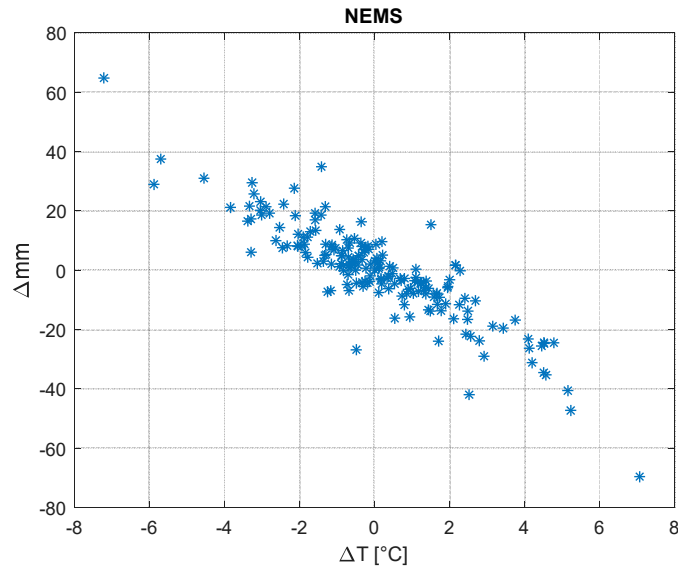
In both cases it can be recognized a negative linear correlation between the two parameters. The correlation coefficient is 0.9 so we can state that there is a strong correlation.

Moreover, using the data recorded, for a temperature variation of 1°C on the NEMS there is a displacement of 6.4mm. While on the other side for the same variation of temperature there is a displacement of 7 mm. These results seem reasonable because if we consider that the length of the main span is 1006m we can calculate how much will be the displacement of the main span according to the linear elasticity theory:

$$\Delta l = \alpha \Delta T l = 12.2 \times 10^{-6} * 1 * 1006 = 12.27 \text{ mm}$$

This measure is the total displacement of the main span, meaning that the span moves of about 6 mm towards north and 6 mm towards south for an increase of 1°C.

Therefore, the sensor data reflect the behaviour of the theoretical model.



## 6.10 Least squares analysis

The Least squares analysis was performed for the NE, SE and SW sides. In these cases, indeed, the correlation between strain and temperature is stronger. Since between strain and temperature we have seen that there is a high value of the Pearson's

correlation coefficient, it is possible to look for the line that best approximates the linear relationship, through the least squares method. The results are presented here:

	$\epsilon_0$	$\alpha$ [ $^{\circ}\text{C}^{-1}$ ]	$m$ [ $\mu\epsilon/d$ ]
NEMS	-61,50	28	-0,39
SEMS	-214,82	0,99	0,48
SWMS	-282,80	0,94	-0,45

Below the covariance matrix of the parameters and their Pearson's correlation are reported.

The diagonal of the covariance matrix for each time span provides the variance of each parameter with itself. The off-diagonal entries in the matrix provide the covariance between each parameter pair.

- NEMS Covariance matrix

$$\begin{bmatrix} 129,0418 & -0,4408 & -6,1585 \\ -0,4408 & 0,0025 & 0,0003 \\ -6,1585 & 0,0003 & 1,5571 \end{bmatrix}$$

- NEMS Pearson's correlation

	$\epsilon_0$	$\alpha$	$m$
$\epsilon_0$	1	-0,7795	-0,4344
$\alpha$	-0,7795	1	0,0056
$m$	-0,4344	0,0056	1

- SEMS Covariance matrix

$$\begin{bmatrix} 213,9862 & -0,7680 & -9,1596 \\ -0,7680 & 0,0047 & -0,0088 \\ -9,1596 & -0,0088 & 2,6966 \end{bmatrix}$$

- SEMS Pearson's correlation

	$\epsilon_0$	$\alpha$	m
$\epsilon_0$	1	-0,7612	-0,3813
$\alpha$	-0,7612	1	-0,0774
m	-0,3813	-0,0774	1

- SWMS Covariance Matrix

$$\begin{bmatrix} 358,6507 & -1,3346 & 15,4863 \\ -1,3346 & 0,0091 & -0,0237 \\ 15,4863 & -0,0237 & 4,7438 \end{bmatrix}$$

- SWMS Pearson's correlation

	$\epsilon_0$	$\alpha$	m
$\epsilon_0$	1	-0,7392	-0,3754
$\alpha$	-0,7392	1	-0,1138
m	-0,3754	-0,1138	1

The figures that represent the trend of the compensated strain of the truss end link are produced as a mean of cancelling the weather effect, hence the temperature variation, from the strain measurements. As a result, they will present the strain that is being induced to the truss end link as a result of all the other factors that affect the link state. The formula below represents the link's strain as a result of all the factors that affect it, including temperature variation. The first of the three set of graphs generated below corresponds to this formula:

$$\Delta\epsilon = \epsilon_0 + \alpha \Delta T + m \Delta t$$

Subtracting the temperature variation is shown below, generating the compensated strain trendline that corresponds to the second of the pair of the three graphs presented.

$$\Delta\epsilon - \alpha \Delta T$$

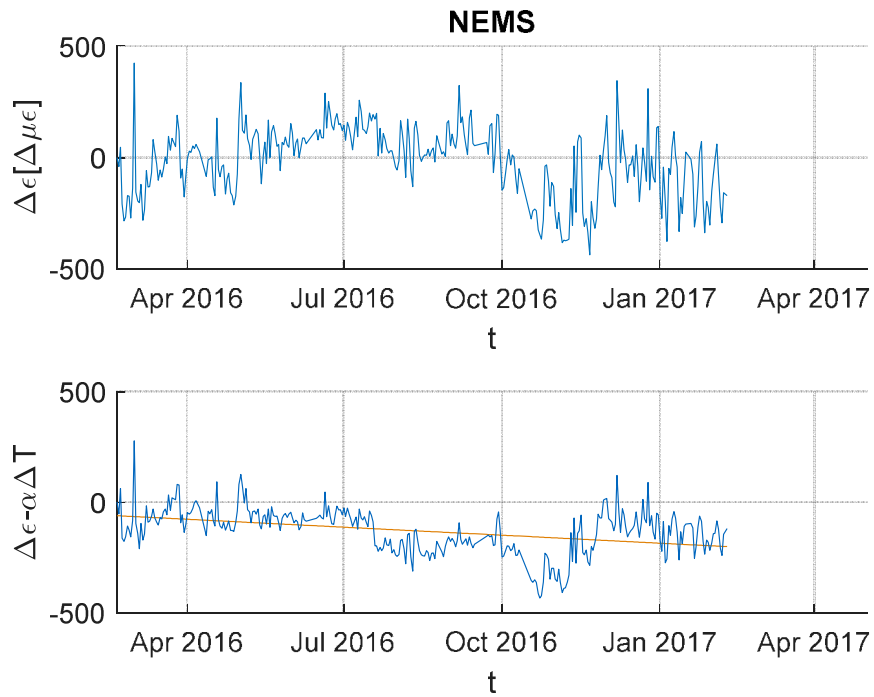


*Figure 6.31: NEMS compensated data*

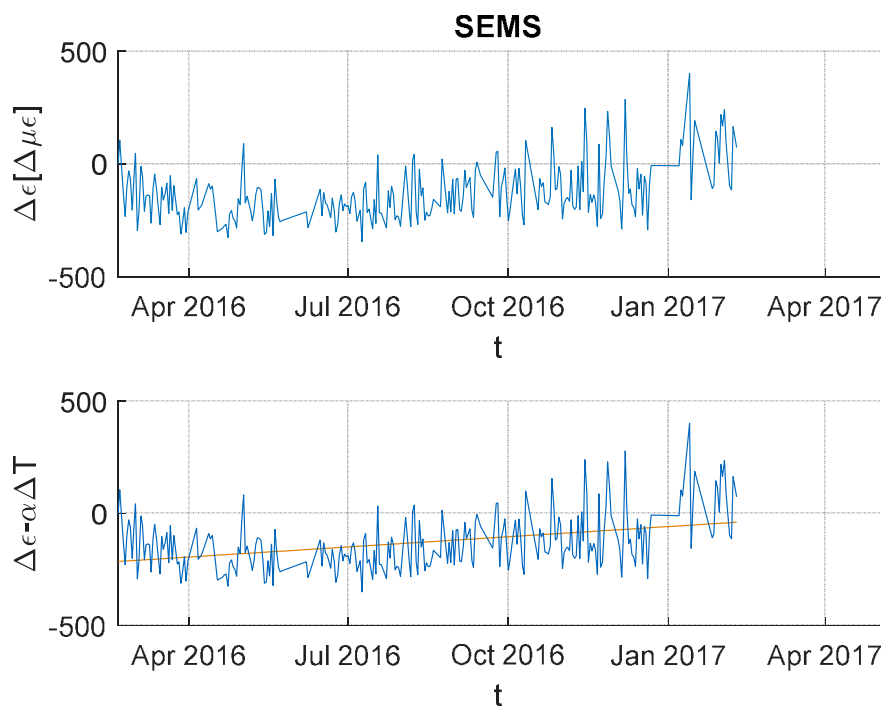


*Figure 6.32: SEMS compensated data*

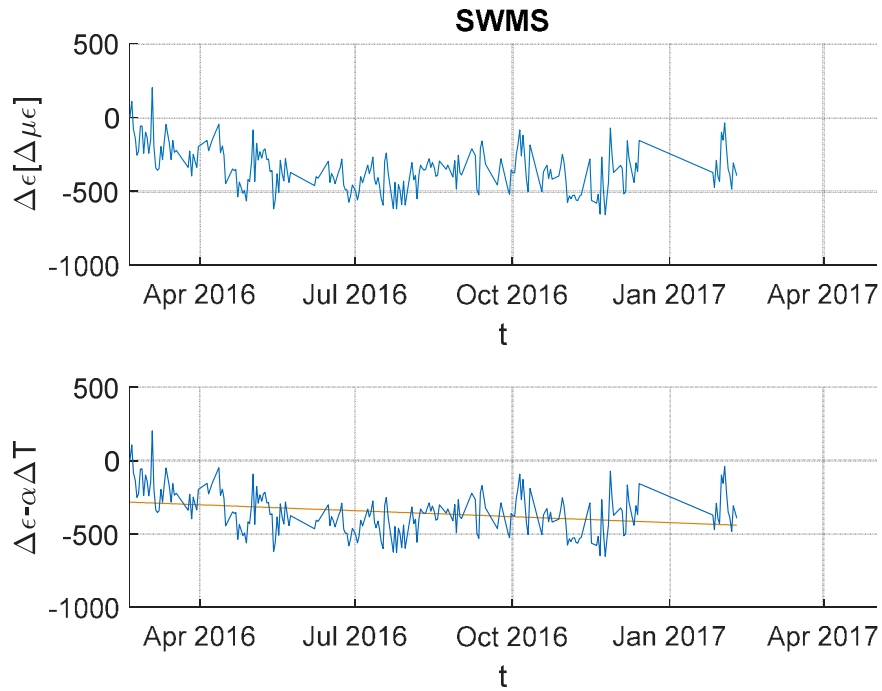


Figure 6.33: SWMS compensated data

The NEMS plot of compensated strain reveals a little retraction of the truss end link as a result of all the other factors that affect it. It should be pointed out that this result contradicts the normal expectations of strain. To be more precise, the truss link was expected to demonstrate a constant strain over the full year, which would have been the natural reaction of the link, because it is subjected to the same traffic/variables loads over the time.

As regard the SEMS and SWMS plots there is an opposite behaviour of the compensated data. In fact, the SEMS compensated strain plot reveals a small elongation of the truss end link over the time. While, a contraction of the truss end link results in the SWMS plot. Moreover, there is a further unexpected result that regards the value of  $\alpha$ . In fact, the apparent thermal expansion coefficient, which takes into account how strain changes due to temperature results a very small value.

## 7.0 New bearing results and discussion

The repair work to replace the links began in August 2016 on the NE side, where the fractured link had been discovered.

The links replacement work resulted in a new configuration in which the function of transmitting loads to the tower, previously carried out by the link, is now carried out by a sliding bearing.

Unfortunately, the only data available at the moment for the new bearings is from the NE side. The works contract to replace the other truss end links with bearings is still ongoing, and while the majority of the works are complete there is still work to be done to get the SHM system live.

Included in this section of the report is the results of analysis of data from the static strain gauges and displacement sensors applying the same method used previously with truss end links data.

### 7.1 Full time history of strain and temperature

Strain and temperature measurements at NEMS were collected for the period from 16/03/2017 to 19/11/2018. However, the plots started on 11/04/2017, day when the load was transferred onto the new bearing.

The analysis of the full-time history of the recorded data was carried out for the strain gauges attached to the bottom chord (STR-BC-05) and to the truss end post (STR-EP-10). In addition, data from the displacement sensor at the top of the truss end post were also analysed.

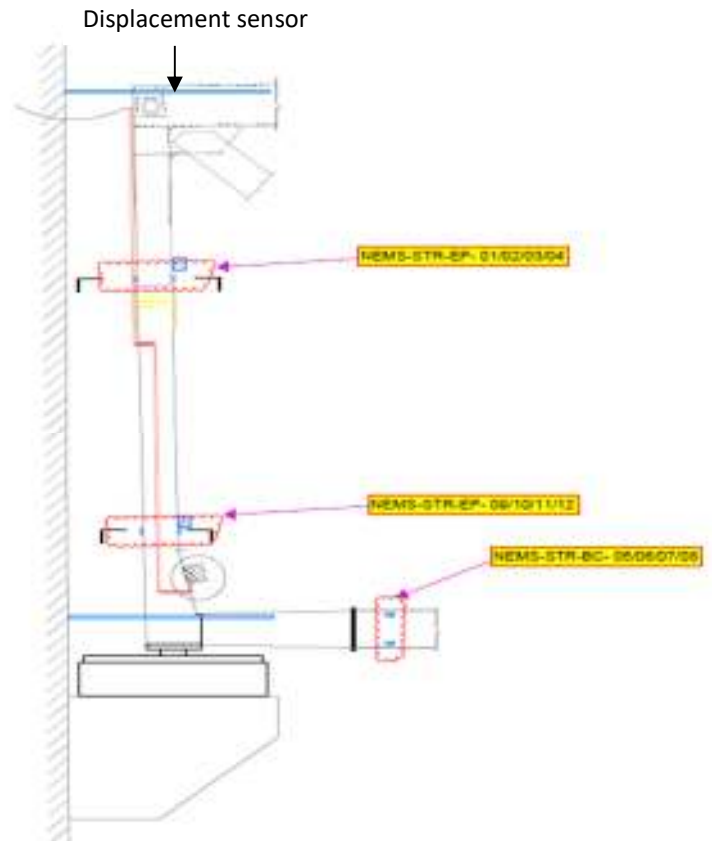


Figure 7.1: New bearing sensors arrangement

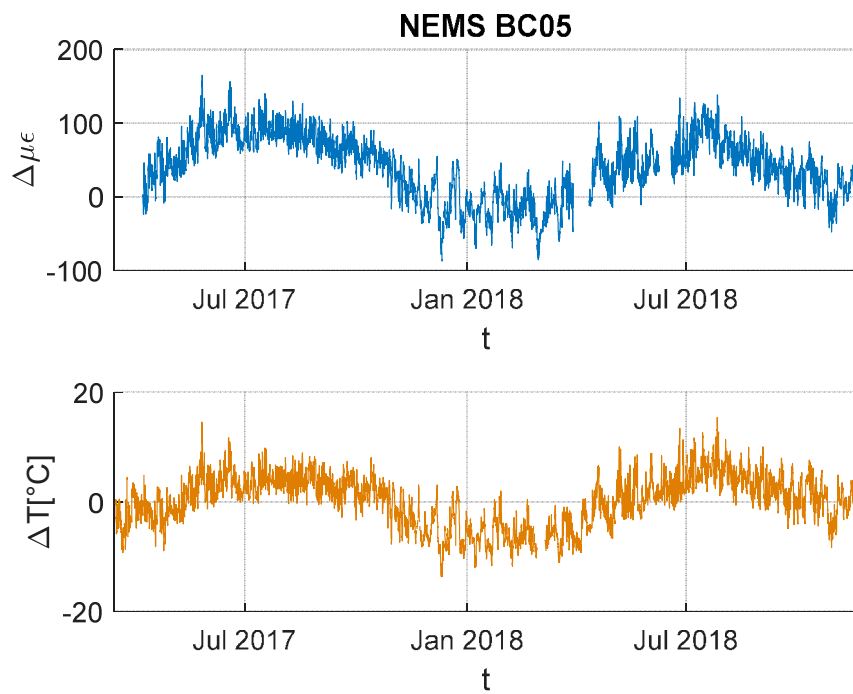


Figure 7.2: BC full time history uncompensated strain and temperature

Looking at the graph it can be seen that the strain and temperature follow the same pattern and that this is repeated during almost two years. This confirms, as before, that changes in strain are directly affected by changes in the temperature of the cable.

Furthermore, it can also be observed that both strain and temperature fluctuate with a constant pattern through the span of the two years for which they were examined, illustrating almost identical values of strain and temperature for the same periods of the year.

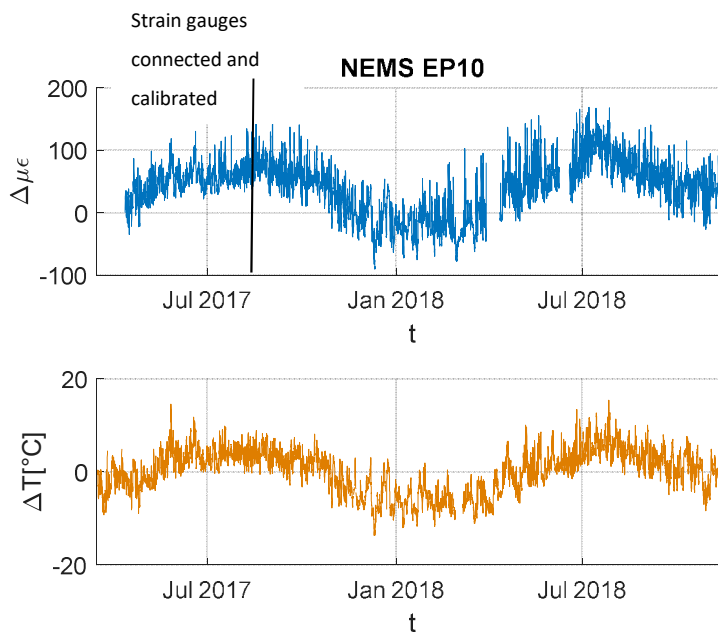


Figure 7.3: EP full time history uncompensated strain and temperature

Observing the truss end post strain plot it can be seen that after September 2017 the signals fluctuations are greater. The reason of this change is that on the 22/09/2017 the end post strain gauges were connected and calibrated. Therefore, the sensors were put into operation since March, like the bottom chord strain gauges, but only in a second moment they were calibrated.

Besides, also in this case the same trend of strain and temperature can be recognized during the two years of recording.

## 7.2 Different periods within the year

In this section, the graphs for uncompensated strain and temperature are presented for a span of three consecutive days, to analyse the daily behaviour of the bottom

chord and of the end post, compared with the temperature. Two different periods were chosen within the year, the summer and winter periods. Those time periods, with their respective 3-day graphs are hereby presented.

### 7.2.1 Summer solstice

The graphs for uncompensated strain and temperature for the summer period, for the full days of 20, 21 and 22 of June 2016 are presented in Figure 7.5 and Figure 7.6 respectively.

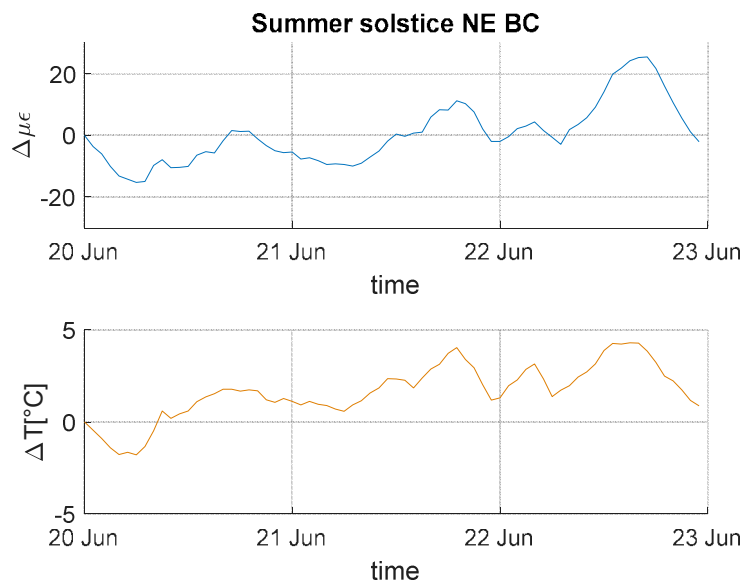


Figure 7.4: BC Summer solstice uncompensated strain and temperature

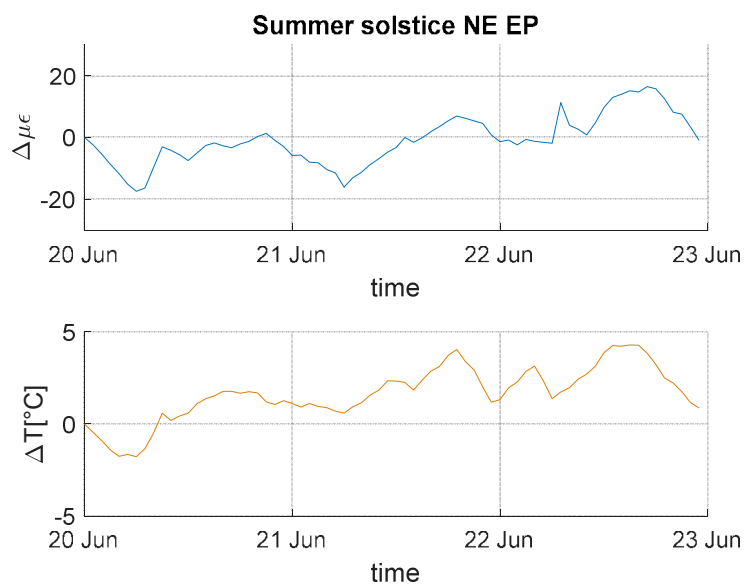


Figure 7.5: EP Summer solstice uncompensated strain and temperature

As observed in the strain and temperature graphs, the daily minimum values for strain and temperature appear at around 6:00, one hour after the sunrise. Moreover, the maximum values for strain and temperature are presented between 17:00 and 19:00.

As we expected the minimum values for strain are reached before sunrise when the structure has cooled down during the night time, therefore dropping their surface temperature and contracting towards their initial length.

During the day the temperature of the structure increases and the strain of the bottom chord and of the end post follow the same trend. To be more precise, strain measures reach the peak shortly before sunset, when the structure surface has been exposed for hours to sun and generally to higher temperatures, as opposed to night time temperatures.

### 7.2.2 Winter solstice

The graphs for uncompensated strain and temperature for the winter solstice are presented for the full days of 18, 19 and 20 of December 2016 because there were temperature data missing for the days of 21 and 22 of December.

Once again it can be seen how the strain gauges measurements recorded for the various times within the day, are directly related to the temperature measurements of the structure, taken for the same timestamps.

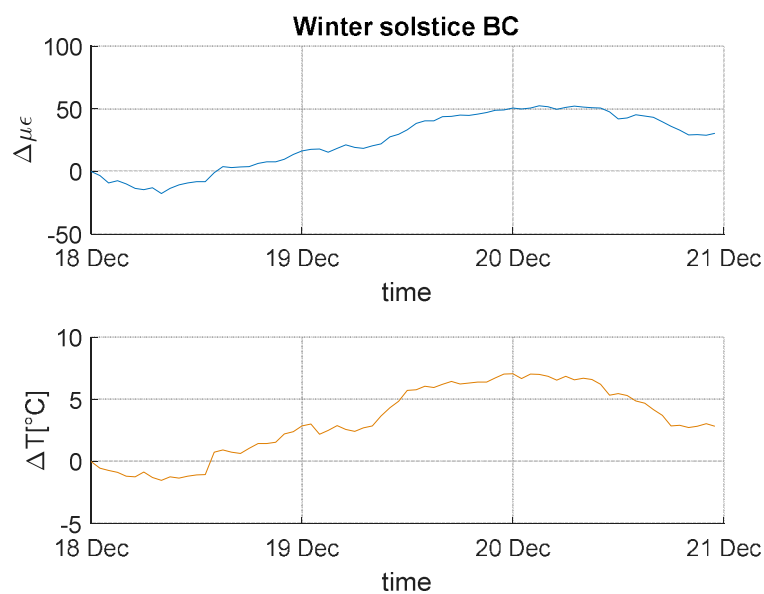


Figure 7.6: BC Winter time uncompensated strain and temperature

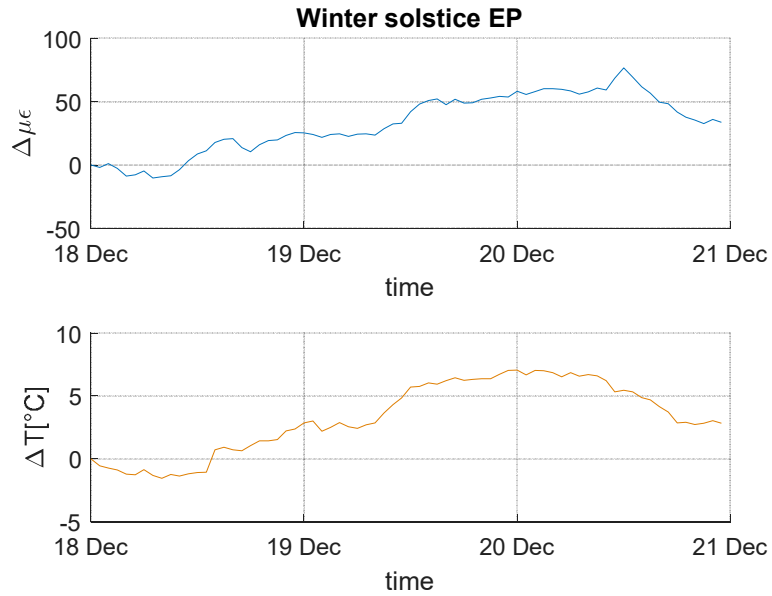


Figure 7.7: EP Winter time uncompensated strain and temperature

### 7.3 Strain and temperature trend with reduced data set

Taking into account the results of the previous section the strain in the truss system is affected by daily temperature variation. Therefore, the dataset was reduced to one significant sample per day, so that the daily temperature effect on the structure could be removed.

The reduced plots were produced selecting a daily sample at 5 am, just before sunrise on average. At this time of the day the surface of the bottom chord and of the truss end post will have been for as many hours as possible under absence of light; therefore, the elements surface temperature will be lower, as well as strain measurements because of it.

Analysing only the daily sample at 5 am, time when the temperature effect is minimal, will help measure strain in the elements that derive from all the other factors that can cause it. In particular, we can observe the strain for reasons of loading of the suspended structure.

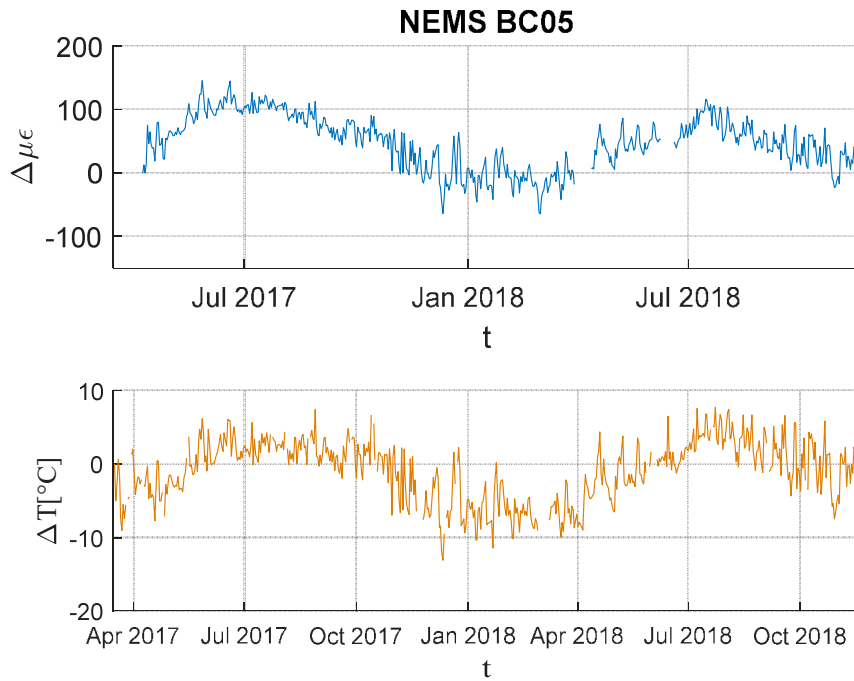


Figure 7.8: BC full-time history of reduced strain and temperature

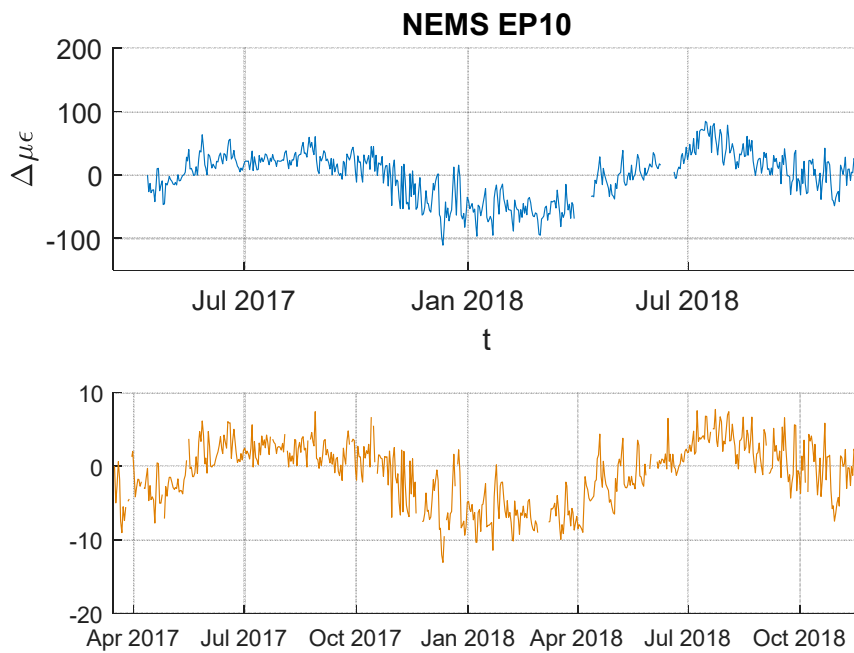


Figure 7.9: EP full-time history of reduced strain and temperature

Comparing the full-time history reduced strain plot to the fulltime history uncompensated strain, we can instantly observe the almost identical pattern with which the two plots fluctuate; a pattern that appears to repeat itself in all two years.

The similarity in the two patterns can be attributed to the contribution of the truss system surface temperature to the strains generated in the truss. To be more precise, looking at the uncompensated and reduced temperature plots that are moving with the same manner, we can understand why this seems to be the case for strain as well, as strain is directly affected by temperature. Therefore, the similarity in the temperature plots determines the similarity observed in the two strain plots.

Now comparing the new bearing plots with those of the truss end links, it can be noted that the strain values measured in the new configuration are smaller than the strain values recorded when there were the truss end links. The reason why there is a different strain variation in the two configurations is that at the beginning of September 2017 the Queensferry Crossing bridge was opened and all the traffic that previously occupied the FRB carriageways was diverted to the new bridge. The Forth Road Bridge was closed for a month and in October 2017 was reopened only to public buses. Hence, the load due to traffic in the new configuration considerably decreased.

#### 7.4 Strain-temperature correlation

To assess the strain sensitivity to temperature the measurements dispersion diagrams are provided in this section.

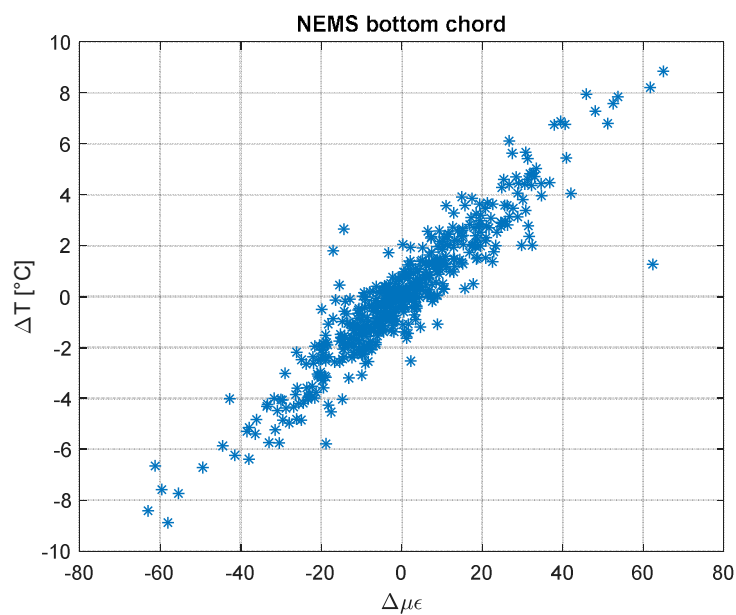


Figure 7.10: BC strain and temperature correlation

At the bottom chord there is positive correlation between strain and temperature with a correlation coefficient of 0.9. The linear relation reveals that for a temperature variation of 1°C the strain variation is about 7  $\mu\epsilon$ .

Considering the thermal expansion coefficient  $\alpha = 12 \times 10^{-6}$  and the following formula:

$$\epsilon = \alpha \Delta T$$

The measured value is compatible with the expected result.

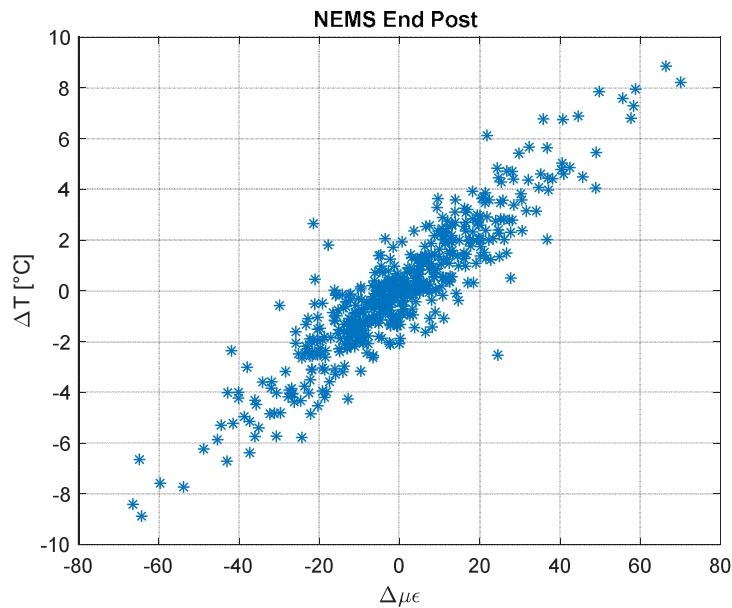


Figure 7.11: EP strain and temperature correlation

Observing the truss end post dispersion diagram, we can see a positive linear correlation between the two variables. Pearson’s correlation coefficient is equal to 0.9. In addition, from the graph we can calculate that for a temperature variation of 1°C the strain varies by 7  $\mu\epsilon$ , which is compatible with the predicted value of 12  $\mu\epsilon$ .

## 7.5 Displacement and temperature trend

In this section the recorded signals coming from the sensor EP-DSP 01 (top displacement transducer) are plotted together with the temperature.

The NEMS displacement monitoring on the new configuration started on 06/04/2017, but the plot starts on 31/05/2017 because all the measurements before this day are variable and with conflicting values.

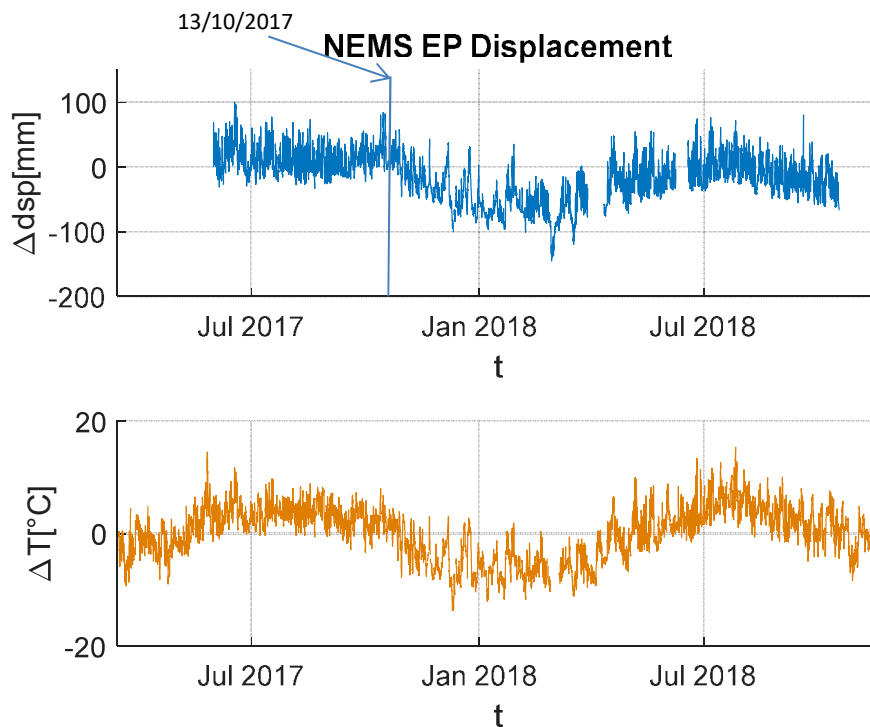


Figure 7.12: EP full-time history uncompensated displacement

Observing the graph, we can see that the displacement trend is initially constant until October 2017 after this time the trend begins to vary and follows that of the temperature. This change is likely due to the reopening of the Forth Road Bridge, after the closure for roadworks, to public buses on the 13/10/2017.

Moreover, comparing this graph with the truss end post displacement plot with the old configuration, it can be seen that in this case the displacement trend follows the temperature trend, while in the old configuration we experienced a reverse behaviour.

The structure behaviour is always the same, it elongates during the warmer months of the year and contracts during winter. However, the reference system in the new configuration is on the contrary compared to before. To be more precise the sensors records a positive displacement when the structure elongates towards the towers, while the measurements results negative when the structure contracts towards the main span. This led to a displacement trend that follows the temperature trend.

## 7.6 Displacement and temperature trend with reduced data set

Following the data processing steps, displacement and temperature data have been reduced picking one sample per day at 5 am to remove the effect of the daily

temperature variation. At this time the structure has cooled down during the night and it is less subjected to elongation due to the air temperature.

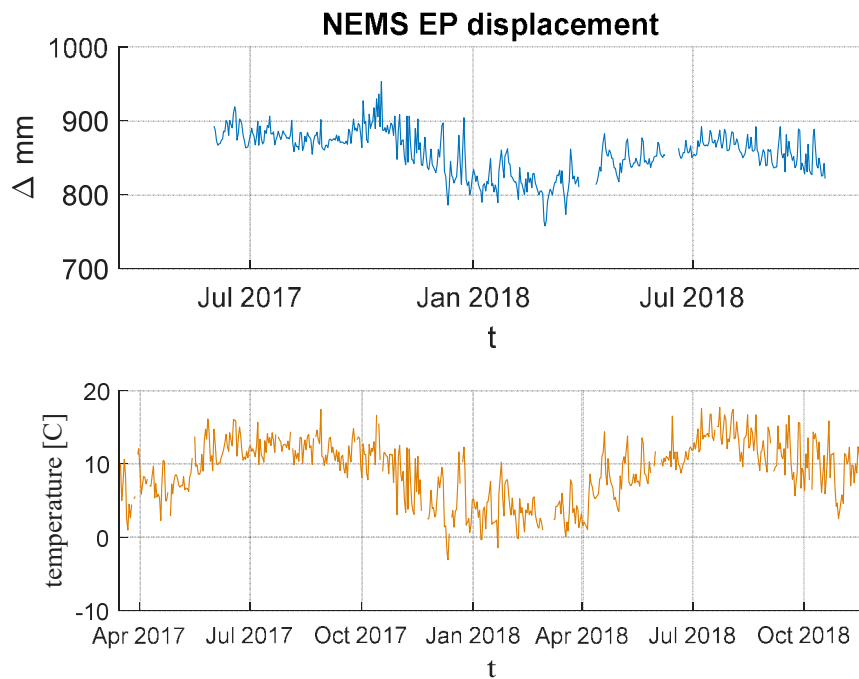


Figure 7.13: EP full-time history of reduced strain and temperature

Relating the full-time history of uncompensated displacement to the plots with reduced data set we can observe that the overall trend doesn't change. This shows the direct influence of temperature on the truss system movement. Therefore, the similarity in the temperature plots determines the similarity observed in the two displacement plots.

## 7.7 Displacement-temperature correlation

To assess the correlation between displacement and temperature, the dispersion diagram has been plotted.

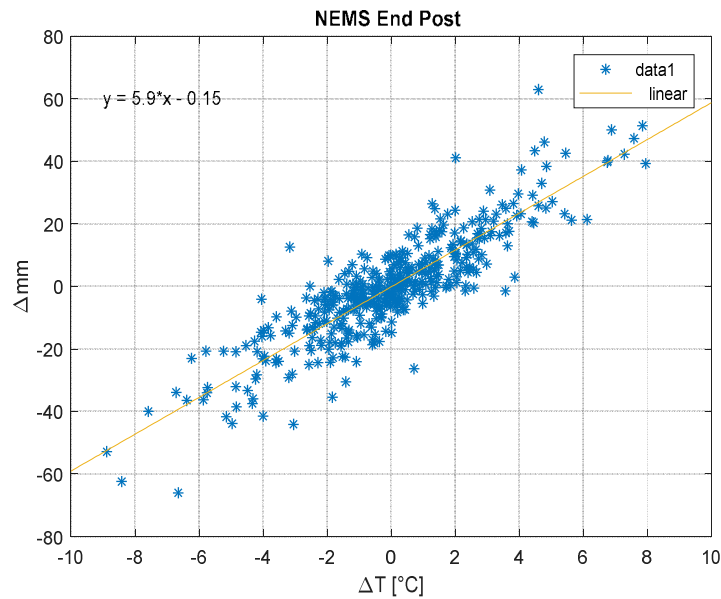


Figure 7.14: EP displacement correlation

Looking at the plot it can be recognized a positive linear correlation between the two parameters. The correlation coefficient is 0.9 hence there is a strong correlation between displacement and temperature.

From the data recorded we can see that for a temperature variation of 1°C the corresponding displacement variation is 6 mm. This value corresponds to the result obtained with the old configuration.

Besides, the length of the main span is 1006 m therefore, the displacement of the main span is:

$$\Delta l = \alpha \Delta T l = 12.2 \times 10^{-6} * 1 * 1006 = 12.27 \text{ mm}$$

This measure is the total displacement of the main span, meaning that the span moves of about 6 mm towards east and 6 mm towards west for an increase of 1°C.

Thus, the result obtained is also compatible with the linear elasticity theory.

## 7.8 Least squares analysis

The mathematical procedure of Least squares analysis will be performed for the full-time history in order to find the best-fitting curve to the full set of data.

	$\epsilon_0$	$\alpha$ [ $^{\circ}\text{C}^{-1}$ ]	$m$ [ $\mu\epsilon/d$ ]
EP	3,69	8,45	2E-4
BC	4,09	8,87	-0,09

Below the covariance matrix of the parameters and their Pearson's correlation are reported.

The diagonal of the covariance matrix for each time span provides the variance of each parameter with itself. The off-diagonal entries in the matrix provide the covariance between each parameter pair.

- Truss end post covariance matrix

$$\begin{bmatrix} 0,6024 & -0,0015 & 0,0055 \\ -0,0015 & 5,2682 & -3,9389 \\ 0,0055 & -3,9389 & 0,0092 \end{bmatrix}$$

- Truss end post Pearson's correlation

	$\epsilon_0$	$\alpha$	$m$
$\epsilon_0$	1	-0,8565	0,0739
$\alpha$	-0,8565	1	0,0178
$m$	0,0739	0,0178	1

- Bottom chord covariance matrix

$$\begin{bmatrix} 1,0180 & -0,0024 & 0,0299 \\ -0,0024 & 8,3402 & 7,6e - 06 \\ 0,0299 & 7,6e - 06 & 0,0148 \end{bmatrix}$$

- Bottom chord Pearson's correlation

	$\epsilon_0$	$\alpha$	$m$
$\epsilon_0$	1	-0,8263	-0,2436
$\alpha$	-0,8263	1	0,0216
$m$	-0,2436	0,0216	1

The figures that represent the trend of the compensated strain of the bottom chord and of the truss end post are produced as a mean of cancelling the weather effect, hence the temperature variation, from the strain measurements.

As a result, the plots will provide the strain that is being induced to the truss system by all the other factors that can affect it. The formula below represents the link's strain as a result of all the factors that affect it, including temperature variation. The first of the set of graphs generated below corresponds to this formula:

$$\Delta\epsilon = \epsilon_0 + \alpha \Delta T + m \Delta t$$

The second pair of graphs with the compensated strain trendline are generated subtracting the temperature variation like it is shown in the formula below:

$$\Delta\epsilon - \alpha \Delta T$$

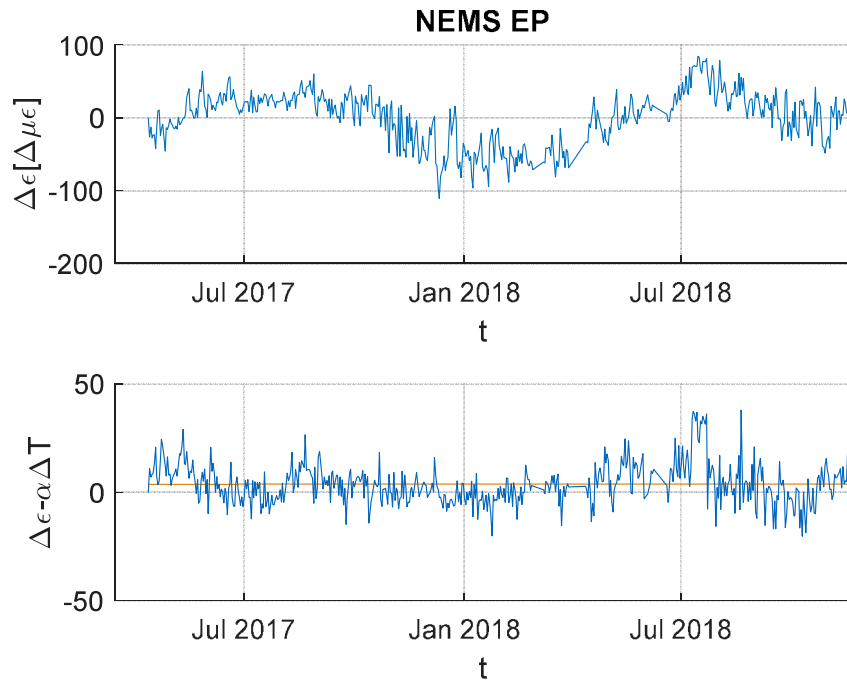


Figure 7.15: EP compensated data

The compensated plot of the truss end post reveals a constant strain over the time as the trend line is almost parallel to X axis.

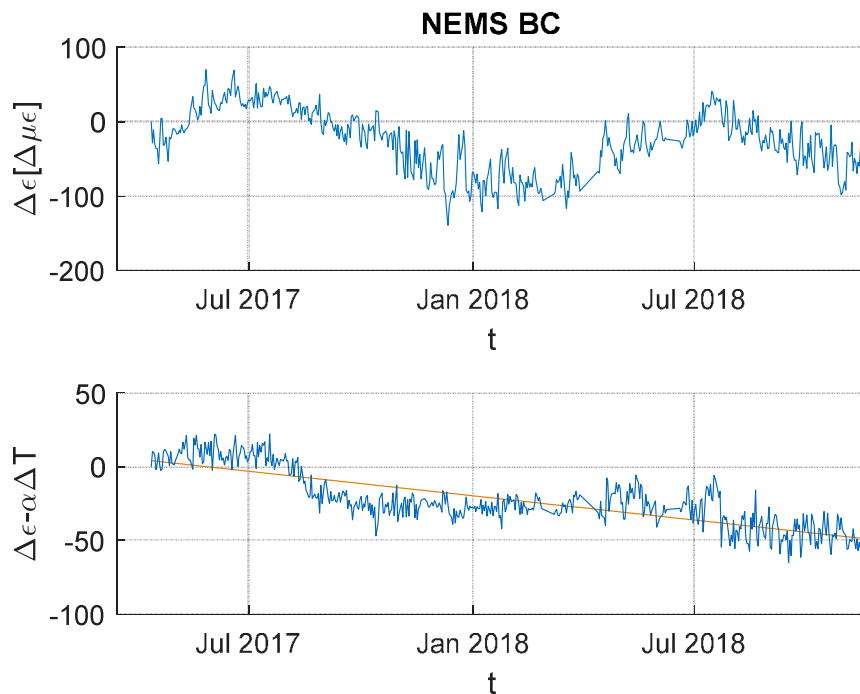


Figure 7.16: BC compensated data

The compensated plot of the bottom chord strain reveals a contraction of the element over the time as a result of all the other factors that could affect it.

It should be emphasized that the normal result that we would expect of a steel truss system concern an almost null variation of strain over the time. However, it should be pointed out that the bottom chord strain trend does not contradict the normal behaviour. In fact, the time stamp considered does not include two full years, but it starts in April 2017 and it ends in November 2018 therefore the last values of strain are smaller because correspond to the winter time.

## 8.0 Conclusion and recommendations

Experience from this bridge has led to the conclusion that SHM can highlight the risk of elements failures and check if all the elements, even those who are difficult to inspect, are behaving as designed. Structural health monitoring of the bending stress in the link would, had it been in place, have shown that risk of fracture was very high.

Sometimes there may be issues with the DAU or with sensors getting broken on site that required them to be reset, as in the case of NWMS data. Therefore, each plot of the measurements must be accompanied by a study of the structural behaviour of the element and if the results do not meet the expectations, further investigations should be made if possible.

In terms of the results of this thesis the structural response of the truss system in the actual configuration is consistent with what we expected from theory. While, regarding the old configuration with the stiffening truss end links, the structural response results strongly influenced by temperature in an unexpected way. Indeed, the values of the truss end link strain recorded vary in a bigger range with respect to the variation visible in the new configuration.

However, the truss end link strain data could be used as a starting point for further analysis, for example comparing these values with the bearing load cell data, as both the elements perform the same function of transmitting the load from the deck to the tower leg.

Another aspect that could be investigated in future is the displacement of the hangers compared to the tower displacement subjected to a uniform increase of temperature in order to calculate accurately the force that the link carries and compare it with the monitoring results.

In conclusion, with the SHM it is possible to validate design assumption and improve future designs or validate new construction methods.

In addition to this the use of the SHM system during the bridge's service life can be used to ensure all load increases, are within safety margins. Which could be used to provide early warnings about any faults in the materials or in the elements if the data received form the system is not as expected.

## References

- Nguyen, D. T., Meng, X., Owen, J. S., Xie, Y., Psimoulis, P., Ye2, G., . . . Madden, P. (2018). Structural Health Monitoring of Long-span Bridges. *9th European Workshop on Structural Health Monitoring*, (p. 13). Manchester.
- Agdas, D., Rice, J. A., Martinez, J. R., & Lasa, I. R. (n.d.). *Comparison of Visual Inspection and Structural-Health Monitoring as Brodge Condition Assessment Methods*.
- Angus, E. (2017). Use of technology in the operation and maintenance of a major asset - The Forth Road Bridge. Amey/Society of Chief Officers of Transportation in Scotland (SCOTS).
- Angus, E. (2018). The use of technology in the operation and maintenance of the Forth Road Bridges. Hong Kong: Amey.
- Angus, E. M. (2018). How integrated technology is driving safety and efficiency on the Forth Road Bridges. *Bridges Scotland 2018*, (p. 61).
- Arndt M., R. O. (2017). Dealing with unpredicted infrastructure failure case study: Forth Road Bridge. Amey.
- Arndt, M. (2015). *Forth Road Bridge - Truss End Link - What has happened? the forth bridges*.
- British Standards Institute BS5400-2. (2006). *Steel, concrete and composite bridges, Part 2*. London.
- Chen, H.-P. (2018). *Structural Health Monitoring of Large Civil Engineering Structures*. University of Greenwich UK.
- Chen, Z., Zhou , X., Wang , X., Dong , L., & Qian, Y. (2017). Deployment of a Smart Structural Health Monitoring System for Long-Span Arch Bridges: A Review and. *sensors*.
- Colford, B. R. (2013). Main cable anchorages investigation at Forth Road Bridge. New York.
- Colford, B. R., & Clark, C. A. (2009). Feasibility Study into the replacement or augmentation of the main cables of a long span suspension bridge. New York.

- Forth Estuary Transport Authority. (2008). *STRENGTHENING OF TRUSS END CONNECTIONS*.
- ICE. (1967). *Forth Road Bridge*. London: William Clowes and Sons Limited.
- J. Fisher and Sons plc. (2015, December 23). BridgeWatch™ plays pivotal role.
- Jack, H. (2003). *The Forth Road Bridge General Arrangement*. Forth Estuary Transport Authority, South Queensferry.
- Kitching. (2017). Smart Infrastructure | Forth Road Bridge. *New Civil Engineer*.
- Kitching, R. (2017, 07 19). Smart Infrastructure | Forth Road Bridge. *New Civil Engineer*, pp. <https://www.newcivilengineer.com/tech-excellence/smart-infrastructure-forth-road-bridge/10021401.article>. Retrieved 08 01, 2018
- Kutner, M. H., Nachtsheim, C. J., Neter, J., & Li, W. (2005). *Applied Linear Statistical Models*. New York: McGraw-Hill Irwin.
- M. L. Wang, J. P. (2014). *Sensor Technologies for Civil Infrastructures*. Woodhead.
- Penistone, J. (2009). A CRITICAL ANALYSIS OF THE FORTH ROAD BRIDGE,. *Proceedings of Bridge Engineering 2 Conference 2009*. Bath,UK.
- Ramboll b. (2013). *SHMS- Sensory system, static strain gauges installed at S2,S1,ST,CT,NT,N1 and N2 design report*. FORTH REPLACEMENT CROSSING - DESIGN JOINT VENTURE:.
- Rehfisch, A. (2016, January 22). Closure of the Forth Road Bridge. *Scottish Parliament Information Centre (SPICe)*.
- Strainstall. (2016, 03 2). NEMS truss end links structural Monitoring DAU-01.
- Strainstall. (2016). *SHMS – DAU FAT TEST PLAN PHASE I*.
- Strainstall. (2016). *SHMS – INDIVIDUAL DAU SAT TEST PLAN*.
- Transport Scotland. (2017). *Forth Road Bridge: Facts and Figures*. Retrieved from <https://www.theforthbridges.org/forth-road-bridge/facts-and-figures/>
- Transport of Scotland. (1964). Retrieved from the forth bridges: <https://www.theforthbridges.org/forth-road-bridge/construction-gallery/>

- Transport Scotland. (2017). *The Forth Bridges: Truss end links repair*. Retrieved July 2018, from <https://www.theforthbridges.org/forth-road-bridge/maintenance/major-projects/truss-end-links-repair/>
- Uhl, T., Stepinski, T., & Staszewski, W. (2013). *Advanced Structural Damage Detection: From Theory to Engineering Applications*. John Wiley & Sons.
- Vaisala ultrasonic wind sensor WS425. (2010). Retrieved from <http://www.vaisala.com/>
- Vishay Precision Group. (2016). Retrieved from vishaypg: <http://www.vishaypg.com/docs/50003/precsg.pdf>
- Watt, D. (2017). *QUEENSFERRY CROSSING: Vision to Reality*. Isle of Man: Lily Publications.
- Wong, K.-Y. (2007). *Design of a structural health monitoring system for long-span bridges*. Retrieved from Structure and Infrastructure Engineering: <https://doi.org/10.1080/15732470600591117>
- X. Meng, D. T. (2018). Design and Implementation of a New System for Large Bridge Monitoring—GeoSHM.

## Acknowledgements

First of all, I would like to thank professor Rosario Ceravolo who gave me the opportunity to take part in this project. I would also like to thank my supervisor professor Daniele Zonta and the PhD students Andrea Verzobio and Andrea Maroni, from the University of Strathclyde, for their help and advices throughout the duration of this dissertation.

Secondly, I would like to thank my family for the support they gave me despite the difficulties they faced. They will always be an anchor in my life.

Finally, a special thanks to Francesco for having always been by my side during these two years, for sharing with me the best and the most stressful years of our life. You are the best (not always though) boyfriend I could ever ask for.